Grant Agreement No: 245163
Project start date: July 2010
Project end date: July 2013

ACROPOLIS
Aggregate and Cumulative Risk Of Pesticides: an On-Line Integrated Strategy
SEVENTH FRAMEWORK PROGRAMME

Deliverable 4.1 a strategy to use internal exposure dose modelling (PBTK) in cumulative and/or aggregate risk assessment.

RIVM National Institute for Public Health and the Environment
Contact person: Jan van Eijkeren, email: jan.van.eijkeren@rivm.nl
Project team: Jan van Eijkeren(RIVM), Bas Bokkers (RIVM) and Jacob van Klaveren (RIVM)

Contents

Abstract

This study discusses the internal dose modelling when considering exposure to different members of a group of neurotoxic pesticides with the same mode of action (cumulative and aggregated exposure) and when relating *in vitro* benchmark dose (BMD) to *in vivo* BMD. Physiologically Based PharmacoKinetic/PharmacoDynamic (PBPK/PD) models for the organophosphorus pesticides (OPs) chlorpyrifos (CPF; Timchalk *et al*. 2002) and diazinon (DZN; Poet *et al*., 2004; Timchalk and Poet, 2008) are applied for cumulative and aggregated dose-effect modelling of acetylcholinesterase (AChE) inhibition. Moreover, PBPK modelling is applied in a reverse dosimetry approach to *in vitro* CPF-oxon cell toxicity data and to *in vitro* rat foetal malformation toxicity of tebuconazole data to obtain *in vivo* BMDs. This approach leads to a refinement of risk assessment both in terms of defining reference values and assessing the relevance of the temporal characteristics of exposure. Modelling is a complex exercise and as such it can be used in those instances when the "standard" risk assessment, that includes a number of conservative assumptions fails to identify safe scenarios. In these cases, PBPK/PD modelling, by reducing the uncertainty of the evaluations, may prove useful in avoiding undue risk management options such as banning o severely limiting the use of certain (groups of) compounds.

Introduction

The EU Acropolis project aims at the improvement of risk assessment strategies in Europe regarding combined exposures to pesticides. One of the objectives is to consider the fate of toxicants within the body and the internal effective dose of different toxicants, to refine, when needed, risk assessment. As exemplary toxicants, the choice is on those that are found on raw food products due to spraying with organophosphorus pesticides (OPs) or fungicides (conazoles). In line with WP4, Bosgra *et al*. (2009) considered an integrated probabilistic framework for cumulative risk assessment with OPs as exemplary. Hinderliter *et al.* (2011) developed a modelling strategy for probabilistic exposure-response modelling with the OP CPF as an example. The objective is to model the internal dose following either dietary exposure (general population) or dietary together professional exposure (mainly dermal).

As a modelling approach the choice is for physiologically based pharmacokinetic (PBPK) modelling that is becoming more and more accepted as a standard. A typical example of a PBPK model is shown in **Figure 1**. For this kind of models, it is not only possible to extrapolate animal models to the human situation, but also it allows for the extrapolation of *in vitro* experimental results to application *in vivo* (reverse dosimetry) and route-to-route extrapolation. In particular, PBPK modelling will help in refining reference doses (e.g. ADI, ARfD) for the compounds under assessment, when this is required by e.g. the "standard" risk assessment indicating a (close to) non-acceptable risk for a (sub)population. Also, since the model incorporates time considerations, this will also provide refinements of risk assessment if information on temporal characteristics of exposure are available.

Moreover, being based on physiological aspects such as tissue weights and regional blood flows, it allows to apply external dose-internal dose-response modelling in a stochastic setting when choosing subjects from a population. So, along with the deterministic PBPK modelling approach, also a stochastic approach is employed for the physiological parameterization of the model. A stochastic approach is applied when considering the population dietary intake of OPs. This study does not consider inter species differences in dynamics. Nevertheless, for the human acetylcholinesterase inhibition PBPK/PD models applied in this study, corresponding rat models exist with a few PD model parameters with different values for humans and rats.

A literature search was performed leading to an overview of PBPK models for OPs (ANNEX Task 4.3; Overview of existing Pharmacologically Based PharmacoKinetic / Pharmaco-Dynamic (PBPK/PD) models for Acetylcholinesterase (AChE) inhibition). From this overview it was decided to chose CPF and DZN as exemplary for modelling the dose-effect relation due to cumulative exposure

to these OPs. This choice was also motivated by the fact that within WP2 cumulative dietary intake distributions have been developed for several OPs along with CPF, DZN and the total of dietary OP exposure. Moreover, the PBPK/PD model

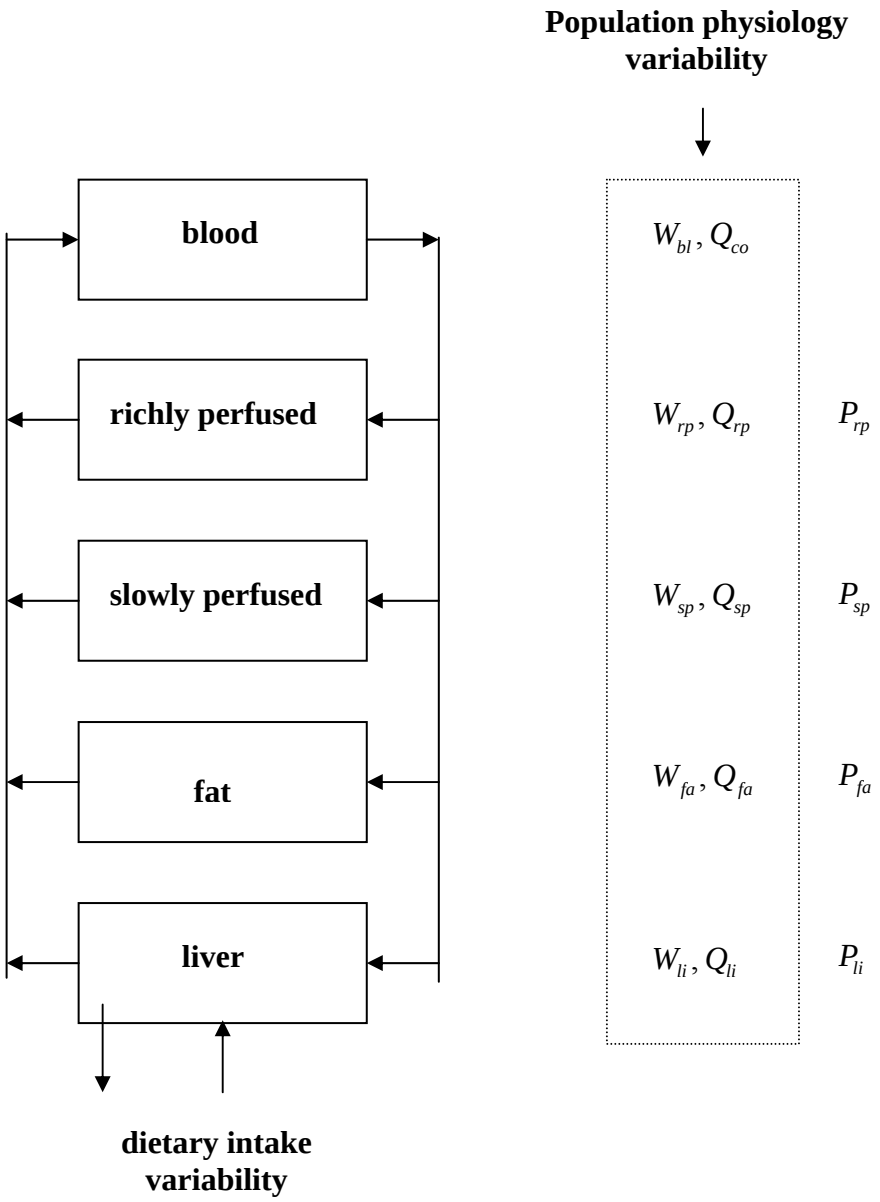

Figure 1. Left: Typical example of a PBPK model for a lipophilic non-volatile compound. The body is represented by 5 compartments: blood (transport means), richly perfused that represent tissues with relative high blood flow, slowly perfused that represent tissues with relative low blood flow, fat (lipophilic compounds storage) and liver (uptake through the portal vein and elimination through metabolism and bile flow). Right: Corresponding compartment weights (*W*) and regional blood flows (*Q*) that vary over the population; bl = blood, co = cardiac output; rp = richly perfused, sp = slowly perfused, fa = fat and li = liver. The distribution over the body is described with tissue:blood partition coefficients (*P*).

for CPF was applied in an aggregated setting, considering a single oral bolus intake and dermal exposure, and for reverse dosimetry estimations of *in vivo* CPF cell toxicity based on *in vitro* cell toxicity data.

Literature search revealed only a few PBPK modelling approaches for conazoles, of which only one, a model for triadimefon and its main metabolite triadimenol, is applied as a fungicide in the field, while the others are used as human medicines. As in WP4 focus is on tebuconazole, both with respect to *in vitro* experiments (malformations in rat foetuses) and to tebuconazole spraying by field workers, a PBPK model for the kinetics of tebuconazole in rabbits was developed, and extrapolated to humans (ANNEX: A PBPK modelling approach for tebuconazole kinetics in male Japanese white rabbit and in humans). This model is applied for reverse dosimetry estimations of human tebuconazole teratogenicity based on *ex vivo* rat malformation data.

In the next section the models and data that are at our disposal are described and the application to the general population as well as to individual exposure is considered in the following section. These two sections are rather technical. The last section examines the benefit of the combination of internal dose modelling or dose-effect modelling with a stochastic approach accounting for population variability in kinetics in risk assessment.

Materials and methods

Organophosphates

In vivo CPF, DZN and total of OPs

A human PBPK/PD model for CPF, essentially based on the model in Timchalk *et al.* (2002) was obtained from C. Timchalk and T. Poet. This model was slightly revised and the naming of variables was systematized as to provide for the extension to a model for the combined exposure to DZN. The corresponding model for DZN in rats, described in Poet *et al.* (2004) and Timchalk and Poet (2008) was co-implemented. The latter reference contains parameter values for both CPF and DZN in rats. It was assumed that the ratios of parameter values for CPF and DZN in humans are the same as the corresponding ratios in rats. Accordingly, parameter values for the human DZN model were obtained from the known model parameter values for CPF. Thus a model for the combined human exposure to CPF and DZN was obtained.

The third Dutch National Food Consumption Inquiry (VCP3; Kistemaker 1998) contains data on the anthropometry (weight, height, age and sex) of 6241 subjects ranging in age of 1 to 97 years. This population of food inquiry participants will serve as exemplary for the general population. From a subject's anthropometry, its physiology in terms of tissue weights and regional tissue blood flows are estimated with the newly introduced model *physB* (Bosgra *et al*., 2012). This model combines a deterministic relation between human anthropometry and physiology with stochastic variation in order to account for human variability around the (deterministic) central trend.

Two other food consumption surveys, VCP Children (Hulshof, 2004) and VCP 2003 (Ocké, 2008), report the food consumption during two consecutive days for children less than 7 years of age and for young adults ranging in age from 19 to 30 years, respectively. Two other data bases, one for the conversion of food consumer products to their primary agricultural food components (CPAP; van Doorn, 1995) and one for residues on primary agricultural food components (KAP: van Klaveren, 1994, 1998), were combined with the two food consumption surveys to estimate the cumulative intake distribution of CPZ, DZN and total of OPs as exemplary for the total Dutch populations of children up to 6 years of age and of subjects from 7 years of age onwards. The cumulative intake distribution tables were implemented in the combined CPF-DZN exposure PBPK/PD model.

The VCP3 population was stratified accordingly to two sub-populations of subjects younger than 7 (530 subjects) and older than 6 (5711 subjects) years of age. For each subject its physiology was obtained from its anthropometry data applying *physB*. The PBPK/PD model was applied to all subjects of the two stratifications. Hinderliter *et al*. (2011) applied it for CPF to a population of 1000 3

year old children and a population of 1000 30 year old adults during 5 consecutive days. Simulating dose intake continuous in time, however, it appeared that steady state at the levels of dietary exposure was reached only after 1 year. Notice that the time to reach steady state is dose dependent. If, *e.g.*, a daily dose of 1000 instead of 10 µg/kg body weight is applied, then steady state is reached in about 75 days. In animal studies such oral levels and higher are common. So, it was decided to consider a simulation time span of 1 year instead of 5 days.

For each day, the daily intake was obtained by random sampling from the uniform distribution and taking the corresponding intake from the linearly interpolated cumulative distribution tables. Just as in Hinderliter *et* al. (2011) the maximum metabolism rates for biotransformation of CPF (DZN) to CPF (DZN)-oxon, of CPF (DZN) to TCP (IMHP) and of CPF (DZN)-oxon to TCP (IMHP) in liver and blood were varied stochastically. In this study lognormal distributions are assumed, Hinderliter *et al*. assume a truncated normal distribution with a lower bound of 0 and an upper bound of fivefold the nominal value. The studied population-minimum AChE activity versus time curve was obtained from the model runs as well as the maximum dose – maximum AChE inhibition relation for each subject. Note for the latter that there is not a direct relation between maximum dose and maximum inhibition as at any time the preceding exposure history of a subject contributes to its inhibition level.

Timchalk *et al*. (2002) introduced a dermal exposure sub-model in order to model human experimental data obtained by Nolan *et al.* (1984). They exposed healthy male volunteers to an acute oral dose of 500 µg CPF/kg body weight followed after 30 days by a dermal exposure to 5000 µg CPF/kg body weight. The sub-model was implemented in the current CPF PBPK/PD model. Timchalk *et al*. (2002) assumed a super skin thin liquid layer containing CPF that was maintained during about 20 hours from CPF application. In our implementation a simple model for absorption from upper skin was assumed. This sub-model allows for aggregated modelling of acute oral and dermal exposure. Aggregated modelling was applied to scenarios of acute oral exposure to 100 µg CPF/kg body weight with concurrent dermal exposure to 5000 µg CPF/kg body weight after 0, 4, 8, 12, 16, 20 and 24 hours. Wiping off CPF was assumed to take place 12 hours after application.

In vitro-in vivo extrapolation CPF

In vitro cell toxicity data for CPF, CPF-oxon, DZN and DZN-oxon were obtained from WP3 (Heusinkveld, reference!). These data were input to the dose-response modelling module PROAST (Slob, 2002) to obtain a benchmark dose – response (BMD) model. $BMD_{0.05}$ served as a surrogate *in vivo* plasma concentration and the corresponding acute external exposure, *i.e.* oral dose, was estimated by reverse dosimetry. The result is compared to the acute oral dose causing 20% decrease in RBC AChE activity, assuming an accepted limit of 20% AChE inhibition (EPA, 2001).

Conazoles

In vivo tebuconazole

A provisional PBPK model for tebuconazole in rabbits was developed in the ANNEX on "A PBPK modelling approach for tebuconazole kinetics in male Japanese white rabbit and in humans". The human model was extrapolated from the rabbit model and **is not verified** due to lack of human data.

In vivo data (tebuconazole, hydroxy- and carboxy-tebuconazole in urine) from field workers exposed to tebuconazoles through spraying were obtained from WP4 (Moretto et al,unpublished results from ACROPOLIS project).

In vivo-in vitro extrapolation tebuconazole

In vitro tebuconazole dose-response data on rat embryo morphologically detected malformation were also obtained from WP4 (Menegola *et al.*, submitted). Like for the *in vitro* CPF data, these data were modelled with PROAST. Neonates in the Dutch population appear to suffer from morphologically detectable malformations (skin, skeleton, muscle) in a range of 0.8 to 1.1% during the years 1997 through 2008 with a significantly ($p < 0.001$) decreasing trend (Mohango *et al.* (2010)). The trend-estimated prevalence in 2012 would be about 0.75%. These malformations are due to unknown causes. If we accept that only exposure to tebuconazole may be the origin, reverse dosimetry

can be applied to the $BMD_{0.0075}$. If, however, we accept that tebuconazole is the cause of only a fraction of 1% of these malformations, reverse dosimetry is applied to the $BMD_{0.000075}$. No uncertainties in BMD are considered.

Results

Organophosphates

In vivo CPF, DZN and total of OPs

As RBC AChE inhibition is an important biomarker of exposure to OPs (Timchalk *et al.* 2002; EPA, 2001) we shall present RBC AChE inhibition/activity results in the sequel. Hinderliter *et al*. (2011) also present their results for RBC AChE. Note that, in contrast to nervous system toxicology, RBC AChE inhibition itself is inconsequential, it simply serves as biomarker.

In **Figure 2** RBC AChE activity is shown after a single bolus oral intake of 500 µg/kg body weight of CPF or DZN and during a (fictive) continuous dosing regimen of 50 µg/kg body weight/day of CPF or DZN. The same CPF bolus exposure was applied to human volunteers in Nolan *et al.* (1984). No signs or symptoms of toxicity were observed in any of the (6) volunteers at this dose level (*ibid*.). Notice that the inhibition level of 8% for CPF is well below the assumed limit of 20% AChE inhibition. The figure shows a difference in potency of CPF and DZN for RBC AChE inhibition. The greater potency for RBC AChE inhibition of CPF is similar to the greater potency of CPF in rats (Timchalk and Poet, 2008). Steady state activity is reached only after about a year. Studies in rats are based on doses of 1000 µg/kg body weight or higher. In humans steady state is reached in about three months or sooner at these levels. In rats this would be still much earlier.

Figure 3 shows the modelled (?) CPF dose – RBC AChE inhibition response in humans. Simulations were performed for CPF continuous dose and acute dose administration. Continuous dose was simulated for 1 year, allowing for reaching steady state at the lowest doses. Dose – response is linear up to about 100 µg CPF /kg body weight/ day for the continuous applied dose and to about 1000 µg CPF/kg body weight for the acute oral dose. Similar results hold for DZN. The figure (left panels) shows typical sigmoid log dose – response curves. Moreover, the right panels show that at low doses, *i.e.* doses below about 1000 µg CPF/kg body weight for acute oral dosing and below about 100 µg CPF/kg body weight/day for continuous dosing, the slope is almost one. Thus the dose response relation is about linear for small doses. Such a relation is derived in the Appendix.

The Dutch VCP3 sub-population anthropometry is shown in **Figure 4**. Body weight and body height of the population subjects are plotted versus their age in dependence of the subject's sex.

The estimated non-parametric cumulative intake distribution of CPF, DZN and total of OPs (children only) is shown in **Figure 5**. This concerns intake **without accounting for cook-**

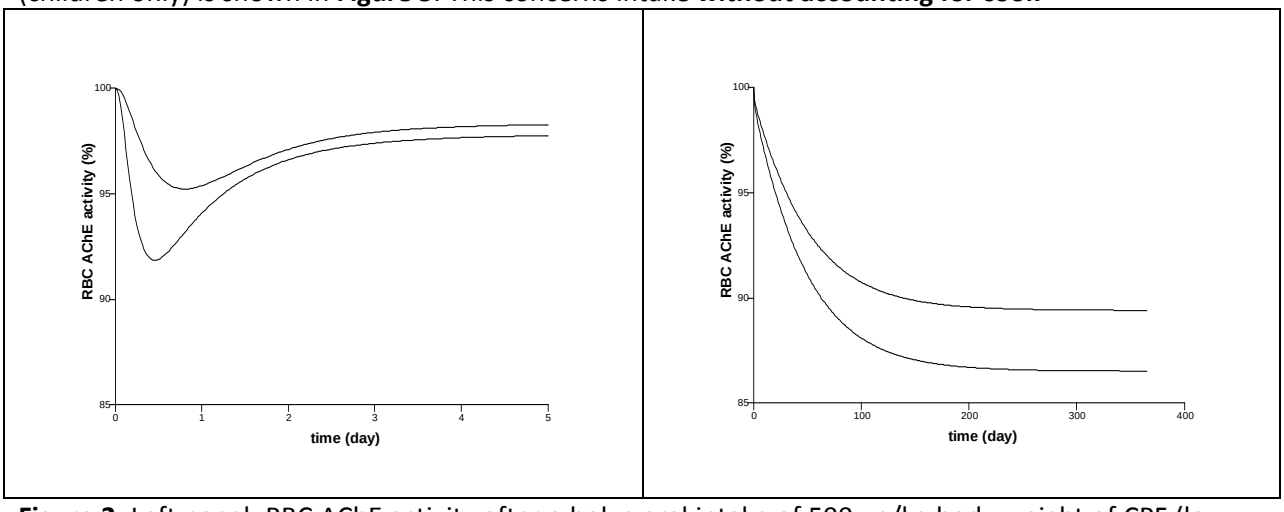

Figure 2. Left panel: RBC AChE activity after a bolus oral intake of 500 µg/kg body weight of CPF (lower line) and DZN (upper line). Right panel: RBC AChE activity during continuous oral intake of 50 µg/kg body weight of CPF (lower line) and DZN (upper line). Standard female.

ing food stuffs or peeling. As such, these distributions reflect **worst case**. All distributions start with a very small non-zero intake value. In the computer code the cumulative distribution tables are extended with the point zero probability on zero dietary exposure. Note that the cumulative dietary intake of CPF exceeds that of DZN and that the cumulative dietary intake per kg body weight for children from 1 to 6 years of age exceeds that of subjects older than 6 years.

For children below 7 years of age Monte Carlo simulations for intake of CPF, DZN and the total of OPs were performed. This includes variation of the subjects physiology based on their anthropometry, variation of the subjects biotransformation characteristics expressed in their maximum metabolism rates and variation in dietary intake. **Figure 6** shows the case for CPF. The left upper panel shows RBC AChE activity during continuous dosing of a standard 5 year old child. After a year steady state inhibition of about 0.15% is reached, therefore the MC simulations per subject are over a range of 1 year. The right upper panel shows the daily minimum activity over the population of 530 children: each day may be represented by a different child that has accidentally the minimum RBC AChE activity at that day. The time course of minimum AChE activity is jagged, but the corresponding maximum inhibition never exceeds 0.5%. The left lower panel shows for each subject its maximum RBC AChE inhibition versus its maximum dose. Note however that the day of maximum inhibition needs not coincide with the day of maximum inhibition, as the preceding inhibition history contributes to the current one. The left lower panel shows the population maximum dose distribution.

Figure 7 shows the results for DZN. A reference continuous dose of 1 µg DZN/kg body weight was used for comparison. Note that in this case RBC AChE inhibition is still smaller than for CPF. This mainly due to the fact that dietary intake of DZN is smaller than dietary intake of CPF (Figure 4 and left lower panel of Figure 5 compared to left lower panel in this figure).

For the total dietary intake of OPs, relative potency factors were used to scale to CPF. Bosgra *et al*. (2009), based on EPA (2001), present a list of estimated relative potency factors with respect to methamidophos of OPs found in food samples from the Dutch market. Boon *et al*. (2009) contains information on the relative contribution of OPs to the total. Based on this information, the % CPF equivalent of each OP the total of dietary OPs can be calculated.

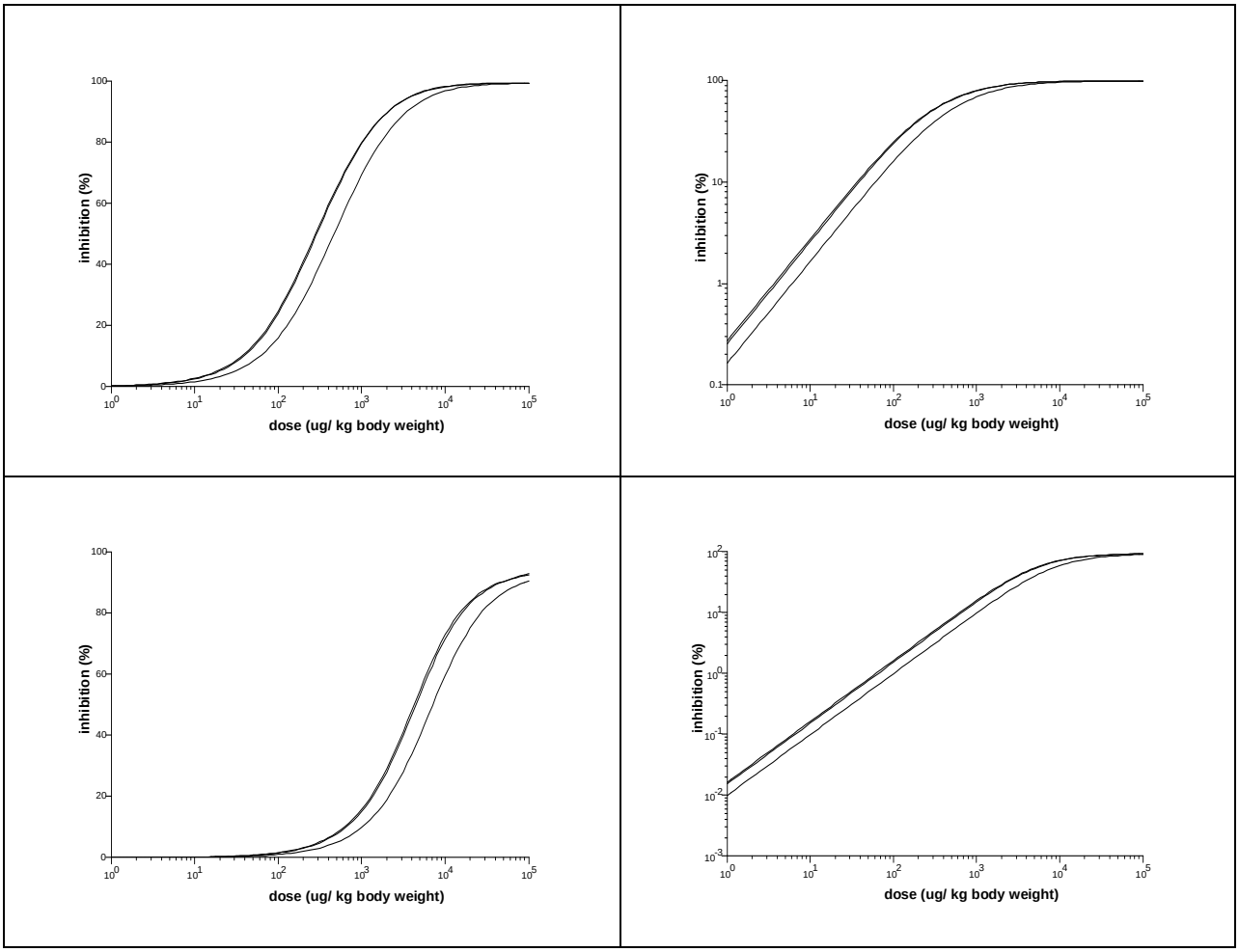

Figure 3. RBC AChE inhibition response versus logarithm of CPF dose for the *physB*-standard female (left lines), *physB*-standard male (lines in middle) and *physB*-standard child five years of age. Upper panels: CPF continuous dose. Simulation time is 1 year to reach steady state for the lowest doses. Lower panels: CPF acute oral. Left panels: response on linear scale showing typical sigmoid log(dose) – response curves. Right panels: response on log scale. The initial slope is 1, implying linear dose – response relations for continuous doses below about 100 µg CPF/kg body weight/ day and for acute oral doses below about 1000 µg CPF/kg body weight.

Moreover, from www.inchem.org data on acceptable daily intakes of these OPs is available. See **Table 1**. In this table, a number of OPs not specified in Boon *et al*. (2009) is assumed **worst case** to consist of the most potent OP monocrotophos in the list of Bosgra *et al*. (2009).

If scaling is performed with respect to CPF, then a dose of 1 µg of total OPs/kg body weight would be equivalent to a dose of about 7.5 µg of CPF/kg body weight and simulated dietary intake has been scaled accordingly **Figure 8** shows the results for the total intake of OPs. A continuous reference dose of 60 µg CPF/kg body weight was taken, leading to steady state RBC AChE inhibition of about 10%. In this case, the dietary exposure leads to a maximum peak of 30% AChE inhibition in one subject of 530 on one day. Note, however, that neither peeling nor cooking of food stuffs is assumed and that the contribution of monocrotophos represents the worst case: if instead DZN would be taken to represent the unspecified OPs, the total OP equivalent to CPF would be about 3.3 instead of 7.5 µg CPF/kg body weight.

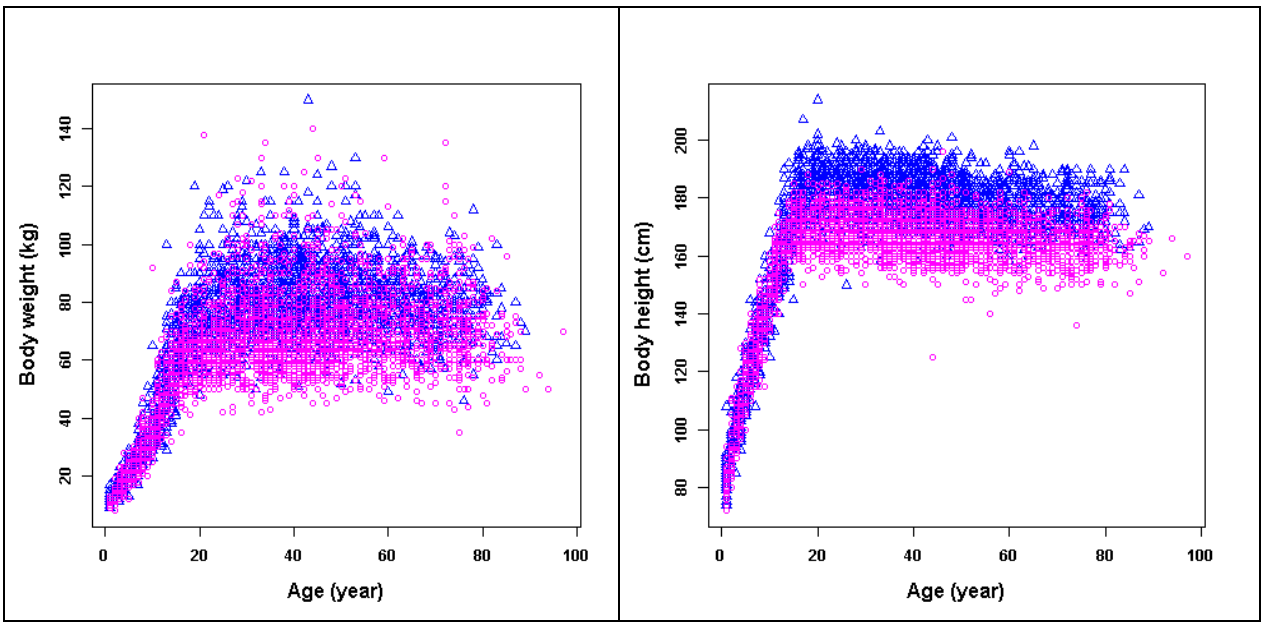

Figure 4. Characteristics of the Dutch VCP3-sub-population. Left panel body weights, right panel body heights for males (blue triangles) and females (pink circles). The VCP3 population is assumed to be exemplary for the total population.

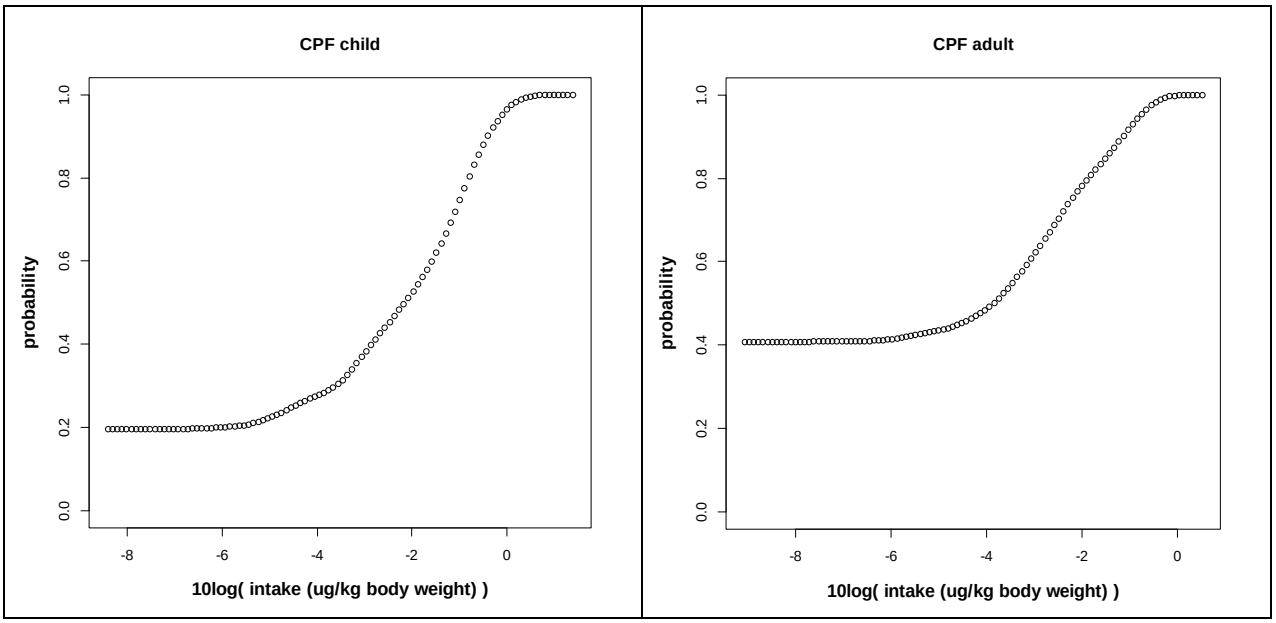

Figure 5. Non-parametric cumulative dietary intake distributions for children below 7 years of age (left panels), subjects from age 7 onwards (right panels; "adults" for short) for CPF (upper panels) and DZN (middle panels) and total of OPs (for children below 7 years only). **continued below…**

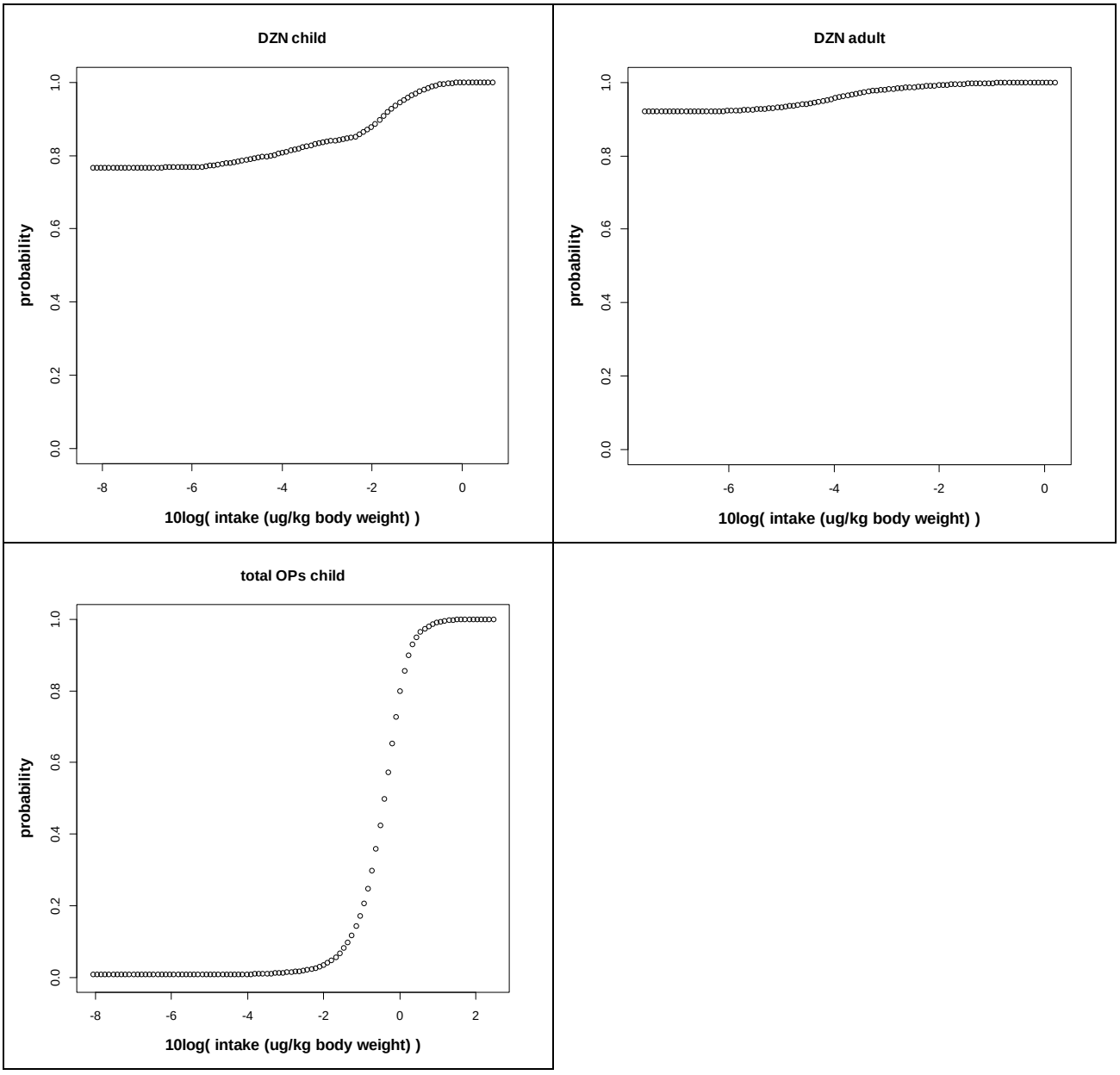

… continued Figure 5.

Table 1. Relative potency factors, % of contribution to total dietary OP exposure and acceptable daily intake (ADI) of OPs found in food samples from the Dutch market.

substance	RPF	% contribution	% CPF equivalent	EU-ADI µg/kg
azinphos-methyl	0.35	6	4.4	5
chlorpyrifos	0.065	4	0.5	10
dichlorvos	0.036	27	2.0	4
dimethoate	0.13	4	1.1	2
fenthion	0.33	14	9.6	1
methidation	0.16	6	2.0	5
rest = **monocrotophos**	5.4	5	56.0	0.6
omethoate	1.5	7	21.8	0.5
pirimiphos-methyl	0.047	27	2.6	10

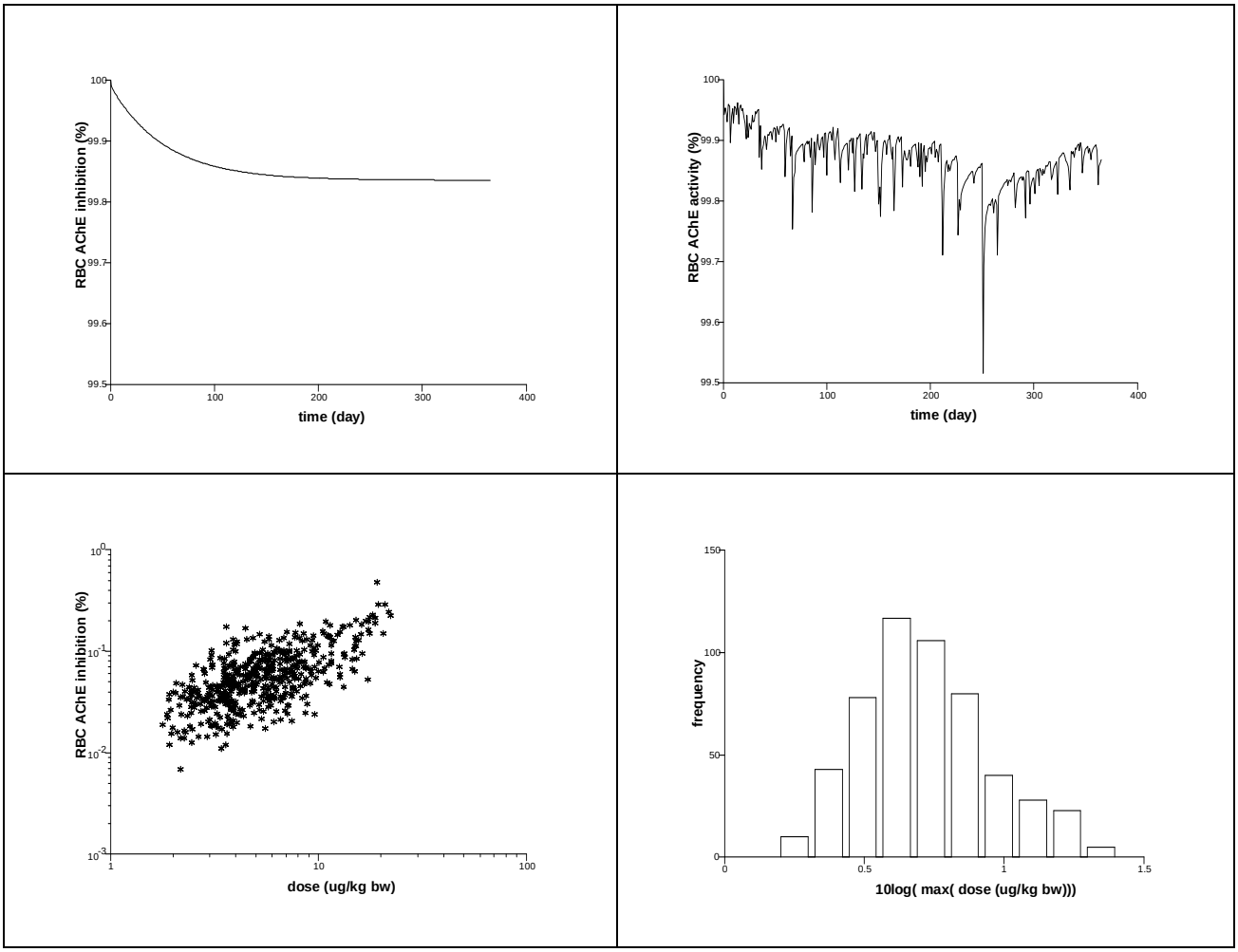

Figure 6. RBC AChE activities and inhibition due to dietary intake of CPF for subjects below 7 years of age. Left upper panel: continuous daily dose of 1 µg CPF/kg body weight/ day for reference. Steady state is reached within a year. Right upper panel: dietary intake randomly drawn from the cumulative distribution in figure 3, right upper panel. Note that the "plateau level" is similar to the steady state level for the fictive continuous daily dose. Left lower panel, maximum RBC AChE inhibition versus maximum dietary dose over a year for each subject. Right lower panel: distribution of maximum dose per subject.

If the acceptable daily amounts for the OPs in Table 1 are summed accordingly to their relative potency with respect to their CPF equivalent, about 50% of the population of children younger than 7 years of age exceeds the AChE limit of 20% inhibition. See **Figure 9** left panel. The children population RBC AChE inhibition mean is 18% (s.d. 8.3%), the median is 17.1% and the geometrical mean is 16.7 %. For subjects above 6 years of age 87% exceeds the limit of 20%. The older than 7 year population RBC AChE inhibition mean is 33.1% (s.d. 11.8%), the median is 32.2% and the geometrical mean is 30.9 %. However, one may question the relevance of such an exposure scenario: a substantial part of the population would show cholinergic symptoms. Moreover, ADIs are derived under the assumption that never anybody would be exposed to all OPs at one day.

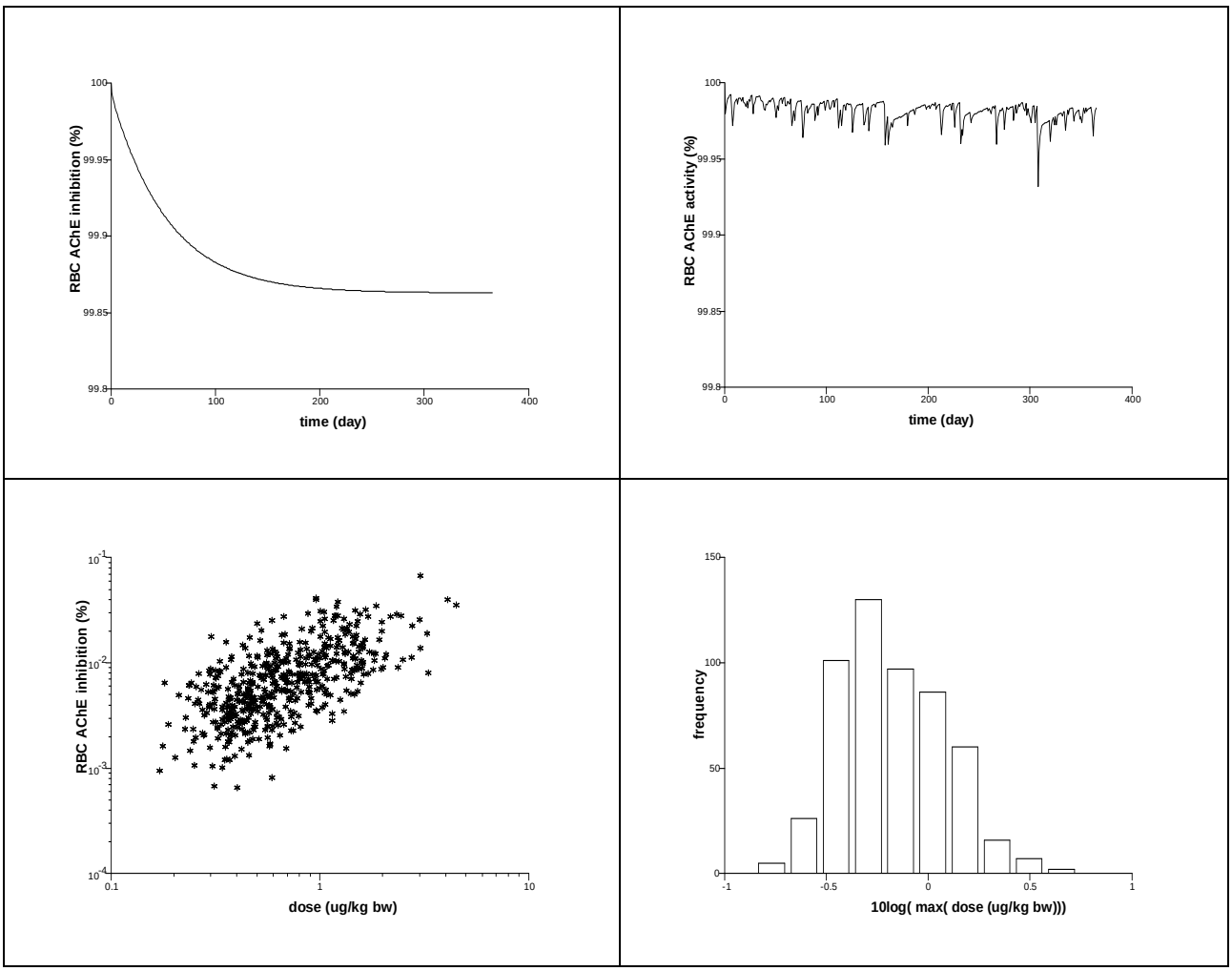

Figure 7. RBC AChE activities and inhibition due to dietary intake of DZN for subjects below 7 years of age. Left upper panel: continuous daily dose of 1 µg DZN/kg body weight/ day for reference. Steady state is reached within a year. Right upper panel: dietary intake randomly drawn from the cumulative distribution in figure 3, right upper panel. Note that the "plateau level" is similar to the steady state level for the fictive continuous daily dose. Left lower panel, maximum RBC AChE inhibition versus maximum dietary dose over a year for each subject. Right lower panel: distribution of maximum dose per subject.

In **Figure 10** results are shown for CPF only for a sub-population of the VCP3 population with subjects older than 6 years of age. For this subpopulation no data on dietary intake of total OPs is available, yet. A reference continuous dose of 1 µg CPF/kg body weight was applied for the standard male and female. Although the RBC AChE inhibition for the standard male and female is greater than for the standard child (Figure 3 and 9 and comparison of left upper panels Figure 6 and 10), the inhibition due to dietary intake is smaller because of the smaller dietary intake of CPF of subjects older than 6 years of age (Figure 5 and comparison of right lower panels in Figure 6 and 10).

It is argued that for instance the sequential intake of carbamates and OPs can be consequential for the resulting AChE inhibition (Bosgra *et al.* (2011) and references therein). Carbamylated AChE does not age and possesses a substantial higher reactivation rate than phosphorylated AChE does (*ibid.*). A combined pseudo-carbamate plus OP dietary exposure was simulated. The pseudo-carbamate was simulated by changing the aging and reactivation parameter values for DZN in the combined CPF-DZN code. DZN-inhibited AChE aging rates were fixed to zero, just like it would be for carbamylated AChE, and DZN-inhibited AChE reactivation rates were taken to be a tenfold of their

corresponding values. **Figure 11**, left panel, shows the result after ingestion of a bolus dose of 100 µg CPF/kg body weight and of 100 µg pseudo carbamate/kg body weight. Note that, due to the faster reactivation, inhibition due to the pseudo-carbamate exposure (line B) is much smaller. Also, due to fast reactivation and no aging, AChE activity levels off to 100% much sooner.

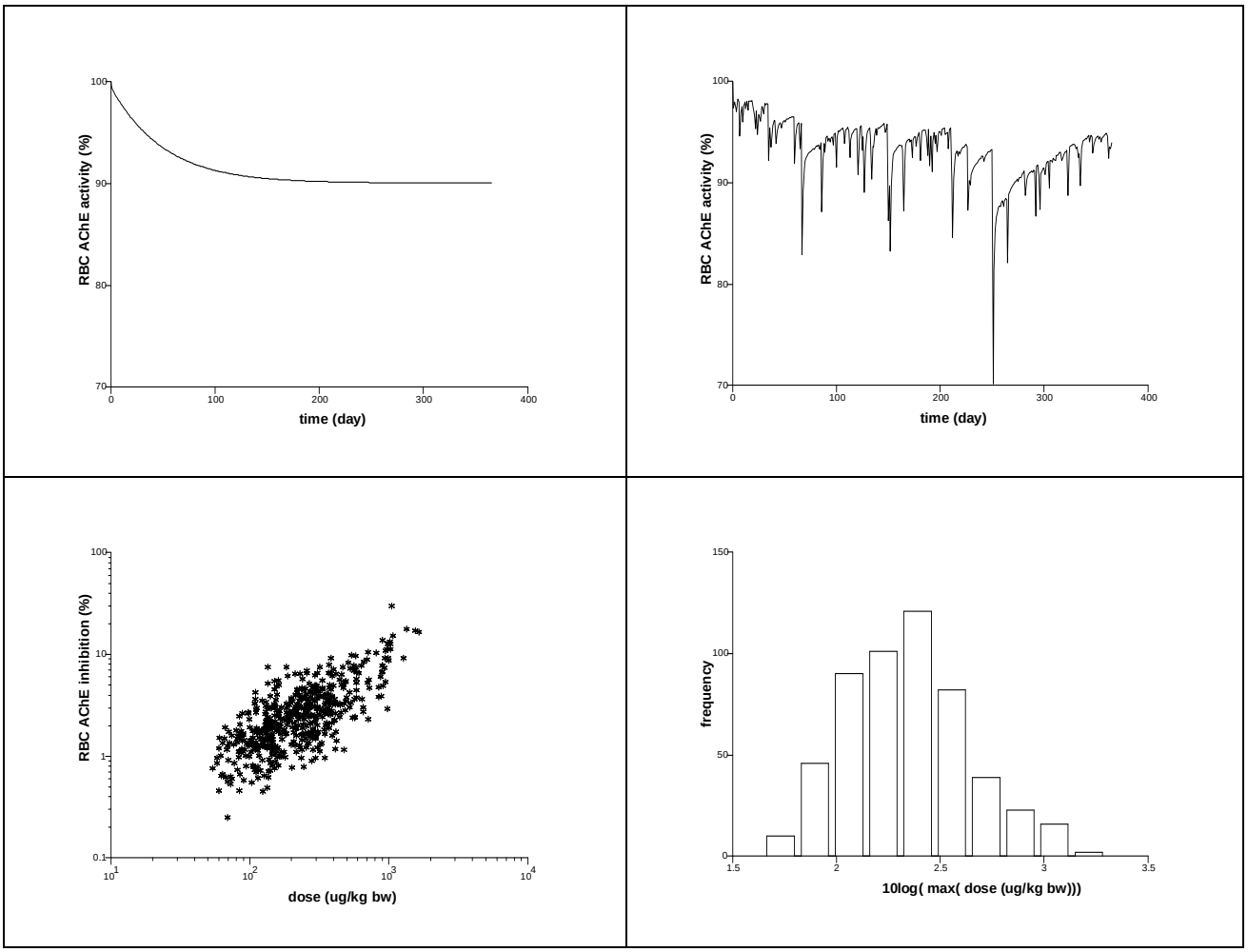

Figure 8. RBC AChE activities and inhibition due to dietary intake of the total of OPs for subjects below 7 years of age. Left upper panel: continuous daily dose of 60 µg CPF/kg body weight/ day for reference. Steady state is reached within a year. Right upper panel: dietary intake randomly drawn from the cumulative distribution in figure 3, right lower panel. Note that the "plateau level" is similar to the steady state level for the fictive continuous daily dose. Left lower panel, maximum RBC AChE inhibition versus maximum dietary dose over a year for each subject. Right lower panel: distribution of maximum dose per subject.

For dietary dosing simulation half of a dietary dose of 7.5 µg CPF equivalent/kg body weight was assigned to CPF, the other half to the pseudo-carbamate. The combined dietary exposure model was applied to subjects younger than 7 years of age. The corresponding cumulative dietary intake for the total of OPs for young children was applied. A random generator seed was used to insure the same stochastics for each of three scenario's: simultaneous intake of OPs and carbamates, intake of OPs 6 hours after intake of carbamates and *vice versa*. Figure 11 right panel shows the resulting population minimum RBC AChE activity during a year.

For the case of simulating aggregated oral and dermal exposure, a dermal exposure compartment was implemented. A subject is considered that is exposed at t = 0 to an acute oral bolus dose of 100µg CPF/kg body weight and additionally to a dermal dose of 5000 µg CPF/kg body weight on a surface area of 5% of total skin surface at t = 0, 4, 8, 12, 16, 20 and 24 hours after oral exposure. The dermal dose is wiped off at 10 hours after onset of dermal exposure. **Figure 12** shows the resulting RBC AChE activities.

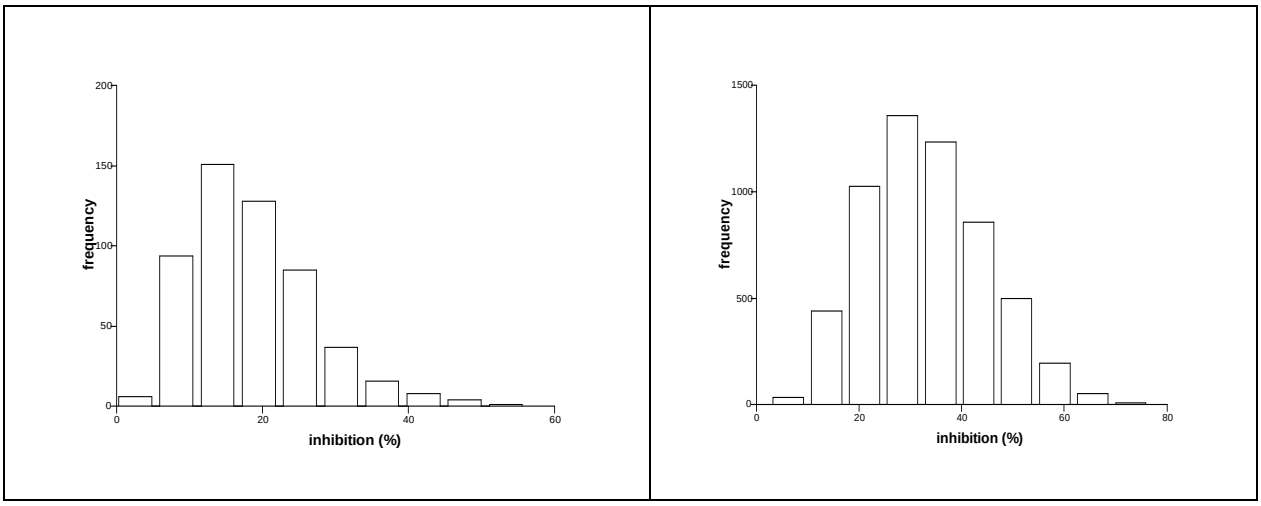

Figure 9. Population distribution of RBC AChE inhibition (%) when subjects are exposed to a daily dietary dose of 130 µg CPF/kg body weight, representing the relative potency weighted sum of OP ADIs in Table 1. Left panel: children below 7 years of age. Right panel: subjects above 6 years of age.

In vitro-in vivo extrapolation CPF

Data on the *in vitro* CPF-oxon and DZN-oxon dose (BMD; µM) – cell toxicity effect (BMR; CFDA 5% level of fluorescence decrease critical effect size) (Heusinkveld, 2012; reference!) was determined to be 5.8 µM with a 90% uncertainty interval range of 5.2 to 6.5 µM for CPF-oxon and 1.4 µM with a 90% uncertainty interval of 0.15 to 8.3 µM for DZN-oxon. See **Figure 13**.

At acute or continuous oral doses as high as 1 g CPF or DZN/kg body weight CPF-oxon levels in blood do not exceed 0.006 or 0.00065 µM, respectively. So, cell-toxicity of CPF-oxon and DZN-oxon is a far less sensitive effect as plasma AChE inhibition of CPF and DZN, respectively.

Conazoles

In vitro-in vivo extrapolation tebuconazole

Data on the *in vitro* tebuconazole dose (BMD; µM) – rat embryo morphological malformation effect (BMR; fraction of control) (Menegola et al, 2012; unpublished results from ACROPOLIS project) was modelled with the Weibull model (**Figure 14**). This model can be inverted easily to obtain a BMD effect – dose model (reverse dosimetry). See **Appendix**.

For a fractional effect of 0.0075 (0.75%) that equals the expected level of skeletal, muscular and skin malformations of Dutch newborn in 2012, the corresponding BMD = 13.7 µM with 90% confidence interval ranging from 4.2 to 26.4 µM. If we accept that tebuconazole may contribute to only 1% of these malformations, the fractional effect is 0.000075 and the corresponding BMD = 1.6 µM with a 90% confidence interval ranging from 0.17 to 5 µM.

The provisional human PBPK model for tebuconazole was adapted to a model for the standard woman of 60 kg. Reverse dosimetry was applied for a daily intake such that the

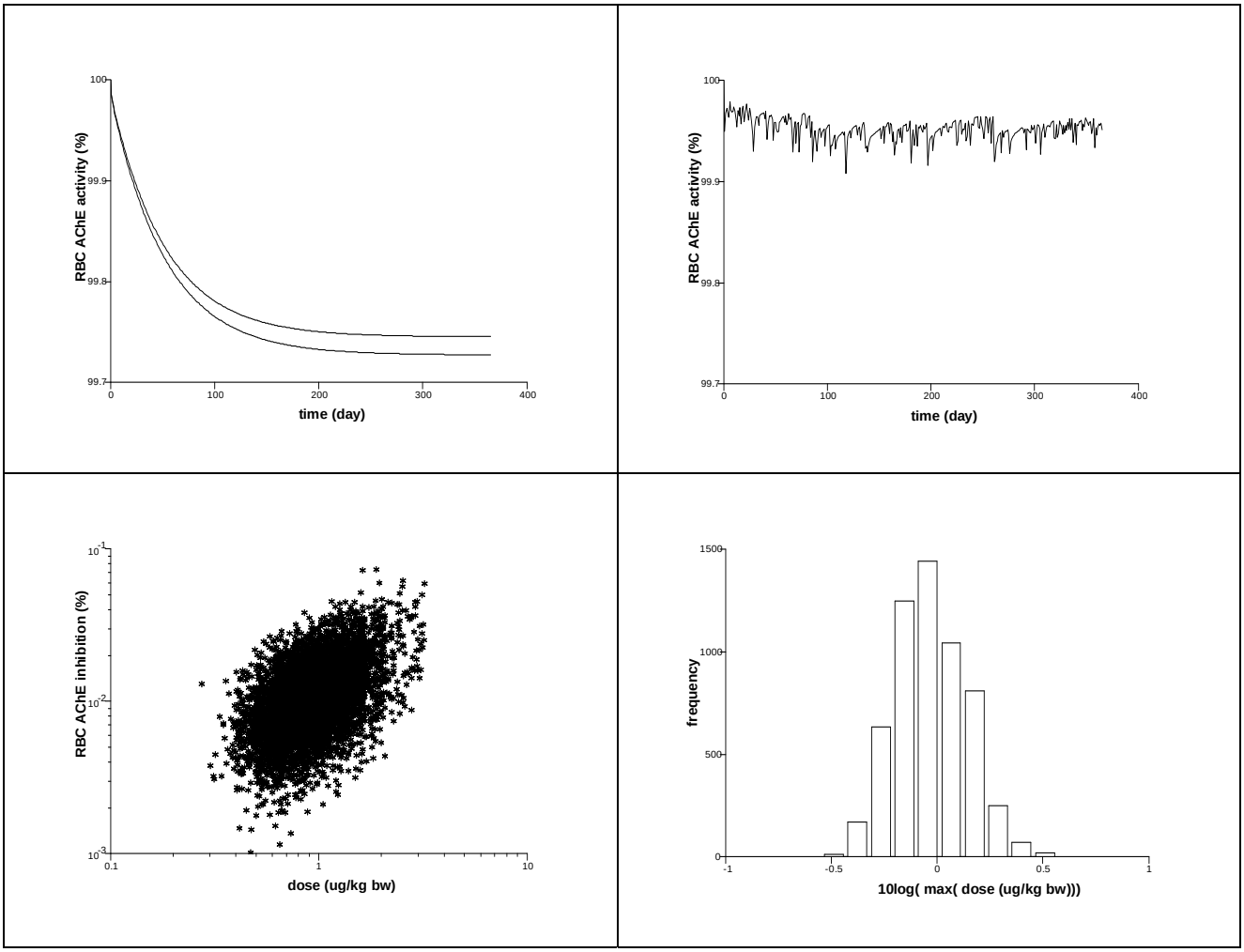

Figure 10. RBC AChE activities and inhibition due to dietary intake of CPF for subjects above 6 years of age. Left upper panel: fictive continuous daily dose of 1 µg CPF/kg body weight/ day (upper line: standard male; lower line: standard female) for reference. Steady state is reached within a year. Right upper panel: dietary intake randomly drawn from the cumulative distribution in figure 3, right upper panel. Note that the "plateau level" is higher to the steady state level for the fictive continuous daily dose. Left lower panel, maximum RBC AChE inhibition versus maximum dietary dose over a year for each subject. Right lower panel: distribution maximum dose per subject.

maximum plasma concentrations (µM) did not exceed the BMDs or confidence limits. Here, it is assumed that *in vivo* plasma concentration represents foetus concentration. Thus, the daily oral BMD for a BMR of 0.0075 was calculated to be 14.5 mg tebuconazole /kg body weight/ day with a 90% confidence limit of 4.5 to 28.5 mg tebuconazole/kg body weight/ day. For BMR = 0.000075, the corresponding BMD = 1.7 mg tebuconazole/kg body weight/ day with a confidence limit of 0.18 to 5.4 mg tebuconazole/kg body weight/ day.

In vivo tebuconazole

Field experiments were carried out by (Moretto, 2012; reference!). Field workers were monitored during spraying tebuconazole and data on exposure of the skin of hands and limbs and of underwear were obtained. The latter category was included to total tebuconazole skin exposure. Inhalatory exposure was neglected as this route typically contributes far less than 10% to skin exposure.

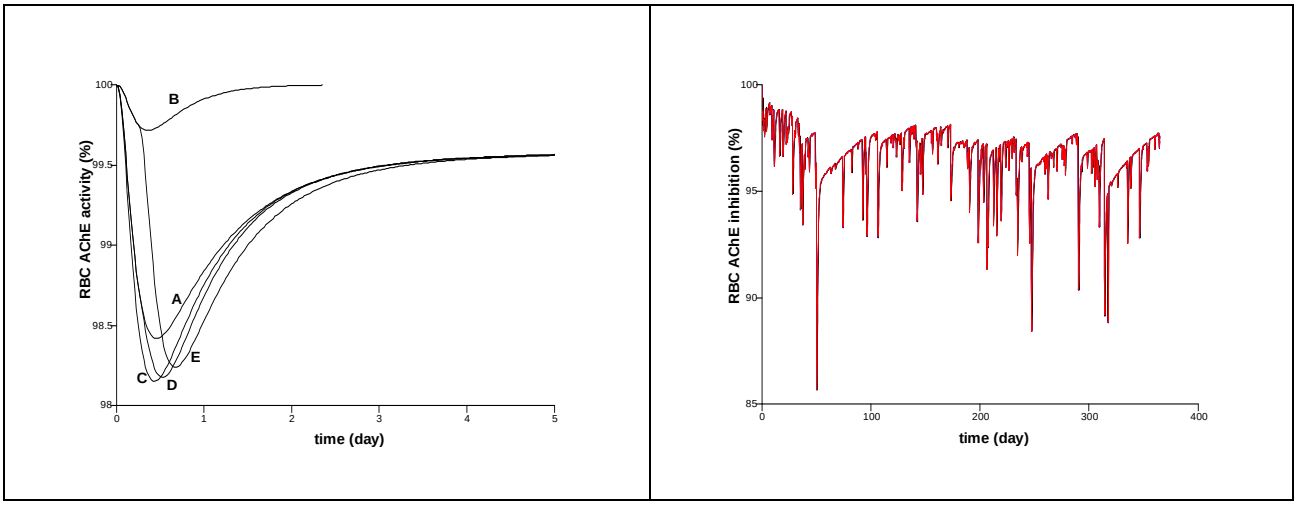

Figure 11. Left panel: RBC AChE activity after a bolus dose. A: 100 µg CPF only /kg body weight; B: 100 µg pseudo carbamate only/kg body weight; C: simultaneous combined dosing of 100 µg CPF and 100 µg pseudo carbamate/kg body weight; D: pseudo carbamate dosing after 6 hours; E: CPF dosing after 6 hours. Right panel: dietary dosing of CPF and pseudo carbamate. Blue line: simultaneous daily dosing; black line: dosing of CPF 6 hours afterwards of pseudo carbamate; red line: dosing of pseudo carbamate 6 hours afterwards of CPF. The blue and the red lines overlap, only the black line is slightly visible. Note that AChE inhibition is almost halved with respect to Figure 7 because the carbamates do hardly contribute.

Besides dermal exposure to tebuconazole urinary data were collected on the excretion of the parent compound and its two main metabolites hydroxy- and carboxy-tebuconazole. Measured concentrations and corresponding urine volumes were combined to obtain a lower limit of total renal tebuconazole excretion and total excretion was compared to the assumed with skin deposition.

It is not feasible to model the data of this pilot experiment. First, it is not clear whether the field workers complied with the spraying regimen. *E.g.*, in half of the cases, tebuconazole and metabolites were already found in samples collected at time points before the arranged start of spraying, indicating a recent history of spraying. All workers washed hands and changed underwear at the end of spraying, but it is not clear when they took a shower. Moreover, it is not known to which extend the contamination of underwear contributes to dermal exposure of limbs. This makes that actual dermal exposure may be less than the amount deposited. **Figure 15** shows the relation for total excretion sampled (black symbols) and for excretion sampled after the agreed time of spraying start (yellow symbols). There seems not to be a clear relation to the amount deposited on hands, limbs and in underwear and the excretion of parent compound and two main metabolites. However, for one case there seems to exist an association between increased urinary excretion and increased skin deposition. Moreover, the ratio excreted deposited is around 0.1. This would indicate a dermal absorption fraction around 10%, which is consistent with the 13% observed in monkeys (EFSA, 2008).

Nevertheless, the amount deposited, which can be considered as a not unrealistic exposure assessment, can be compared to the BMR derived above. Amount deposited was expressed in terms of mg tebuconazole/kg body weight. A geometric mean of 0.011 mg/kg was obtained with a 90% uncertainty range of 0.002 to 0.06. If the upper limit of 0.06 mg/kg is compared to the lower confidence limit of 0.18 mg tebuconazole/kg body weight (which is a **daily** exposure limit) for a BMR of 0.000075 (as a worst case), it may be concluded that there is no unacceptable risk for pregnant women and their foetuses. Note that the BMR is derived for oral exposure. Generally, oral uptake rate is much faster than dermal uptake rate. In this comparison with dermal exposure no account was made for difference in uptake rate, making it **worst case**.

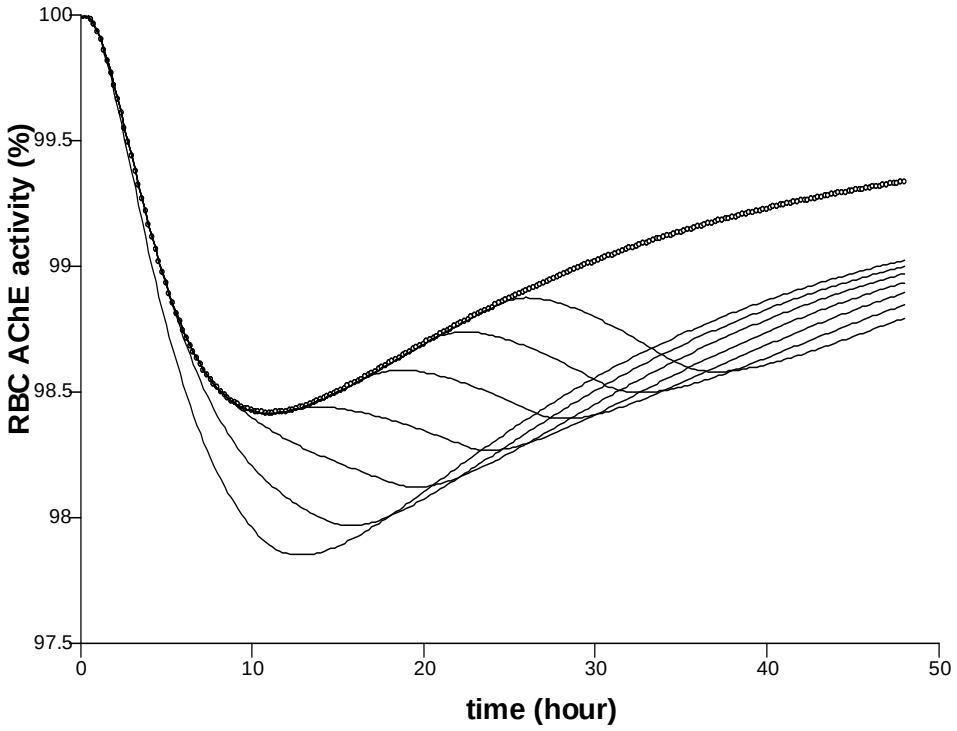

Figure 12. RBC AChE activity in a person that is exposed to an acute oral dose of 100 µg CPF/kg body weight and an additional dermal dose of 5000 µg CPF/kg body weight on 5% of total skin surface at t = 0, 4, 8, 12, 16, 20 and 24 hours after oral exposure. CPF is wiped off skin 10 hours after onset of dermal exposure. The thick upper line shows AChE activity after the acute oral dose only.

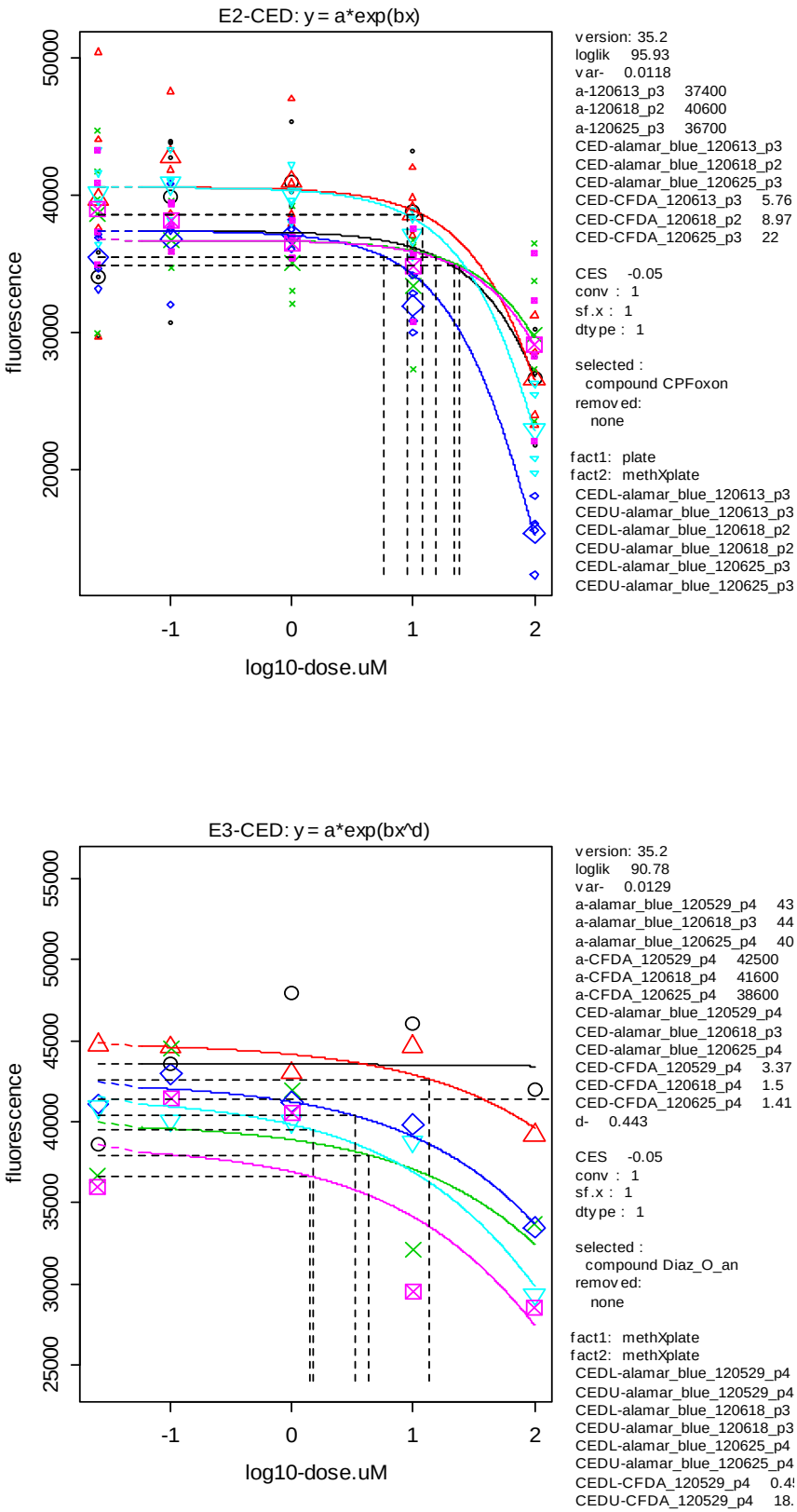

Figure 13. *In vivo* dose – response (CFDA, blue, light blue and pink lines; alamar-blue, red, black and green lines) relations for CPF-oxon (upper panel) and DZN-oxon (lower panel). CFDA is more sensitive.

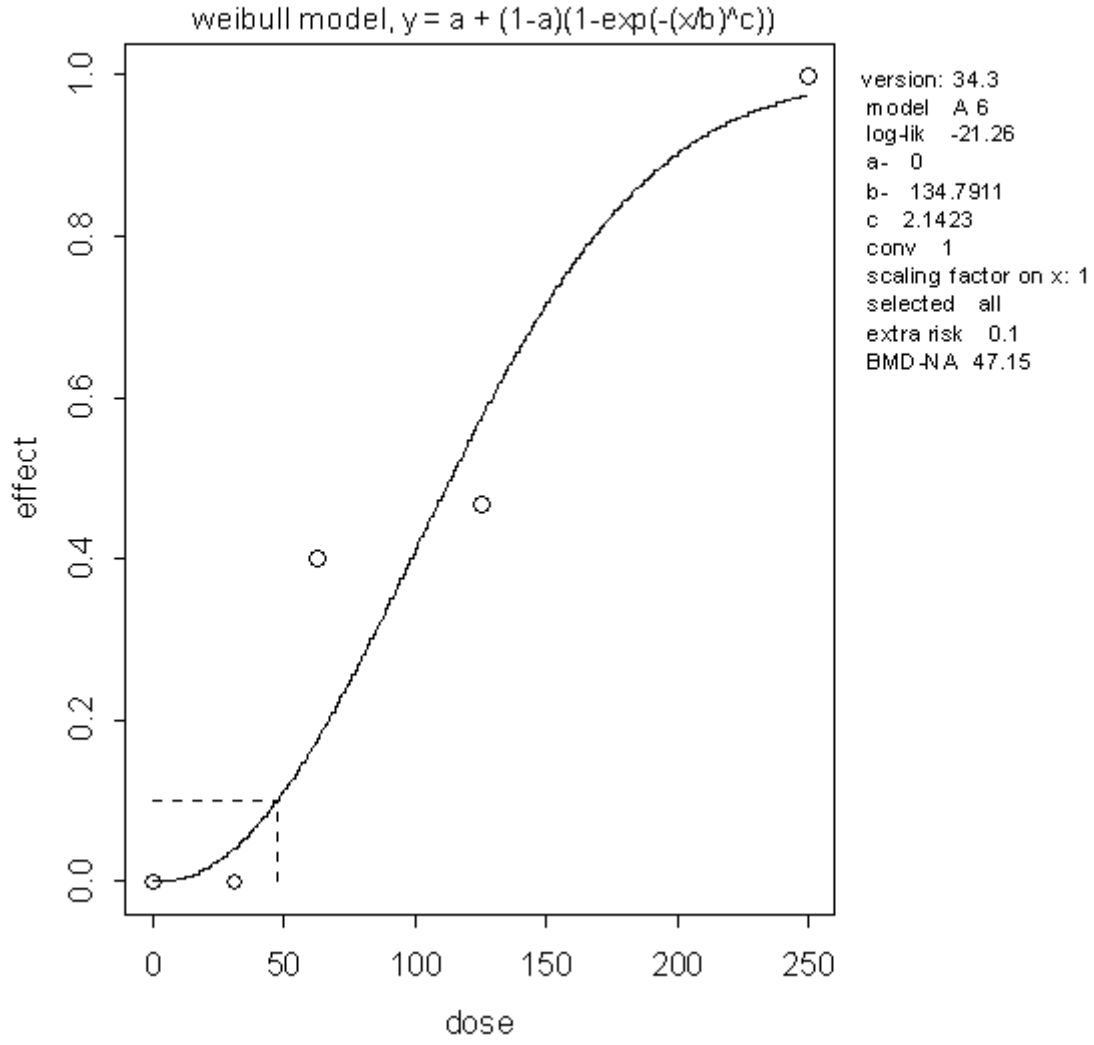

Figure 14. Symbols: tebuconazole dose (µM) rat embryo morphological malformations effect (fraction of control) data from Menegola et al., (2012, unpublished results from ACROPOLIS project). Line: Weibull BMD model.

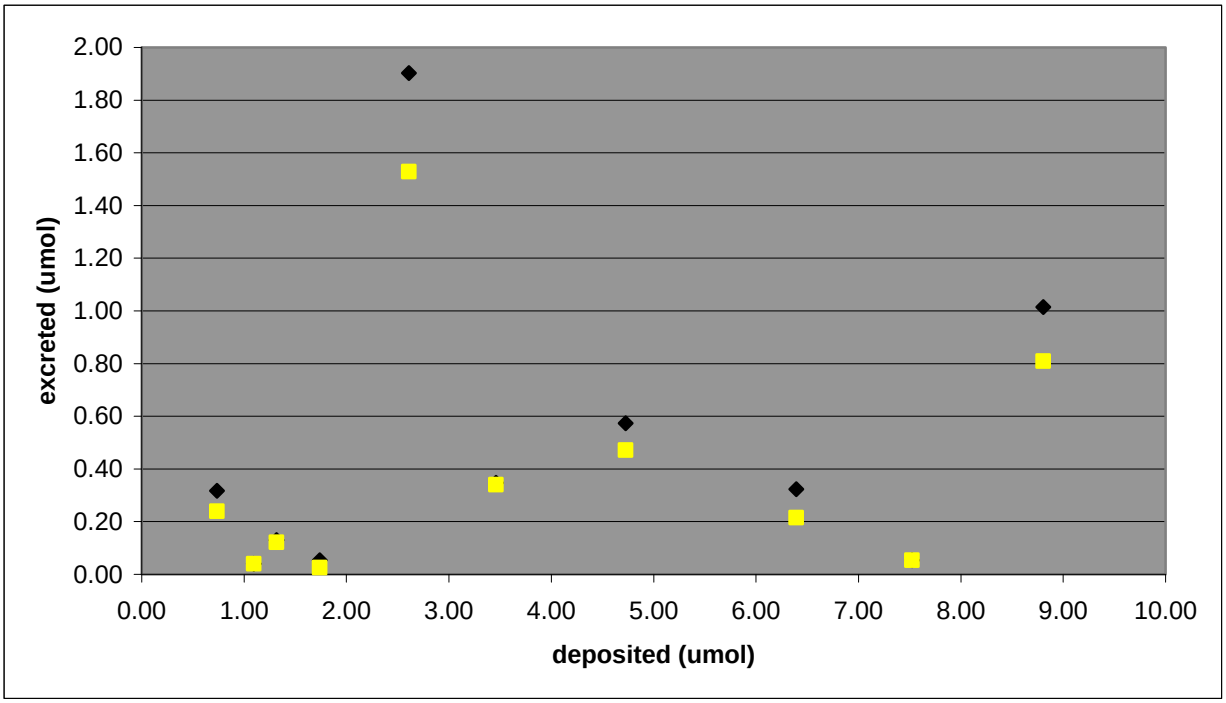

Figure 15. Amount of tebuconazole deposited on skin, limbs and underwear and total excretion of tebuconazole, hydroxy- and carboxy-tebuconazole. Black symbols including all urine samples, yellow symbols excluding samples taken before agreed time of spraying.

Discussion

General

One of the targets of the EU Acropolis project is to study the benefit of bio-kinetic modelling in order to link external dose (exposure) to internal dose (plasma concentration) and related effects. This link might improve the risk assessment of substances.

Classical risk assessment relies heavily on *in vivo* experiments with laboratory animals (mice, rats, dogs, monkeys, guinea pigs, etc.). From these experiments, effect doses are derived and typically assessment factors are applied to extrapolate from animals to humans. Moreover, assessment factors are used to protect vulnerable and susceptible subgroups. However, applying multiple assessment factors might result in too conservative reference values. Considering exposure to different substances, exposure on several times a day or exposure via several routes, it is not clear whether one may "sum up" to estimate the effect level. In order to get some insight, in tricky matter, this study was proposed.

It is well known that the EU within their REACH program strives for the reduction of *in vivo* experiments and replacing them by *in vitro* experiments. However, this raises the question of how to extrapolate *in vitro* dose response relations to the *in vivo* situation. Since the kinetics of a substance in the experimental *in vitro* system is generally not known nor determined, the nominal dose at the start of the experiment is related to the observed effect. However, different experimental dose-effect relations may be based on different experimental time durations. Generally it is assumed that the substance concentration in medium is representative for the concentration in blood or plasma, but the bio-kinetics of the substance in blood/plasma may be quite different from the *in vitro* kinetics. Another relevant issue is whether the effects are C_{max} (maximum plasma concentration) or AUC (area under the concentration-time curve) dependent. These problems are far beyond the scope of this study and we have focussed on deriving by reverse dosimetry the *in vivo* from the *in vitro* BMD and

considering maximum *in vitro* concentration. This is likely to be correct for both teratogenic effects and AChE inhibition. Nevertheless, the results of extrapolation should be interpreted with caution.

As a modelling approach it was decided to apply PBPK(/PD) modelling. In PBPK models, physiological tissues and regional blood flows are considered. Blood to tissue transfer is based on the chemical potential of a substance with respect to blood or plasma as reference liquid. This is expressed as tissue to blood partition and partition coefficients can be obtained by *in vitro* experiments or from QSARs. From *in vitro* experiments liver metabolic pathways and metabolism rates can be obtained or absorption rates of substances across the gut wall. All this information can be integrated in the PBPK model. Additionally, these models allow for route-to-route extrapolation once the kinetics after systemic absorption is known. Moreover, the extrapolation of physiology of laboratory animals to humans is immediate and additional physiological characteristics such as liver metabolism rate can be estimated using allometric scaling. This also concerns the fact that species may differ in their CYP-systems.

In this study PBPK modelling was integrated in an approach to estimate a populations cumulative dietary dose – effect relation. This integration concerns a newly developed physiological model, *physB*, that generates human physiologic characteristics (tissue weights, tissue regional blood flows) based on anthropometry. From these characteristics the required PBPK model compartments and blood flows can be composed. Another ingredient in the integration is formed by the VCP3, VCP Child and VCP 2003 Dutch National Food Consumption enquiry. The first served a population of anthropometry data, the second cumulative dietary intake distributions for children younger than 7 years of age for CPF, DZN and the total of OPs and the third cumulative dietary intake distributions for young adults (19 – 30 years of age) for CPF and DZN. The latter was assumed exemplary for a population of subjects older than 6 years of age.

Secondly, PBPK modelling was applied to aggregated exposure of CPF due to exposure to an oral bolus dose and dermal exposure and to aggregated inhalatory and dermal exposure to tebuconazole. Moreover, in this study PBPK modelling was applied to *in vitro* data on cell viability for CPF and on rat foetus malformations for tebuconazole. BMD modelling with the module PROAST was performed and the *in vitro* BMD was extrapolated through reverse dosimetry to *in vivo* BMD.

<u>Organophosphates</u>

For organophosphates this study focus on AChE inhibition with RBC AChE inhibition as a biomarker. In Figure 2 it is shown that different OPs may possess different potency for AChE inhibition. From the modelling approach one can see that several mechanisms cause this difference. First of all, both CPF and DZN are metabolized to their oxon equivalent and concurrently detoxified to TCP and IMHP, respectively. So, the rates of both these processes determines the rate and extend of oxon formation. In the second step, the CPF- or DZN-oxon is bound to AChE (inhibition step), but also is concurrently detoxified to TCP or IMHP. So, the rates of both these processes then determine the rate and extend of AChE inhibition. Regeneration and aging rates are the same for both oxon-AChE complexes.

An important observation in Figure 3 is that the oral dose – AChE inhibition response relation is linear at low doses. This implies that, as long as dietary doses of different OPs are low, dietary exposure to them can modelled using relative potency factors and summing up the different contributions. Of course, there is an effect of “arrival” caused by being exposed during lunch and 6 hours later during dinner. If relevant knowledge is available about the differences in exposure during lunch and dinner, this may be used for a refined risk assessment. However, it is doubtful whether such information is available and one has to the conservative assumption that all OPs are ingested at one time.

In the cumulative dietary exposure simulations no peeling or cooking of food stuffs is assumed. This means that the **worst case** has been considered. The population AChE inhibition during one year of dietary exposure, sufficient to extrapolate to more years as steady plateau level is reached after one year, has been simulated for children younger than 7 years of age in Figure 6 – 8. The exposure to CPF or DZN only does not lead to exceeding the AChE inhibition limit of 20%. Moreover, as expected from the fact that both DZN has about half the potency of CPF and that dietary expo-

sure to DZN is smaller than to CPF, AChE inhibition is still smaller than for CPF dietary exposure. In Figure 7, the total OPs CPF-equivalent dose exceeds the CPF limit of about 100 µg/kg body weight for dose – response linearity. However, as long as the separate contributions of the OPs, expressed in their CPF equivalent, is smaller this not of a problem. From Table 1 it can be seen that omethoate and the remaining of OPs, considered as consisting of monocrotophos only, do not comply with this limit. Especially monocrotophos exceeds this limit. In our calculations monocrotophos, as representing the remaining OPs, contributed about 56% of the total equivalent dose of OPs. So, this is a second **worse case** assumption. Note that only in one of 530 subjects AChE inhibition of 30% exceeds the limit of 20% on one day.

If the EU ADIs for the different OPs in Table 1 are expressed in their CPF equivalents, it appears that all ADIs stay well below the CPF limit of about 100 µg/kg body weight where the response is linear with dose. When summing up these CPF dose equivalents a total dose equivalent of 130 µg CPF/kg body weight results which lies just beyond the limit. We assumed that dose addition is still a fair approximation of the sum of (CPF equivalent) ADIs found on Dutch food products. A dietary exposure to 130 µg CPF/kg body weight for each subject with no daily or inter-individual variability is considered. Under these extreme conditions, it appears that about 50% of the children younger than 7 years and about 87% of the subjects older than 6 years of age would exceed the 20% AChE inhibition limit. So, the sum of different OP ADIs does not comply with the limit of 20% RBC AChE inhibition. However, the question is whether ADIs were ever derived in this sense.

Figure 10 shows that for subjects older than 6 years of age, for which no cumulative dietary exposure distribution for the total of OPs is available, AChE inhibition due to dietary exposure is much smaller than for the young children. Although the dose – effect relation in Figure 3 shows a greater sensitivity for the older ones than for children, dietary exposure per kg of body weight appears much smaller for this group.

Carbamates also cause AChE inhibition, inhibited (carbamylated) AChE does not age and quickly reactivates, much quicker than phosphorylated AChE. In the combined CPF-DZN exposure model DZN was defined as a pseudo carbamate by fixing its aging rate to zero and by taking its regeneration rate to tenfold its nominal value. From Figure 11 it can bee seen that due to the much greater regeneration rate of AChE inhibited by the pseudo carbamate, the final inhibition level is much smaller than that of CPF. Moreover, recovery to the 100% activity level is much faster for the pseudo carbamylated than for the phosphorylated AChE. There are arguments that application of carbamates could be favourable in combination with OP exposure in that the resulting AChE inhibition would smaller. In Figure 11 an exposure like in Figure 8 is considered, however with half of the exposure caused by carbamates and the other half by OPs. Three scenarios are considered: simultaneous exposure, exposure of OPs 6 hours after exposure to pseudo carbamates and *vice versa*. No noticeable differences were found. Based on the left panel of Figure 11 noticeable difference were not expected either.

Aggregated exposure to CPF is simulated in Figure 12. The exposure concerns a single oral bolus intake of 100 µg CPF/kg body weight and dermal exposure starting simultaneously or after 4, 8, 12, 16 or 24 hours. Dermal uptake effectiveness is low. Nolan *et al.* (1984) report a fraction of dermal dose in the order of a few percent only to be taken up. This depends of course also on the time of wiping off, which was in the order of 10 to 20 hours. Due to the small fraction absorbed, even an applied dose of 5000 µg CPF/kg body weight has only a small AChE inhibition effect. Based on the guidance document EFSA (2010) it was estimated that a field worker spraying 8 ha of vineyard would be skin exposed to about 2600 µg CPF/kg body weight if mounted on a tractor and to about 5300 µg CPF/kg body weight if using a knapsack.

Finally, the PBPK model was applied in a reverse dosimetry approach to find CPF and DZN exposure levels that would lead to plasma CPF-oxon and DZN-oxon BMD levels found *in vitro* for cell toxicity. It appeared that, compared to AChE inhibition due to binding of the oxons to AChE, cell toxicity has a very weak sensitivity.

Conazoles

A provisional model for tebuconazole was developed. Experimental data regarding field workers show that the model should at least be extended with a renal elimination route besides metabolism for the parent compound. The data however do not allow for improving further the provisional model. The model was employed in a reverse dosimetry approach to derive the *in vivo* BMD from the *in vitro* BMD. *In vivo* derived BMD was compared to the dose, *i.e.*, the amount of tebuconazole deposited on skin and underwear considered as **worst case** exposure, sprayers are exposed to. The lower limit *in vivo* BMD of 0.18 mg/kg body weight appears to be about 5 times as large as the upper confidence limit of 0.035 mg/kg body weight (n = 10) of tebuconazole exposure to workers in this field experiment. Note that **worst case** was considered by taking the BMD lower limit and the exposure upper limit.

Conclusion

This study shows that PBPK and PBPK/PD modelling can be applied in cumulative and aggregated risk assessment. It allows reverse dosimetry calculations relating *in vitro* (or *ex vivo*) BMD data to human *in vivo* BMD and hence refinement of risk assessment. Modelling is a complex exercise and as such it can be used in those instances when the "standard" risk assessment, that includes a number of conservative assumptions fails to identify safe scenarios. In these cases, PBPK/PD modelling, by reducing the uncertainty of the evaluations, may prove useful in avoiding undue risk management options such as banning o severely limiting the use of certain (groups of) compounds.

Acknowledgements

Polly Boon and Gerda van Donkersgoed provided the data on estimated daily intake of OPs.

Jan Dirk te Biesebeek performed the exposure assessment of field workers to CPF.

Angelo Moretto and Harm Heusinkveld provided the *in vitro* data needed to derive BMDs through reverse dosimetry calculations.

Angelo Moretto not only made extensive comments to the first draft of this report but to both annexes as well.

This study has much profited from the continuous scientific work of Charles Timchalk and Torka Poet on the risk assessment for OPs in general and for CPF and DZN in particular. They also kindly provided the latest updates of their computer codes for CPF dietary risk assessment.

Literature

Bosgra, S., van der Voet, H., Boon, P.E. and W. Slob; An integrated probabilistic framework for cumulative risk assessment of common mechanism chemicals in food: An example with organophosphorus pesticides; *Regul. Toxicol. Pharmacol.* **54** (2009) 124 -133

Bosgra, S., van Eijkeren, J.C.H., van der Schans, M.J., Langenberg, J.P., and W. Slob; Toxicodynamic analysis of the inhibition of isolated human acetylcholinestase by combinations of methamidophos and methomyl *in vitro*; *Toxicol. Appl. Pharmacol.* **236** (2009) 1-8

Bosgra, S., van Eijkeren, J.C.H., Bos., P.,Zeilmaker, M.J., and W. Slob; An improved model to predict physiologically based model parameters and their inter-individual variability from anthropometry; *Crit. Rev. Toxicol.* (2012) accepted for publication

Van Dooren, M.M.H., Boeijen, I., van Klaveren, J.D., and G. van Donkersgoed; Conversie van consumeerbare voedingsmiddelen naar primaire agrarische producten. RIKILT Report 95.17, 1995, Wageningen, The Netyherlands. In Dutch

EFSA; Scientific Opinion on Preparation of a Guidance Document on Pesticide Exposure Assessment for Workers, Operators, Bystanders and Residents; *EFSA Journal* **8**, (2010) [65 pp.]. doi:10.2903/j.efsa.2010.1501

EFSA Scientific Report Conclusion on the peer review of tebuconazole (2008) 176, 1-109

EPA; Preliminary cumulative hazard and dose-response assessment for organophosphorus pesticides: determination of relative potencyand points of departure for cholinesterase inhibition; Office of Pesticide Programs, US Environmental Protection Agency, Washington, DC; 2001.

Hinderliter, P.M., Price, P.S., Bartels, M.J., Timchalk, C. and T.S. Poet; Development of a source-to-outcom model for dietary exposures to insecticide residues: An example using chlorpyrifos; *Regul. Toxicol. Pharmacol.*, **61** (2011) 82-92

Hulshof, K.F.A.M., Ocké, M.C., van Rossum, C.T.M., Buurma-Rethans, E.J.M., Brants, H.A.M., Drijvers, J.J.M.M., and D. ter Doest; Resultaten van de Voedselconsumtiepeiling 2003; RIVM rapport 350030002/2004, 2004, Bilthoven, The Netherlands. In Dutch.

Kistemaker, C., Bouman, M., and K.F.A.M. Hulshof; De consumptie van afzonderlijke producten door de Nederlandse bevolkingsgroepen- Voedselconsumptiepeiling 1997-1998. TNO-rapport V98.812, 1998, Zeist, The Netherlands. In Dutch.

van Klaveren, J.D., van Donkersgoed, G., and M.M.H. van Flipsen; *Bouw van de databank van het Kwaliteitsprogramma Agrarische Producten (KAP) en de gegevensverwerking van monitoringsprogramma's*; 1994, ISBN 9056010050, 9789056010058 (In Dutch)

J.D. van Klaveren*; Results residue monitoring in The Netherlands, Programme for the Quality of Agricultural Products*; KAP-report, RIKILT-DLO, Wageningen 1998, 1-84 ISBN: 90-5601-013-1

Mohango, A.D., van der Pakl-de Bruin, K.M., and S.E. Buitendijk; Aangeboren afwijkingen in Nederland 1997-2008; TNO-rapport, KvL/P&Z 2010.090, 2010, Leiden, The Netherlands. In Dutch.

Nolan, R.J., Rick, D.L., Freshour, N.L., and J.H. Saunders; Chlorpyrifos: Pharmacokinetics in human volunteers. *Toxicol. Appl. Pharmacol.*, **73** (1984) 8 – 15

Ocké, M.C., van Rossum, C.T.M., Fransen, H.P., Buurma, E.J.M., de Boer, E.J., Brants, H.A.M., Niekerk, E.M., van der Laan, J.D., Drijvers, J.J.M.M., and Z. Ghameshlou; Dutch National Food Consumption Survey – Young Children 2005/2006; RIVM Report 350070001/2008, 2008, Bilthoven, The Netherlands

Poet, T.S., Kousba, A.A., Dennison, S.L. and C. Timchalk; Physiologically based pharmacokinetic/pharmacodynamic model for the organophosphorus pesticide diazinon; *NeuroToxicology*, **25** (2004) 1013-1030

W. Slob; Dose-response modeling of continuous endpoints. *Toxicol Sci* **66**, (2002) 298-312.

Timchalk, C., Nolan, R.J., Mendrala, A.L., Dittenber, D.A., Brzak, K.A. and J.L. Mattsson; A a physiologically based pharmacokinetic and pharmacodynamic (PBPK/PD) model for the organophosphorus insecticide chlorpyrifos in rats and humans; *Toxicol. Sci.*, **66** (2002) 34-53

Timchalk, C. and T.S. Poet; Development of a physiologically based pharmacokinetic and pharmacodynamic model to determine dosimetry and cholineterase inhibitioenfor a binary mixture of chlopyrifos and diazinon in the rat; *NeuroToxicoloy*, **29** (2008) 428-443

Appendix 1 – Dose-effect relation

Dose-effect relation

The following set of 4 differential equations contains all the essentials of the dynamic model for AChE inhibition:

$$\begin{aligned}
\frac{dC}{dt} &= D - \frac{V_{max,CO} C}{K_{M,CO} + C} - \frac{V_{max,CT} C}{K_{M,CT} + C} \\
\frac{dO}{dt} &= \frac{V_{max,CO} C}{K_{M,CO} + C} - \frac{V_{max,OT} O}{K_{M,OT} + O} - k_i \cdot O \cdot A \\
\frac{dA}{dt} &= S - k_d \cdot A - k_i \cdot O \cdot A + k_a \cdot \overline{OA} \\
\frac{d\overline{OA}}{dt} &= k_i \cdot O \cdot A - \left(k_r + k_r\right) \cdot \overline{OA}
\end{aligned} \tag{1}$$

The first line shows the mother compound continuous source, its metabolism to its oxon equivalent and detoxification. The second line shows oxon formation from the mother compound, its detoxification and its binding to AChE. The third line shows endogenous AChE formation and degradation which, by absence of the compound, would lead to a steady AChE level of S / k_d, its inhibition by complex formation with the oxon and its regeneration from the complex. The fourth line shows inhibited AChE formation, regeneration and aging of the inhibited AChE.

When *C* and *O* are "small enough", the Michaelis-Menten relations in the first two lines may be linearized and the resulting set of differential equations is:

$$\begin{aligned}
\frac{dC}{dt} &= D - k_{CO} C - k_{CT} C \\
\frac{dO}{dt} &= k_{CO} C - k_{OT} O - k_i \cdot O \cdot A \\
\frac{dA}{dt} &= S - k_d \cdot A - k_i \cdot O \cdot A + k_r \cdot \overline{OA} \\
\frac{d\overline{OA}}{dt} &= k_i \cdot O \cdot A - \left(k_r + k_a\right) \cdot \overline{OA}
\end{aligned} \tag{2}$$

Steady state analysis is more easy now than for the set of equations (1), but still cumbersome. We introduce the steady AChE level $A_0 = S / k_d$ in absence of parent compound. Further, the inhibition $I = A_0 - A$ is introduced. If inhibition is "small enough", then the state variable *A* can be approximated by A_0 and thus the following set of differential equations is considered:

$$\begin{aligned}\frac{dC}{dt} &= D - k_{CO}C - k_{CT}C \\ \frac{dO}{dt} &= k_{CO}C - k_{OT}O - k_i \cdot O \cdot A_0 \\ \frac{dI}{dt} &= k_i \cdot O \cdot A_0 - k_d \cdot I - k_r \cdot \overline{OA} \\ \frac{d\overline{OA}}{dt} &= k_i \cdot O \cdot A_0 - \left(k_r + k_a\right) \cdot \overline{OA}\end{aligned} \tag{3}$$

Straightforward analysis shows that in steady state

$$\begin{aligned}C_{ss} &= \frac{D}{k_{CO} + k_{CT}} \quad O_{ss} = \frac{1}{k_{OT} + k_i \cdot A_0} \cdot \frac{k_{CO} \cdot D}{k_{CO} + k_{CT}} \\ \overline{OA}_{ss} &= \frac{1}{k_r + k_a} \cdot \frac{k_i \cdot A_0}{k_{OT} + k_i \cdot A_0} \cdot \frac{k_{CO} \cdot D}{k_{CO} + k_{CT}} \\ I_{ss} &= \frac{1}{k_d} \cdot \frac{k_a}{k_r + k_a} \cdot \frac{k_i \cdot A_0}{k_{OT} + k_i \cdot A_0} \cdot \frac{k_{CO} \cdot D}{k_{CO} + k_{CT}}\end{aligned} \tag{4}$$

and as a result, the steady state inhibition is linear with parent compound dose as long as the dose is "small enough".

In the derivation above it was silently assumed that initially *C*, *O*, *I* and $\overline{OA}$ are zero and *D* is a continuous constant forcing. Suppose now an acute bolus dosing instead, than the first line in equation (3) reads

$$\frac{dC}{dt} = -k_{CO}C - k_{CT}C; \quad C(0) = C_0 \tag{5}$$

As the system is linear, the solution is linear with C_0. *E.g.*, $C(t) = C_0 \exp\left(-\left(k_{CO} + k_{CT}\right) \cdot t\right)$. So the maximum inhibition will be linear in C_0.

Benchmark dose model.
The Weibull model with three parameters reads:

$$\mathrm{BMR(fraction\ of\ control)} = a + (1-a) \cdot \left(1 - \exp\left(-\left(\frac{\mathrm{BMD(\mu M)}}{b}\right)^c\right)\right)$$

Here, BMR is the fraction of response with respect to the control and BMD is the dose applied *in vitro* that corresponds to the observed effect. The model was optimized for the rat embryo malformation data with for the BMR $a = 0$, $b = 135$ and $c = 2.14$, for the BMRL $a = 0$, $b = 128$ and $c = 1.43$ and for the BMRU $a = 10^{-6}$, $b = 152$ and $c = 2.79$.

Given a BMR the corresponding BMD follows:

$$\mathrm{BMD}(\mu\mathrm{M}) = b \cdot \left(\ln\left(\frac{1-a}{1-\mathrm{BMR(fraction)}} \right) \right)^{1/c}$$

Annex 1.
Tebuconazole kinetics in male Japanese white rabbit

Jan C.H. van Eijkeren; RIVM/IF/EMI

Abstract
In this study a physiologically based pharmacokinetic (PBPK-) model is developed to describe tebuconazole kinetics in male Japanese white rabbit. The model is extrapolated to a PBPK-model for tebuconazole in humans.

Introduction
In the EU project "Acropolis" (www.acropolis-eu.com) interest is in the exposure of workers to the fungicide tebuconazole (Angelo Moretto, WP 4). In order to interpret sampled data a model for the kinetics of tebuconazole in workers is desirable.

There appears to be little information about the kinetics of this substance. Weber (1987, 1988) and Ecker *et al.* (1987; unknown reference, most probably located at Bayer AG, Germany) studied the kinetics of radioactivity of labelled tebuconazole in rats. These references are unpublished reports of Bayer AG, Germany. Results and references are summarized in:
www.fao.org/ag/AGP/AGPP/Pesticid/JMPR/Download/94/tebucona.pdf,
www.fao.org/ag/AGP/AGPP/Pesticid/JMPR/Download/94/tebucon1.pdf,
www.fao.org/ag/AGP/AGPP/Pesticid/JMPR/Download/94/tebucon2.pdf.
This same reference also summarizes the kinetics of radioactivity of labelled tebuconazole in dairy goats (Lee and Wood ,1990) and in laying hens (Ecker and Weber, 1991; Lee *et al*., 1991). Although radioactivity includes all metabolites as well, some specific information about parent compound and metabolites is presented.

Zhu *et al.* (2007) studied the stereoselective degradation kinetics of a well defined racemic mixture of tebuconazole in rabbits. They present concentration data in plasma, brain, fat, heart, kidney, liver, lung, muscle and spleen. Andreu-Sánchez *et al.* (2011) studied acute toxicity and bioconcentration of tebuconazole in zebra fish and present concentration data in basin water and in total zebra fish body.

These last authors present a classical pharmacokinetic model for tebuconazole total body burden in zebra fish, taken up through the gills from basin water, which is not really scalable to humans. There seems not to be any model for tebuconazole in mammals. There is a physiologically based pharmacokinetic (PBPK-) model for triadimefon and its metabolite triadimenol in rats and humans (Crowell *et al*. (2011)). However, the data for triadimefon and triadimenol are from rats only and the kinetics shown by the data in plasma, liver, kidney, brain and fat and modelled kinetics do not really match. Also, it is not clear at all how to scale a model for triadimefon and triadimenol to tebuconazole.

It was decided to develop a PBPK-model for tebuconazole in the rabbit, based on the experimental findings of Zhu *et al.* (2007).

Materials and methods
Tebuconazole in rabbit
Data for tebuconazole in plasma, brain, fat, heart, kidney, liver, lung, muscle and spleen of male Japanese white rabbits in Zhu *et al.* (2007) were digitized. These data concern the two tebuconazole enantiomers R(-) and S(+)-tebuconazole. Differences in kinetics are not only related to metabolic elimination, but also to stereoselective plasma binding and to chiral conversion of tebuconazole in plasma. To avoid problems of over parameterization and parameter identifiability, the model is based on the total tebuconazole concentration as the sum of the concentrations of both enantiomers.

The PBPK-model needs physiological data of the rabbits such as tissue volumes and regional blood flows. PBPK-model physiological data on mice, rats, dogs and humans are to be found in Brown *et al*. (1997). In table 34 they also present some data on male and female rabbits weighing 2.8 and 2.5 kg, respectively. The rabbits in Zhu *et al.* (2007) weighed 2 – 2.25 kg. However, considering the tissues that were sampled, only relative weights for heart, kidney, liver and spleen are available. In table 36 of Brown *et al*. (1997 interspecies allometric equations for organ weights for adipose tissue, brain, heart, kidneys, liver, lung, and spleen are presented. Moreover, considering body tissues not sampled by Zhu *et al.* (2007), also allometric equations for skin and gastrointestinal tract (GI-tract) are available, not however for the sampled muscle tissue and also not for plasma or blood.

For reason of consistency, it was decided to make use of the interspecies allometric equations for adipose tissue, brain, heart, kidney, liver, lung and GI-tract. The allometric scaling equations can be found in the Appendix. *For relative muscle and bone weights (50% and 7.5%, respectively) d*ata on rabbit muscle and skeleton were taken from from www.**rabbit**farming.org/uncategorized/**anatomy**-of-the-**rabbit**-2*. Relative blood weight was assumed to be 7.5% of body weight and plasma weight to be 50% of blood weight. As for humans (ICRP, 2003), it is assumed that about one third of blood is arterial blood and two third is venous blood. Beside the sampled tissues and plasma, the GI-tract, skin and skeleton were lumped as a "remaining tissues" compartment. See* ***Figure 1****. The missing 0.9% of body weight was assigned to the remaining tissues compartment.*

Cardiac output was allometrically scaled to body weight following Andersen et al. *(1987). By lack on data about regional blood flow in rabbits, regional blood flow percentages as for rats (Brown* et al. *(1997), table 23) were taken. Part of the remaining tissues compartment regional blood flow,* i.e. *GI-tract blood flow, is assumed to flow through the liver via the* vena porta*. See* ***Figure 1****. Brown* et al. *(1997) do not provide regional blood flow to spleen. It is assumed that the specific spleen blood flow,* i.e. *regional spleen blood flow per unit of spleen volume, is equal to the specific blood flow to the GI-tract. Relative regional blood flows do not sum to 100%. Corrected blood flows are obtained by assigning the difference to all regional blood flows proportional to their uncorrected values.*

Plasma:tissue tebuconazole partition coefficients and the liver clearance rate (see ***Figure 1****) of tebuconazole were fitted to the data available. It is not possible, given the data, to identify whether tebuconazole is not only metabolized in the liver or is also eliminated through bile.*

PBPK-model equations are in the Appendix. The model is implemented in ACSL code and data were fitted with ACSL-Optimize (www.acslX.com *).*

<u>*Rabbit to human model extrapolation*</u>

In extrapolating the tebuconazole PBPK-model for the rat to the human one should be cautious not to exaggerate the confidence in the rabbit model developed and the procedure of extrapolating. So, the number of compartments of the model for the rabbit will be reduced. The compartments heart, kidney, muscle, spleen and part of the remaining tissues will be lumped into one compartment only. As neurotoxic effects are also studied in WP4 brain will be considered as a separate tissue. However, there is no evidence from in vivo and *in vitro* studies conducted for ACROPOLIS that conazole have any significant neurotoxic effect (unpublished data).

As the kinetics of field workers, that are exposed to tebuconazole through the inhalatory and dermal route, skin is detached from the remaining tissues and considered as a separate compartment. See ***Figure 2****.*

Physiological data for a male and females in Bosgra et al. *were used to parameterize the compartment volumes and regional blood flows. Tissue:plasma tebuconazole partition coefficients are taken as for the rabbit. The remaining tissues:plasma partition coefficient was determined by the volumetric weighted mean of the constituting tissue:plasma partition coefficients for the rabbit. Liver clearance was allometrically scaled proportional to the ratio of human to rat body weights to the power 0.75 (*E.g.*, West* et al.*, 2002).*

Results

Tebuconazole in rabbit

The following body composition in percentage of body weight was obtained from the allometric scaling equations, from the World Wide Web and as assumed:

Adipose tissue:	7.5%	allometric scaling
Brain:	0.9%	allometric scaling
Heart:	0.4%	allometric scaling
Kidney:	0.6%	allometric scaling
Liver:	3.2%	allometric scaling
Lung:	0.8%	allometric scaling
Spleen:	0.3%	allometric scaling
Skin:	13.3%	allometric scaling
GI-tract:	7.1%	allometric scaling
Skeleton:	7.5%	world wide web
Muscle:	50%	world wide web
Blood:	7.5%	assumption

These values sum up to 99.1%. The percentage of 0.9% that is left was assigned to the remaining tissues compartment, consisting of skin, skeleton and GI-tract and thus comprising a total of 28.8% of body weight.

The allometrically scaled value for cardiac output is 0.44 L/min.
The following regional blood flows in percentage of cardiac output was obtained from table 23 in Brown *et al.* (1997) for rats:

Adipose tissue:	7.0%	after correction:	7.7%
Brain:	2.0%		2.2%
Heart:	5.1%		5.5%
Kidney:	14.1%		15.3%
Liver:	2.1%		2.3%
Skin:	5.8%		6.3%
GI-tract:	15.3%		16.6%
Skeleton:	12.2%		13.3%
Muscle:	27.8%		30.2%

From the first column of this table, the relative regional blood flow to spleen was determined from the specific blood flow to the GI tract to be 0.6%. Totally, the values in this column sum up to 92% of cardiac output. The remaining 8% is distributed over all regional flows in proportion to the relative flows above (second column; the value for spleen is 07% after correction). Note that the total flow to the liver is the sum of the flows through liver artery and *vena porta*, 18.9% of cardiac output.

A model fit was performed to all available data simultaneously to estimate parameter values for the partition coefficients and the liver clearance. A relative error model for the residuals was assumed. The optimized parameter values for the tebuconazole tissue:plasma partition coefficients are

Adipose tissue:	12 (3)
Brain:	3.1 (0.6)
Heart:	3.3 (0.5)
Kidney:	3.5 (0.6)
Liver:	6.7 (1.5)

Lung:	23 (6)
Spleen:	4.0 (0.7)
Muscle:	0.9 (0.2)
Remaining tissues:	1.9 (0.8)

The optimized value for liver clearance is 0.052 (0.007) L/min

The fitted model is compared to data in plasma in **Figure 3** and to data in brain, adipose tissue, heart, kidney, liver, lung, muscle and spleen in **Figure 4**. For comparison the picture corresponding to Figure 4 is taken from Zhu *et al.* (2007) in **Figure 5**. The apparent maximum concentration they find for all tissues but lung can not be explained with the model. It is not really conceivable how such a concentration-time course, which such relative large values for maximum concentration time, can exist together with the concentration-time course in lung and, as shown in Figure 3, in plas-ma, with relative fast decreasing concentration levels.
The resulting concentration-time course of tebuconazole in the remaining tissues compartment, for which no data are available, is shown in **Figure 6**.

The terminal phase, when all tissue concentrations are in steady equilibrium with plasma concentration and the terminal elimination rate is reached for all tissues, starts at about 300 min (5 h) and the terminal elimination rate is about 120 min (2 h).

Rabbit to human model extrapolation
A "standard" male human weighing 73 kg has the following body composition (Bosgra et al*., 2011):*

Adipose tissue:	23.3%
Liver:	2.5%
Lung:	0.7%
Remaining tissues:	65.8%
Blood:	7.7%

The "standard man" cardiac output is 390 L/h
The relative regional blood flows as percentage of cardiac output are

Adipose tissue:	5.3%
Liver:	6.9%
Remaining tissues:	87.8%
GI-tract:	20.0%

Note that of the 87.8% relative blood flow to the remaining tissues, 20% (absolute) flows via the *vena porta* to the liver and 67.8% (absolute) directly to the venous pool. So, the total relative regional liver flow is 26.9%.

The liver clearance of 0.052 L/min of the rabbit scales to 44 L/h for the standard man.

The remaining tissues:plasma tebuconazole partition coefficient as a volumetric weighed mean of the constituting tissues:plasma partition coefficients in rabbit is 1.3.

The terminal phase half life time of tebuconazole in humans is, following this modelling approach, about half a day.

In **Figure 7** two administration scenarios are compared: intra-venous bolus dosing and acute oral exposure to 1 mg tebuconazole per kg of body weight. The implied smaller tebuconazole AUC for oral dosing is caused by the so called "first pass" effect through the liver. **Figure 8** shows the time course of daily administered tebuconazole (1 mg / kg / day). Plateau values are reached after a few days of administration.

Note: the results in these figures are hypothetical and not supported by data on the kinetics of tebuconazole in humans.

Discussion

General

Although the widespread application of conazoles as fungicide and drug, there appears to be little research on the kinetics of these substances in laboratory animals, let alone in humans. As a consequence PBPK-models, but one only, have not been developed for conazoles in laboratory animals and humans (besides the zebra fish (Andreu-Sánchez, 2011, that cannot serve as a starting point for PBPK-modelling in humans). Crowell *et al.* (2011) seem to be the first authors that developed such a model, *i.e.* a PBPK-model for triadimefon and its metabolite triadimenol in rats, based on experimental data that was extrapolated to a model for humans.

At the start of this study, it was assumed that somehow the model of Crowell *et al.* (2011) could be adapted to tebuconazole. But first of all, their model for tebuconazole in the rat is not convincing as compared to the experimental data. See **Figure 9A** and **B**. The data in plasma, liver, kidney and brain clearly show bi-phasic behaviour that is not well represented by their model results. It was tried to improve modelling results by simplifying assumptions on metabolism (not saturated instead of saturated) and the kinetics of the adipose tissue compartment (flow limited instead of diffusion limited), but when, *e.g.* improving the result for triadimefon in plasma to almost perfect, modelled triadimefon in other tissues and/or modelled triadimenol did not compare well. Somehow, the experimental data and several model concepts are not compatible.

So, the starting point would introduce a great uncertainty of itself. Two ways exist of extrapolating the model for triadimefon in the rat to that of tebuconazole in humans. One way is the extrapolation of the triadimefon model in the rat to a model for triadimefon in humans as Crowell *et al*. did (additional uncertainty 1)and then relating that model to the kinetics of tebuconazole in humans (additional uncertainty 2). Another way is relating the kinetics of triadimefon in rats to that of tebuconazole in rats (additional uncertainty 1) and then extrapolating the tebuconazole kinetics in rats to that in humans (additional uncertainty 2).

Ongoing literature search revealed the work of Zhu *et al.* (2007) that was not considered in the first literature screening period, because of its focus on the chiral aspects of tebuconazole. In fact, in our study, that aspect was ignored because *in vivo* chiral conversion rates can not be identified from these data. It was decided to use their data to directly model the kinetics of tebuconazole in a laboratory animal, *in casu* the rabbit, and extrapolate to a model for tebuconazole in humans. This avoids both additional uncertainties, described in the section above, due to the extrapolation of triadimefon to tebuconazole and the extrapolation from rat to human.

Tebuconazole in rabbit

The data in Zhu *et al.* (2007) for plasma and lung tissue seem to be not compatible to those in the other tissues. The first ones, at least from the first sample time point onward, steadily decline as expected, but the other ones reach a maximum at a relative long time, 30-60 minutes, after iv-dosing. So, just like for the data of Crowell *et al.* (2011) in the rat, there seems to be, at least from the view point of the model concept, inconsistency in the data for the rabbit as well. Note however, that all data from a sampling time point are obtained from one rabbit only.

Given the data in Zhu *et al.* (2007) the simplest model to describe all data is in Figure 1 and the model, optimized to all the data available, is compared to the data in Figures 3 to 4. The latter

figure is compared to Figure 5, presenting the original data in Zhu *et al.* (2007) together with some suggestive, data connecting lines. From the point of view of kinetic modelling one could not imagine, *e.g.*, how tebuconazole, a lipophilic compound, would be eliminated from adipose tissue so relatively fast as compared to the other tissues.

So, as for Crowell *et al.* (2011) for triadimefon in the rat, also this model for tebuconazole in uncertain. In order to check whether the uncertainty in both models is similar, the model for triadimefon in the rat in comparison to the rat data on logarithmic scale as in Crowell *et al.* (2011), presented in Figure 9A and B, is compared to the model for tebuconazole in the rabbit in comparison to the rabbit data on logarithmic scale, presented in **Figure 10A** and **B**. Our conclusion is that the uncertainty for the model of tebuconazole in the rabbit is certainly not greater than the uncertainty for the model of triadimefon in the rat.

So, it is to be expected that starting from the data in Zhu *et al.* (2007) less uncertainty is introduced, as now only additional uncertainty in the extrapolation of the rabbit PBPK-model for tebuconazole to a model in humans is demanded and not the extrapolation from triadimefon to tebuconazole.

Rabbit to human model extrapolation

The extrapolation of rabbit physiology data (though itself uncertain, because obtained from allometric scaling and an assumption on blood percentage) to human physiology data is immediate.

The extrapolation of tebuconazole tissue:plasma partition coefficients is less trivial, as tissue:plasma partition coefficients in general depend on the tissue and plasma composition in terms of water, fat and protein fraction and on the binding properties of tebuconazole to albumin an other plasma proteins and to tissue proteins. So, this extrapolation step is uncertain and it is not known how to quantify this uncertainty.

The power law applied for the extrapolation of the tebuconazole liver clearance (West *et al.*, 2002) is a general one and typically depicted on a logarithmic scale. It may be expected that the human clearance rate thus estimated is at least a factor 3 higher or lower. Such a variation has a rather great impact on tebuconazole kinetics in humans. See **Figure 11** where the hypothetical tebuconazole plasma kinetics after acute bolus dosing is compared for tebuconazole liver clearances of 1.5, 44 and 132 L/h.

Literature

Andersen, M.E., Clewell, H.J., Gargas, M.L., Smith, F.A. and R.H. Reitz; Physiologically based pharmacokinetics and the risk assessment process for methylene chloride; *Toxicol. Appl. Pharmacol.* **87** (1987) 185-205

Andreu-Sánchez, O., Paraiba, L. C., Jonsson, C. M. and J. M. Carrasco; Acute toxicity and bioconcentration of fungicide tebuconazole in zebra fish (*Danio rero*); *Environ. Toxicol.* **21** (2011), www.wileyonlinelibrary.com DOI 10.1002 tox.2061

Bosgra, S., Bos, P., van Eijkeren, J., Zeilmaker, M., Vermeire, T., Rompelberg, C., and W. Slob; A novel model to predict physiologically based model parameters and their inter-individual variability from anthropometry; to be submitted

Brown, R.P., Delp, M.D., Lindstedt, S.L., Rhomberg, L.R. and R.P. Beliles; Physiological parameter values for physiologically based pharmacokinetic models; *Toxicol. Indust. Health* **13** (1997) 407-484

Crowell, S.R., Henderson, W.M., Kenneke, J.F. and J.W. Fisher; Development and application of a physiologically based pharmacokinetic model for triadimefon and its metabolite triadimenol in rats and humans; *Toxicology Letters*, **205** (2011) 154-162

Ecker, W. and Weber, H. 1991 (chlorophenyl-U-14) tebuconazole absorption, distribution, excretion, and metabolism in laying hens. Report No. PF3587. Bayer AG, Germany. Unpublished.

ICRP, 2003. *Basic Anatomical and Physiological Data for Use in Radiological Protection: Reference Values*. Elsevier Science, Amsterdam, The Netherlands.

Lee, S.G.K., Hanna-Bey, L.A., Johnston, K., Wood, S.E. and Leimkühler, W.M. 1991. The metabolism of 14C-Folicur(TM) in chickens. Report No. MR87156. Mobay corporation, USA. Unpublished.

Lee, S.G.K. and Wood, S.E. 1990. The metabolism of Folicur(TM) in dairy goats. Report No. MR94882. Mobay corporation, USA. Unpublished.

Weber, H. 1988. (Phenyl-UL-14) HWG 1608 Whole-body autoradiographic distribution of the radioactivity in the rat. Report No. PF2962. Bayer AG, Germany. Unpublished.

Weber, H. 1987. (Phenyl-U-14) HWG 1608: Study of biokinetic behaviour in the rat. Report No. PF2859. Bayer AG, Germany. Unpublished.

Weber, H. *et al.* 1987. Report No. PF2907 212/1987. Bayer AG, Germany. Unpublished.

West, G.R., Woodruff, W.H. anf J.H. Brown; Allometric scaling of metabolic rate from molecules and mitochondria to cells and mammals; *PNAS* **99, suppl 1** (2002) 2473-2478

Zhu, W., Qiu, J., Dang, Z., Lu, C., Jia, G., Li, L. and Z. Zhou; Stereoselective degradation kinetics of tebuconazole in rabbits; *Chirality* **19** (2007) 141-147

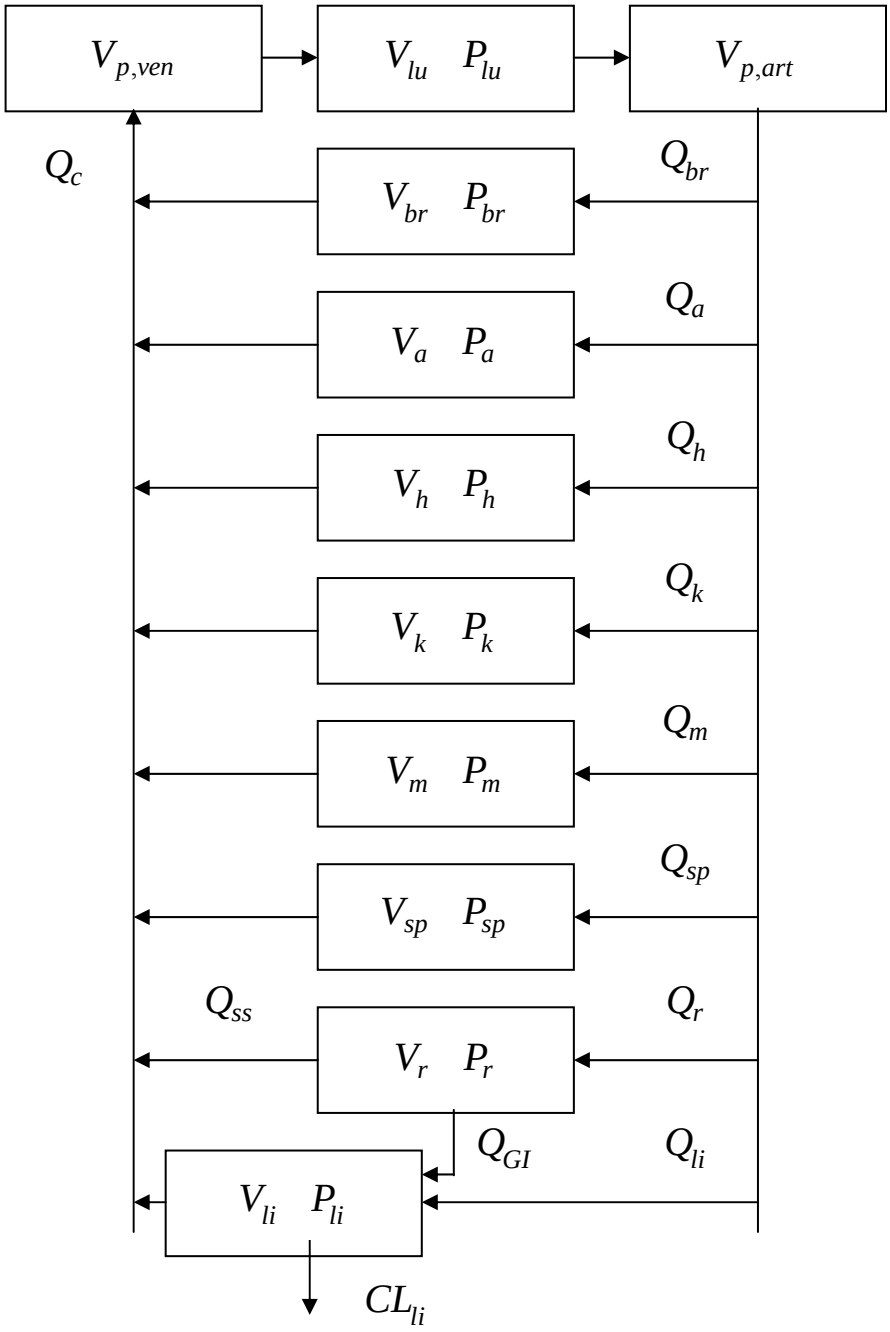

Figure 1. Tissue volumes (*V*), regional blood flows (*Q*) and tissue:plasma tebuconazole partition coefficients (*P*) for lung (lu), brain (br), adipose tissue (a), heart (h), kidney (k), muscle (m), spleen (sp), remaining tissues (r) and liver (li). Total cardiac output is Q_c. The flow to the lumped remaining tissues splits in a part that flows through the liver (Q_{GI}) and directly into the venous plasma pool (Q_{ss}), for skeleton and skin). Liver clearance (metabolism and bile excretion) is denoted by CL_{li}.

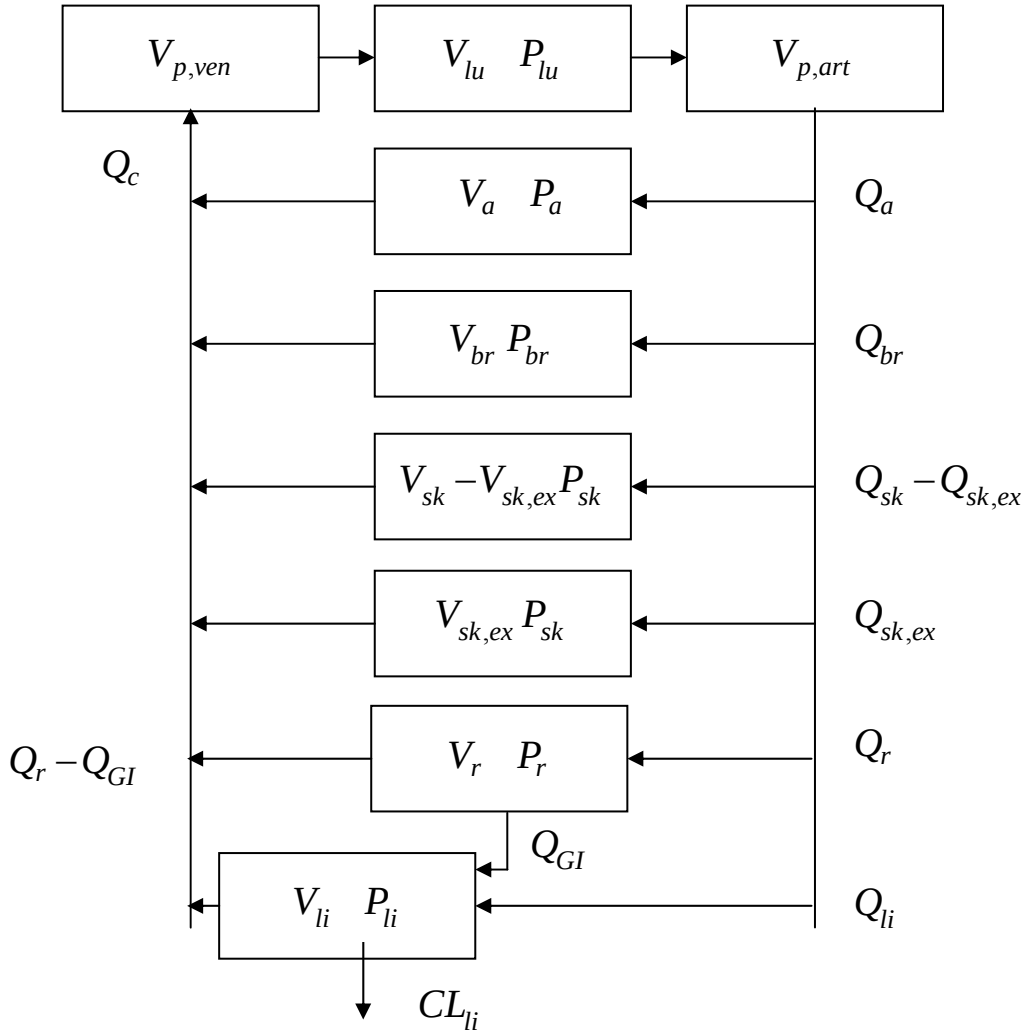

Figure 2. Proposed PBPK-model for tebuconazole in humans. Heart, kidney, muscle, spleen and part of the remaining tissues of the PBPK-model for rabbits are lumped into one remaining compartments tissue. Skin is detached from the remaining tissues. Exposed skin is considered as a separate compartment. Physiological data are from humans instead of rabbits, tebuconazole tissue:plasma partition coefficients are from rabbits. The rabbit liver clearance rate is allometrically scaled to humans with power 0.75.

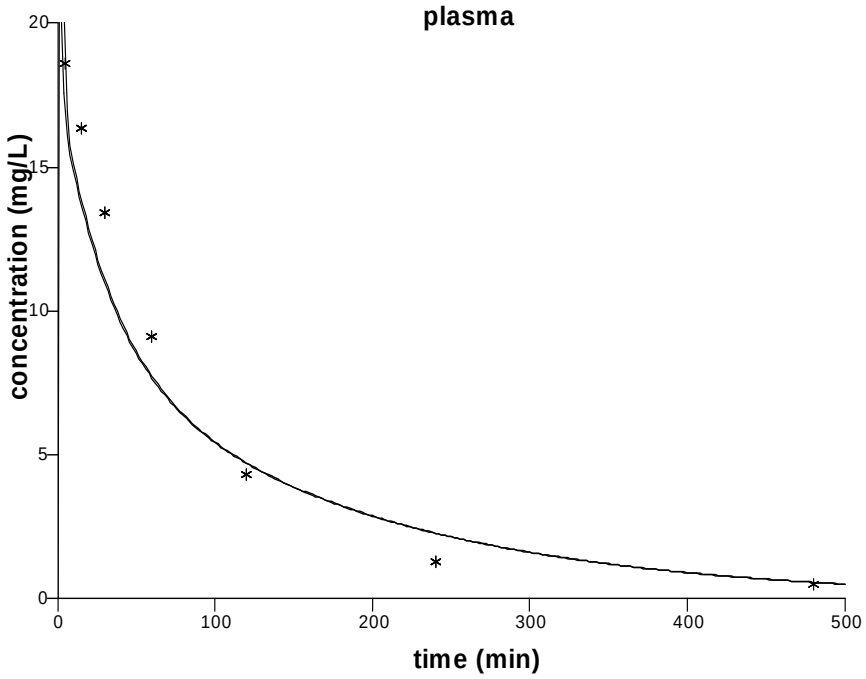

Figure 3. Tebuconazole in plasma. Comparison of optimized model (straight line) and experimental data from Zhu *et al.* (2007). The number of animals is one per experimental time point.

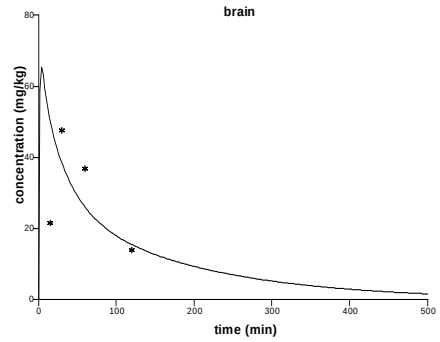
brain
concentration (mg/kg)
time (min)

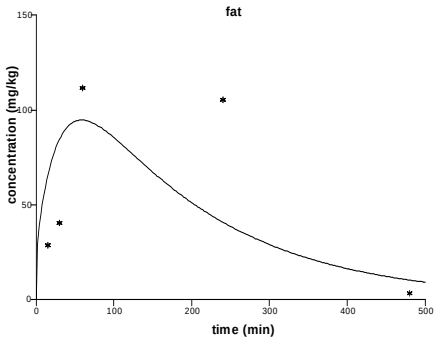
fat
concentration (mg/kg)
time (min)

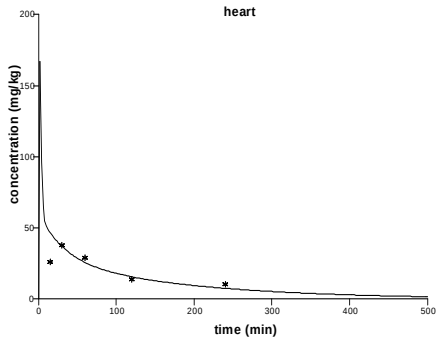
heart
concentration (mg/kg)
time (min)

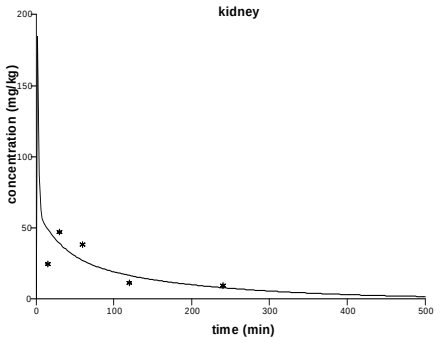
kidney
concentration (mg/kg)
time (min)

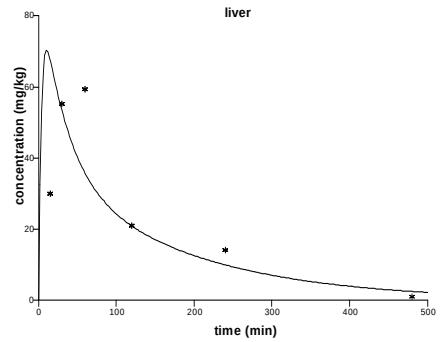
liver
concentration (mg/kg)
time (min)

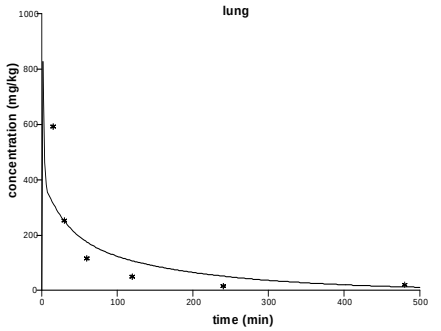
lung
concentration (mg/kg)
time (min)

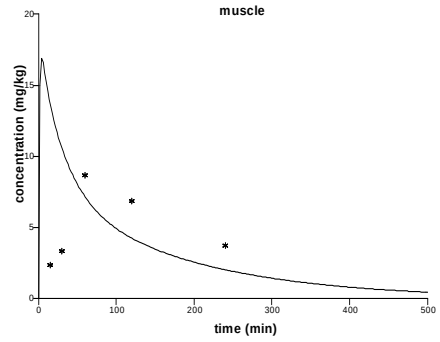
muscle
concentration (mg/kg)
time (min)

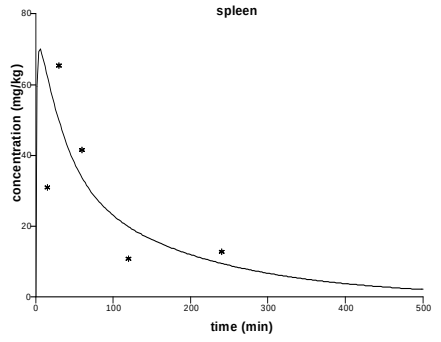
spleen
concentration (mg/kg)
time (min)

Figure 4. Tebuconazole in several tissues. Comparison of optimized model (straight line) and experimental data from Zhu *et al.* (2007). The number of animals is one per experimental time point.

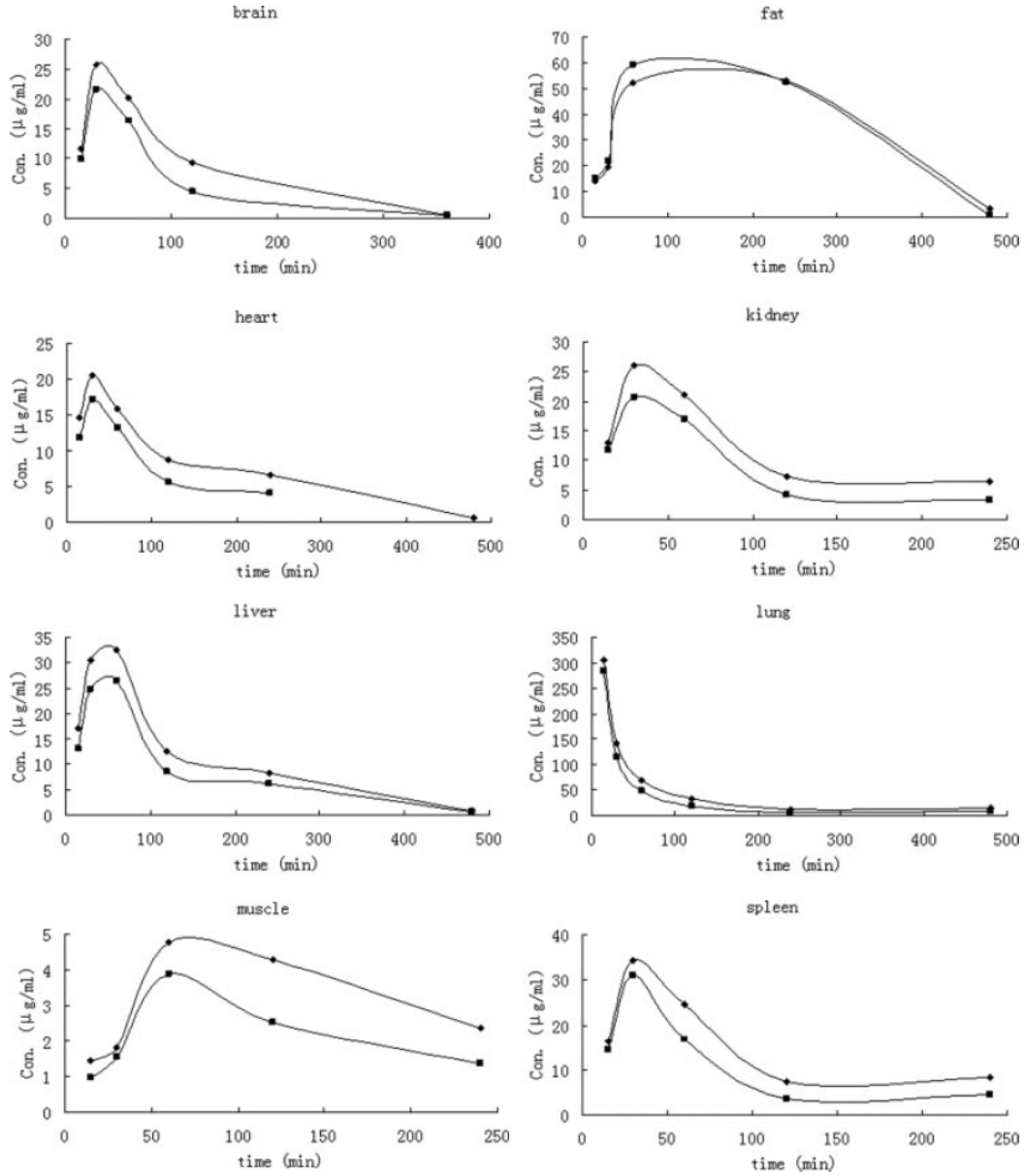

Figure 5. Picture taken from Zhu *et al.* (2007) corresponding to figure 4, but split into two points for each of the two enantiomers. The apparent maximum between 30 – 60 minutes cannot be explained by the PBPK-model. Each pair of data is from one rabbit.

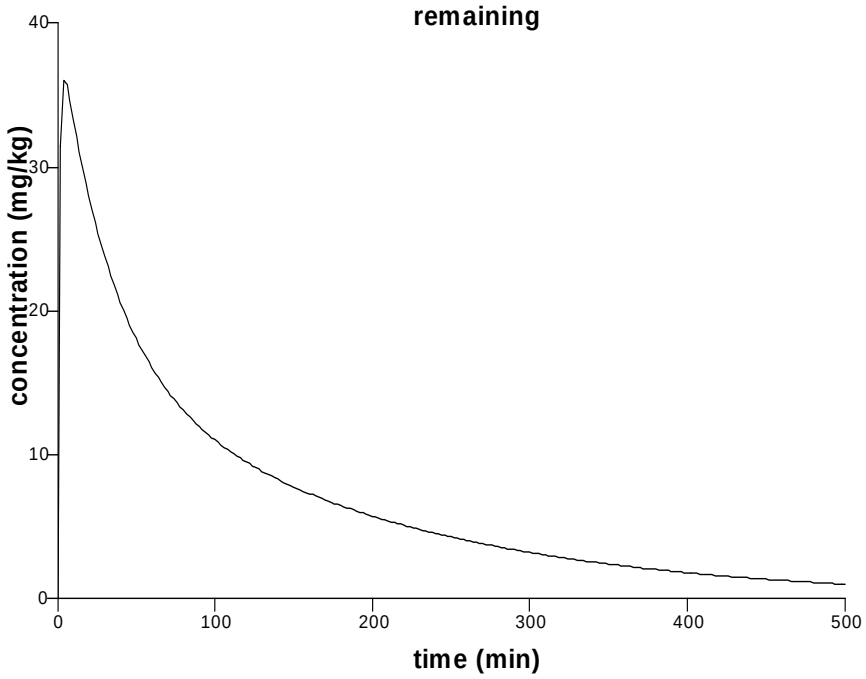

Figure 6. Resulting tebuconazole in remaining tissues for which no data in Zhu *et al.* (2007) are available..

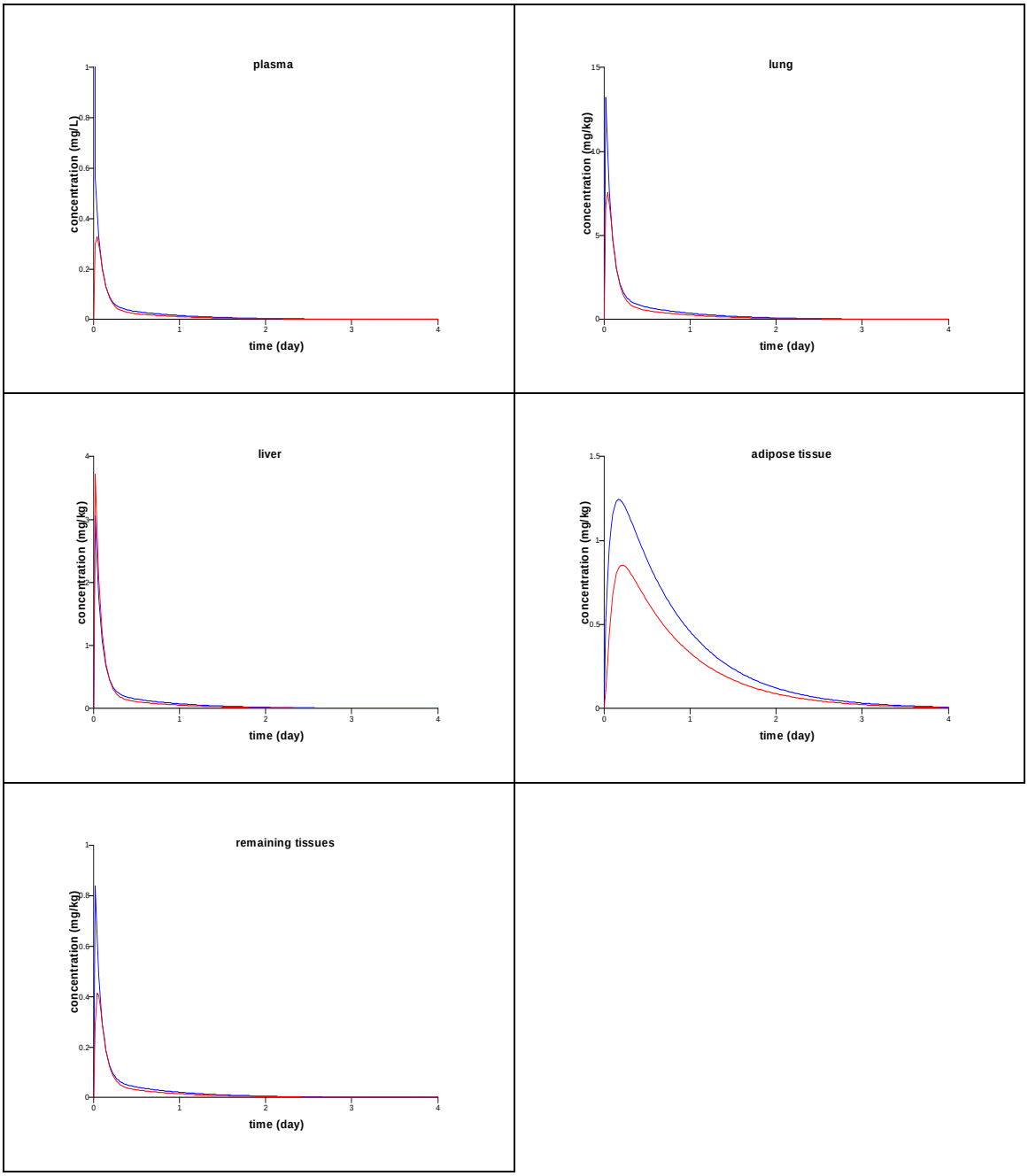

Figure 7. Hypothetical tebuconazole kinetics in humans. Intravenous (blue lines) and acute oral (red lines) bolus dosing regimen of 1 mg/kg. The initial concentration in plasma after i.v. bolus dosing is about 40 mg/L.

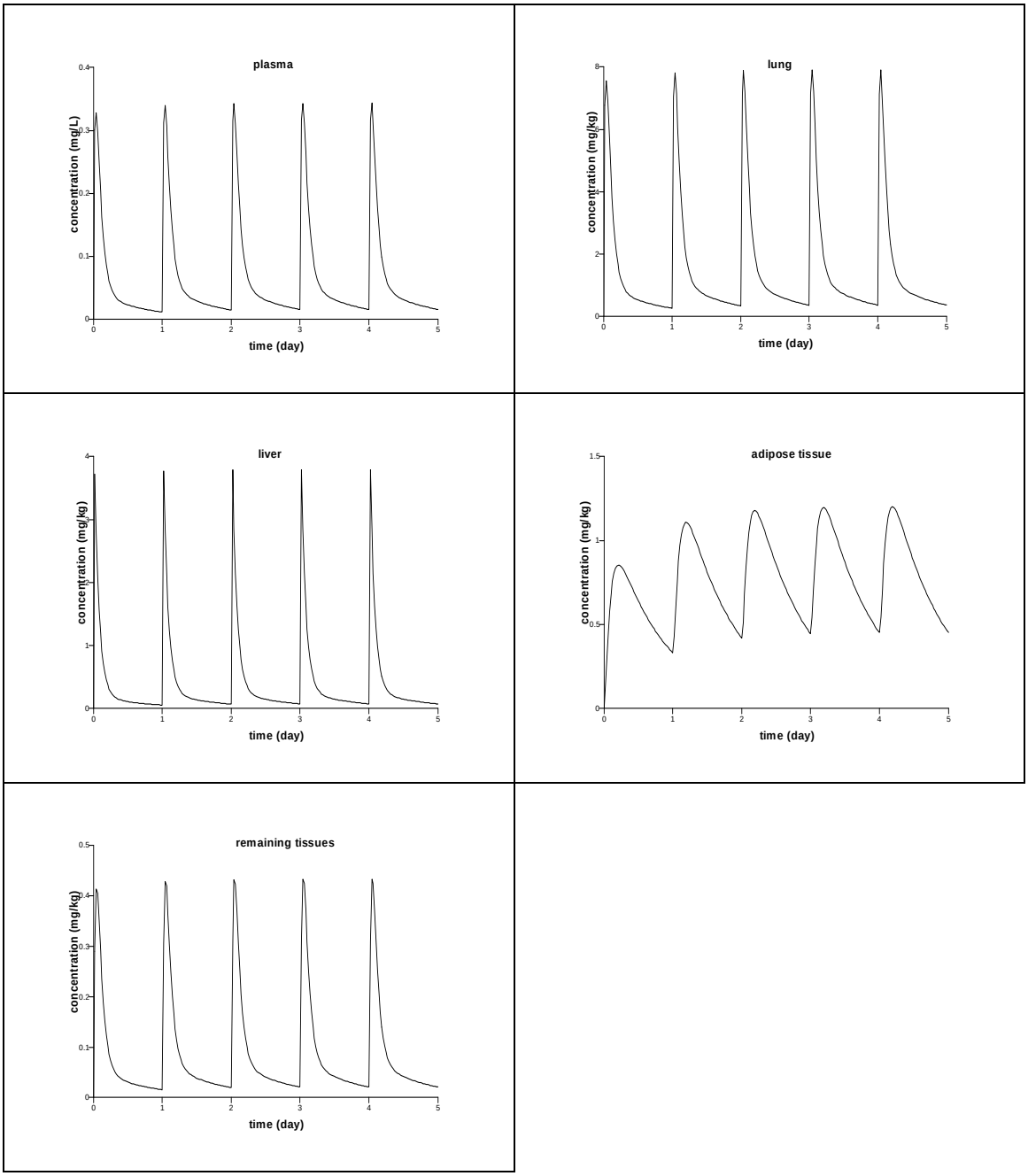

Figure 8. Hypothetical tebuconazole kinetics in humans. Chronic dosing regimen of 1 mg/kg/day as an oral bolus.

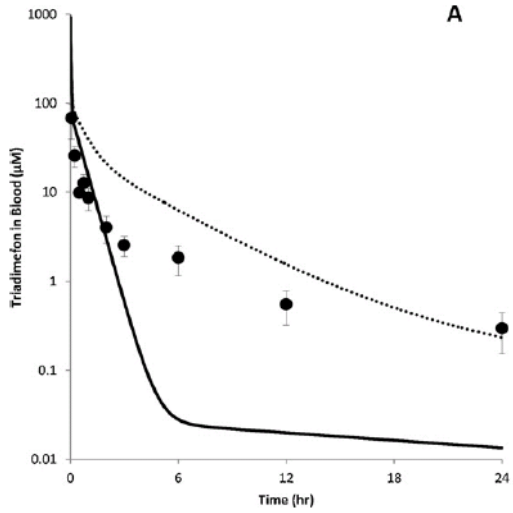

Figure 9A. Triadimefon in rat plasma. Model in Crowell *et al*. (2011) compared to data. Note the logarithmic scale.

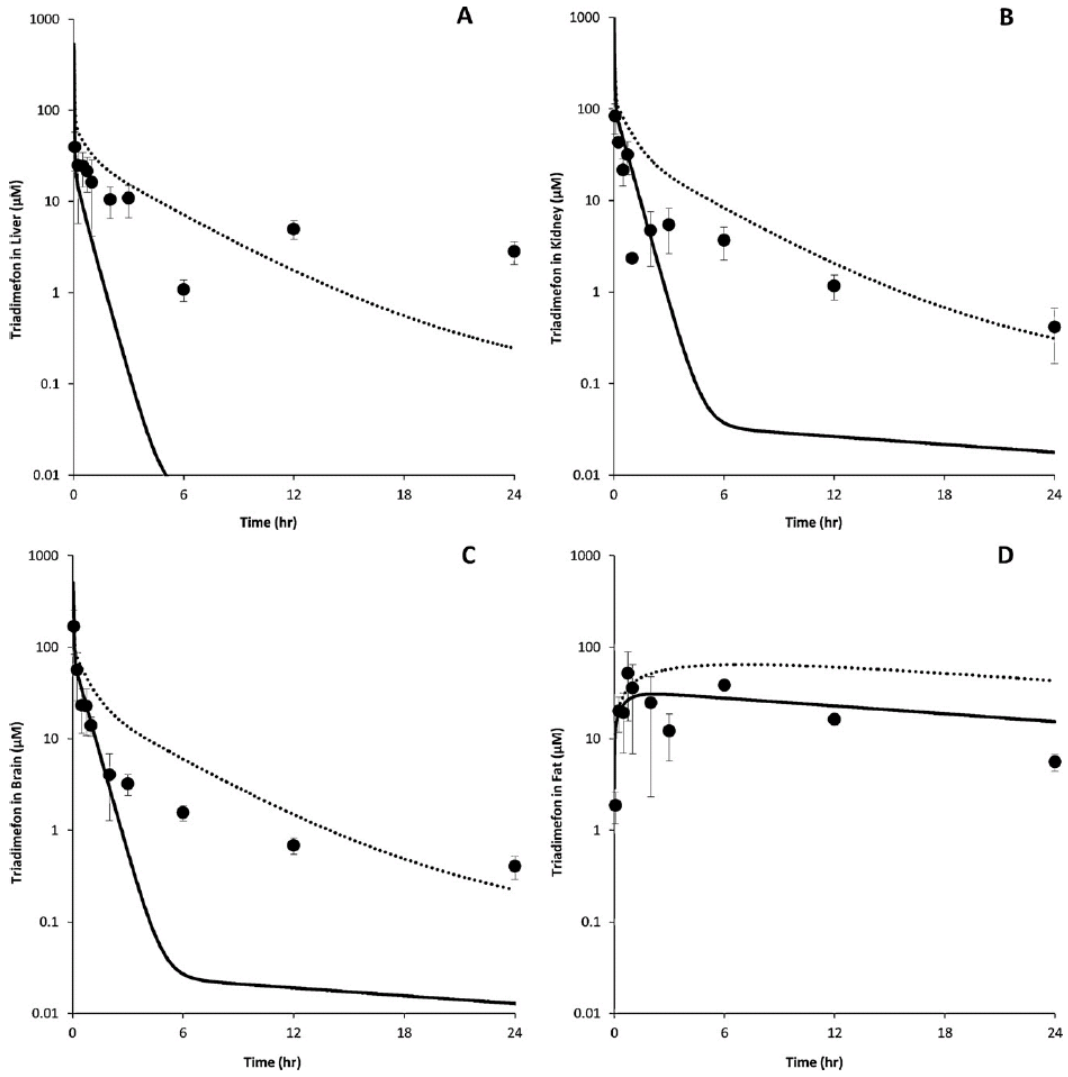

Figure 9B. Triadimefon in rat liver, kidney, brain and adipose tissue. Model in Crowell *et al*. (2011) compared to data. Note the logarithmic scale.

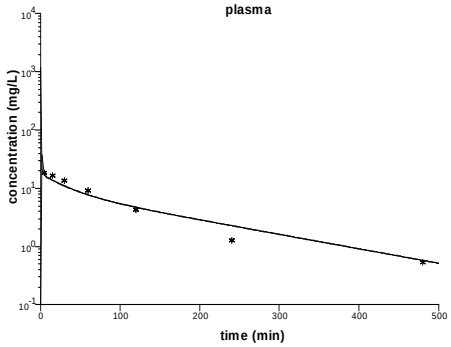

Figure 10 A. Tebuconazole in rabbit plasma. Model compared to data on logarithmic scale to compare to figure 9A.

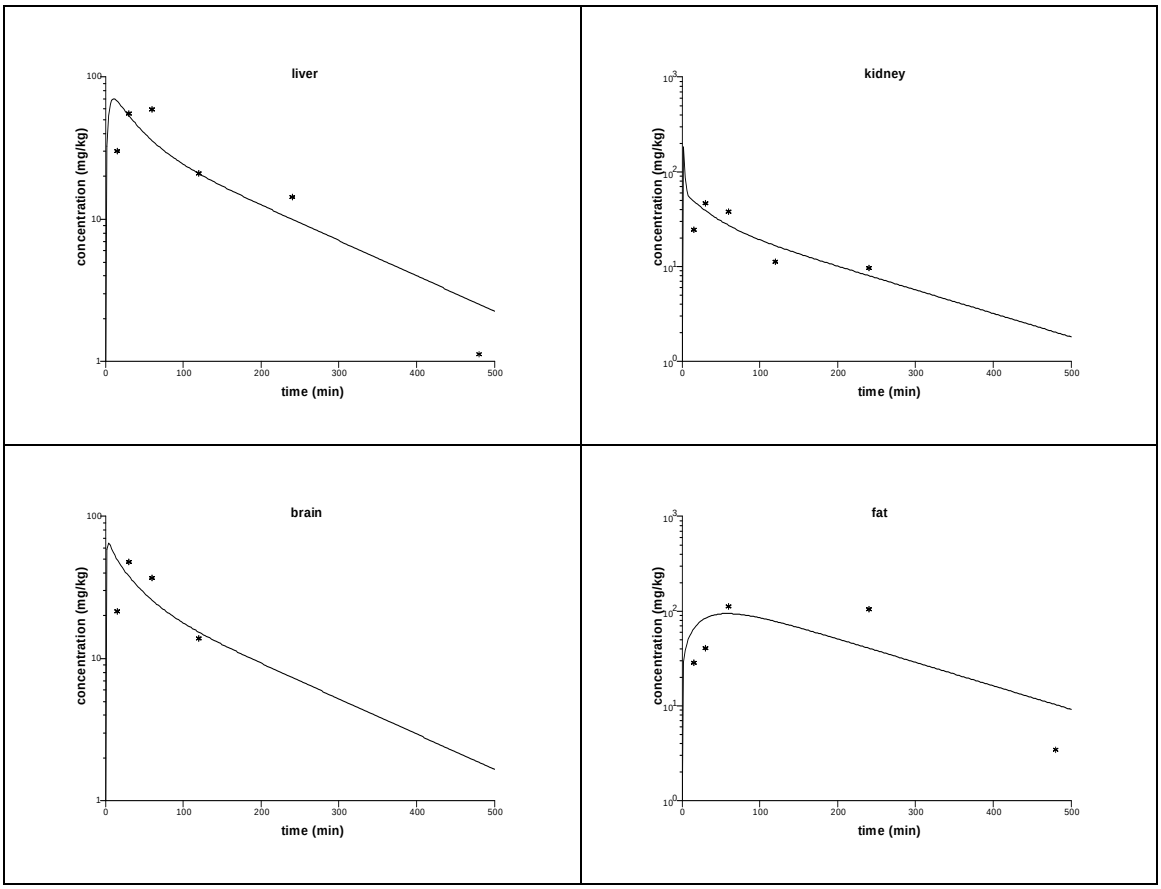

Figure 10 B. Tebuconazole in rabbit liver, kidney, brain and adipose tissue. Model compared to data on logarithmic scale to compare to figure 9B.

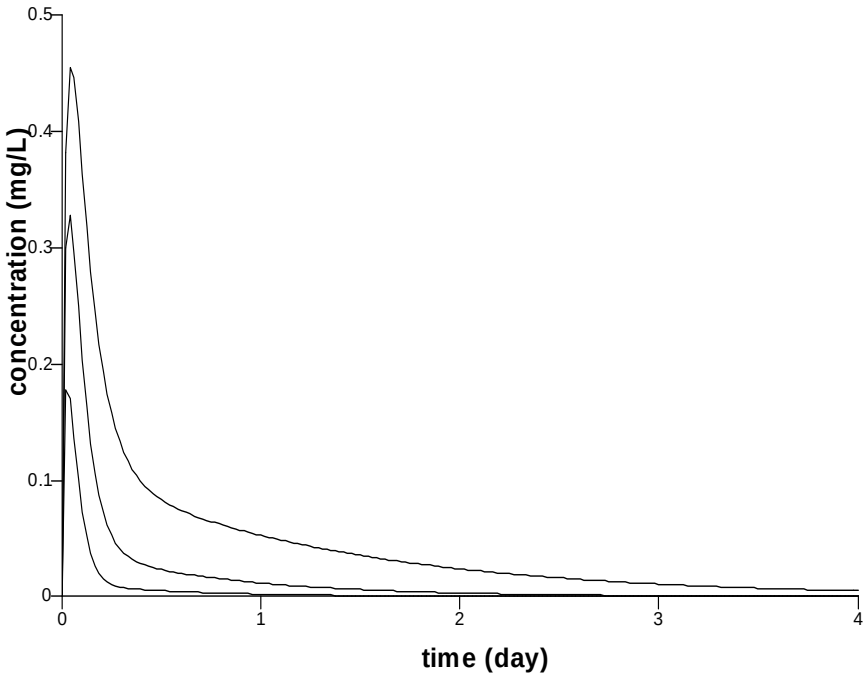

Figure 11. Hypothetical tebuconazole concentration-time courses in plasma after acute bolus dosing (1 mg/kg) with the model nominal liver clearance value (middle line), threefold lower value (upper line) and threefold higher value (lower line).

Appendix

Allometric scaling equations for organ weights

The allometric scaling equations require body weight value. A value of W = 2.125 kg was taken for the rabbits in Zhu *et al.* (2007). They reported body weight values to lie between 2 and 2.25 kg for the experimental white Japanese rabbits. The equations, with references, can be found in Brown *et al.* (1997).

Adipose tissue: $67.1 \times W(kg)^{1.14}$ g

Brain: $10.9 \times W(kg)^{0.755}$ g

Heart: $4.34 \times W(kg)^{1.0}$ g

Kidney: $7.1 \times W(kg)^{0.85}$ g

Liver: $35.44 \times W(kg)^{0.87}$ g

Lung: $7.72 \times W(kg)^{1.03}$ g

Spleen: $2.5 \times W(kg)^{1.02}$ g

Skin: $139 \times W(kg)^{0.942}$ g

GI-tract: $74 \times W(kg)^{0.94}$ g

Allometric scaling equation for cardiac output

$0.25 \times W(kg)^{0.74}$ L/min Andersen *et al.* (1987)

PBPK-model equations

For tissue $x \in \{\text{adipose tissue, brain, heart, kidney, spleen, muscle, remaining tissues}\}$ the time rate of change of the amount of tebuconazole is given by the difference between the amount entering the tissue through arterial blood and leaving through venous blood:

$$\frac{dA_x}{dt} = Q_x(C_{p,art} - C_x / P_x) \quad (6)$$

where A_x is the amount of tebuconazole in tissue *x*, Q_x is the tissue *x* regional blood flow, $C_x = A_x / V_x$ is the tebuconazole concentration in tissue *x*, P_x is the tebuconazole tissue *x*:plasma partition coefficient (hence, C_x / P_x is the tissue *x* leaving venous concentration of tebuconazole) and $C_{p,art}$ is the tebuconazole concentration in arterial plasma.

For the liver the time rate of change of the amount of tebuconazole is given by the difference between the amount entering through arterial blood and through remaining tissues leaving venous blood via the GI-tract and the liver leaving through venous blood and clearance:

$$\frac{dA_{li}}{dt} = Q_{li}(C_{p,art} - C_{li}/P_{li}) + Q_{GI}(C_r/P_r - C_{li}/P_{li}) - CL_{li} \cdot C_{li}/P_{li} \quad (7)$$

For venous plasma the time rate of change of the amount of tebuconazole is given by the difference between the amount entering the venous pool through venous blood from the tissues in the equations (6) and (7) and the amount leaving the pool to lung:

$$\frac{dA_{p,ven}}{dt} = \sum_{x \neq \text{remaining tissue}} Q_x \cdot C_x/P_x + Q_{ss} \cdot C_r/P_r + (Q_{li} + Q_{GI}) \cdot C_{li}/P_{li} - Q_c \cdot C_{p,ven} \quad (8)$$

For lung the time rate of change of the amount of tebuconazole is given by the difference between the amount entering through venous blood and the amount leaving to the arterial blood pool:

$$\frac{dA_{lu}}{dt} = Q_c \cdot (C_{p,ven} - C_{lu}/P_{lu}) \quad (9)$$

For arterial plasma the time rate of change of the amount of tebuconazole is given by the difference between the amount entering from the lung and the amount leaving to the tissues in the equations (6) and (7):

$$\frac{dA_{p,art}}{dt} = Q_c \cdot (C_{lu}/P_{lu} - C_{v,pla}) \quad (10)$$

where, of course, cardiac output equals the sum of the regional blood flows.

Annex 2.
Overview of existing Pharmacologically Based PharmacoKinetic/PharmacoDynamic (PBPK/PD) models for Acetylcholinesterase (AChE) inhibition

J.C.H. van Eijkeren, RIVM/IF/EMI

Abstract
This study overviews existing PBPK/PD models for neurotoxic effects of organophosphates and carbamates. It is concluded that the human models for CPF and DZN (Timchalk *et al.*, 2002; Poet *et al.*, 2004; Timchalk & Poet, 2008; Hinderliter *et al*., 2011) are best suited when proceeding with the tasks on organophosphorus pesticides as described in Task 4.4.

Introduction
Within WP4 of the EU Acropolis project, interest is in the development of methods for the risk assessment of cumulative and aggregated exposure to neurotoxic substances. This general objective is narrowed to the case of pesticides and more explicitly described in the following:
Objective
Determination of the fate of the pesticide within the body and the possible internal effective dose of different pesticides with possible additive effects.
Moreover, focus is on the following:
Case study
Neurotoxic pesticides are chosen because this group is relatively well studied. This is needed in order to model the internal dose (PBPK/PD modelling).
Within that case-study Task 4.3 is planned to be an:
Overview of existing PBPK/PB models
RIVM will overview the available PBPK/PD models that may be used in this project.

In Task 4.4 mention is made of *conazoles* and *chlorpyrifos* (CPF). Of conazoles only one PBPK model reference was found in the literature and no PBPK/PD model reference. A PBPK model for triadimefon and its main metabolite triadimenol in rats is developed in (Crowell *et al*., 2011) and extrapolated, based on human *in vitro* data, to a PBPK model for conazole in humans. Comparison of the rat model with experimental data is moderate and no comparison is available of the extrapolated model with human data. Within the work package interest is in tebuconazole and a provisional PBPK model for tebuconazole in rabbits was developed in van Eijkeren (2012). *However, there is no evidence from in vivo* and *in vitro* studies conducted for ACROPOLIS that conazole have any significant neurotoxic effect (unpublished data).

Organophosphates (OPs), such as CPF, and carbamates do cause the neurotoxic effect of cholinesterase inhibition. For five OPs and two carbamates PBPK/PD models for acetylcholinesterase inhibition have been developed. Therefore, this overview concerns these neurotoxic agents.

A brief description of PBPK models and of the mode of action (PD) of OPs and carbamates is given, followed by a short history of the development of different models for different of OPs and carbamates. Next, these models will be compared as to their properties and relevance for human dietary exposure as meant in WP4.

PBPK models

PBPK models are compartment models that that describe the disposition of a compound in humans and animals in terms of gross physiological properties such as tissue volumes and regional blood flows. These gross properties may be refined to more fine tuned ones such as tissue composition and enzyme activities. Generally these model consider absorption of a compound (across the gut wall after oral uptake, across the skin or across the alveolar wall), its distribution among the different compartments, its metabolism (assumed mainly in liver, but other tissues may be considered if relevant) and its excretion (through bile or urine).

A typical example is the following seven compartment PBPK model in **Figure 1** taken from Ramsey and Andersen (1984):

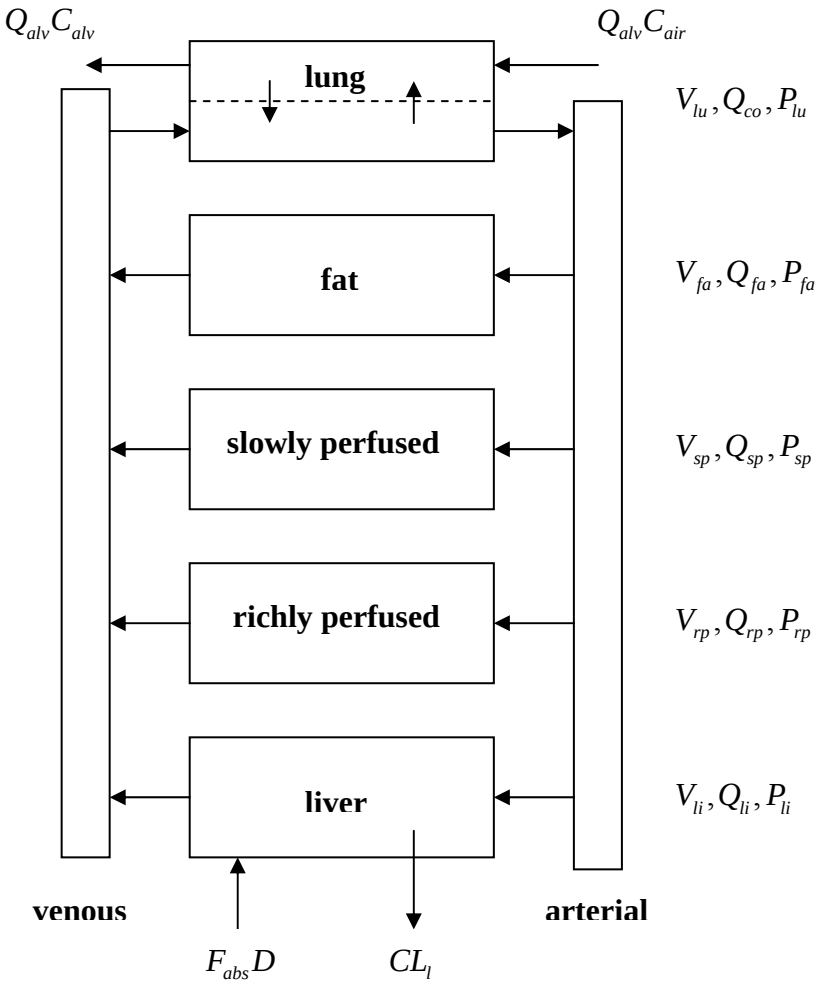

Figure 1. Example of a PBPK model. The compartments considered are venous and arterial blood, separated by the lung for possible uptake or elimination of volatile compounds, fat (adipose tissue) for storage of lipophilic compounds, liver for oral uptake (= fraction absorbed times dose) end hepatic metabolism (clearance) and two lumped tissue compartments discerned by their specific regional blood flows: slowly perfused (muscle, bone and skin) or richly perfused (all other tissues). Each compartment is characterised by is physiological volume *V* (or weight) and regional blood flow *Q* (Q_{co} is the cardiac output). Moreover, substance dependent tissue:blood partition coefficients *P* determine the distribution

The choice for modelled compartments depends on the compound's characteristics and the target tissues that should be modelled. *E.g.*, for AChE inhibitors brain and diaphragm are compartments to be considered or red blood cells (RBC) as an AChE inhibition indicator. In the introduction of models below, not only metabolism and detoxification processes in the liver are considered, but in blood and other compartments as well.

Mode of action of OPs

Organophosphates inhibit the so-called B-esterases: acetylcholinesterase (AChE), butyrylcholinesterase (BuChE) and Carboxylesterase (CaE). However several do not so directly, but have to be metabolized through CYP450 activity to their active oxygen analogue. Competing detoxification through CYP450 activity may also take place, *e.g.* the OPs chlorpyrifos (CPF) and diazinon (DZN) are hydrolysed to trichloropyridinol (TCP) and isopropylmethylhydroxypyrimidine (IMHP).

The mode of action of the active oxon analogue is depicted in **Figure 2** obtained from Bosgra *et al*. (2009). The oxon binds to a B-esterase (inhibition, reaction 1). The oxon-esterase complex may be reactivated (reaction 2) under hydrolysis of the oxon, or it may be dealkylated (aging, that is irreversible, reaction 3). The rates of reaction 2) and 3) depend on the characteristics of the R residues (e.g. reaction 2 is significant when R is CH_3-, almost nil if R is C_2H_5-). Carbamates do not age, and relatively quickly undergo reaction 2 ($t_{1/2}$ 30-60 minutes). The oxon metabolite, just as the parent compound may be detoxified through hydrolysis (so called A-esterase activity, reaction 4). B-esterases are synthesised *de novo* and then degraded, causing a steady B-esterase activity and providing for recovery of full B-esterase activity after inhibition. after exposure

So, a PBPK/PD model should provide for the kinetics of the OP in question and, if necessary, its oxon analogue together with the dynamics of the B-esterases inhibition.

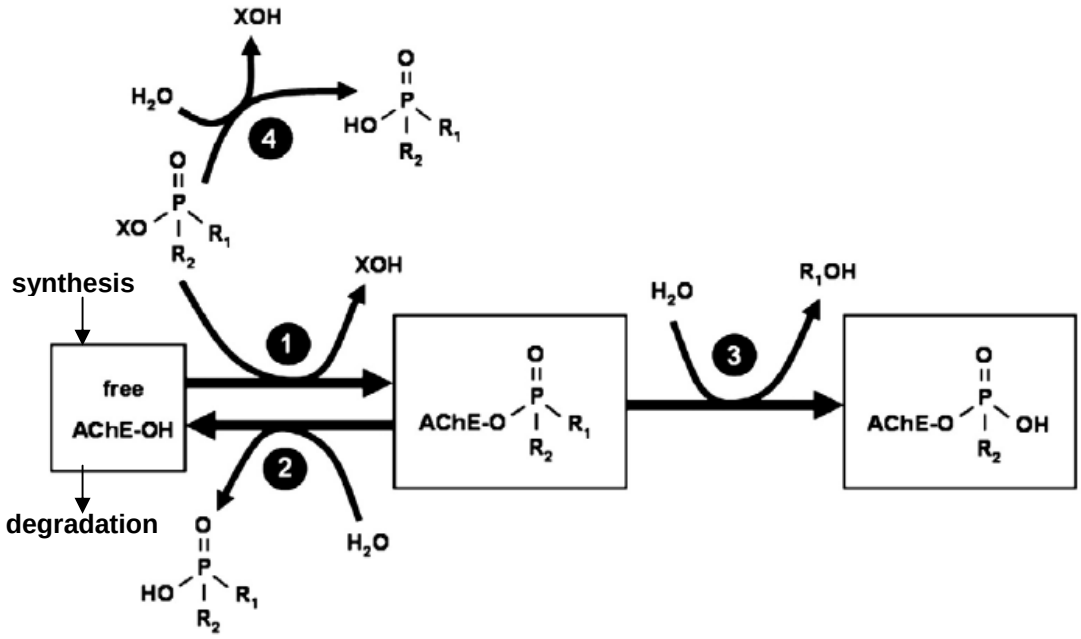

Figure 2. Mode of action of OPs. Inhibition of the parent or active metabolite by phosphorylation of the B-esterase (1) followed by reactivation through hydrolysis (2) or aging by dealkylation (3). Hydrolysis by A-esterase activity of the active compound (4) results in detoxification. B-esterases are synthesized and degraded throughout. From Bosgra *et al*. (2009). Carbamates do not age.

Short history of PBTK/TD models of OPs and carbamates

Soman in rats

The first PBPK/PD model found in the literature is a model for soman in the rat (Maxwell *et al*., 1988).

Although in figure 1 *ibid.* of their paper venous and arterial blood/plasma are shown explicitly as compartments, the PBPK model presented at the bottom of page 179 and the top of page 180 *ibid.* consists of the nine compartments: plasma (referred to as blood in figure 4 *ibid.*), lung (obvious from figure 2 and table II, not from page 180 *ibid.*), brain, heart, kidney, diaphragm, muscle, liver and carcass. Soman itself is the active agent and needs not to be metabolised. This model includes soman chirality.

All tissues compartments are assumed to have B-esterase activity, but carcass has no AChE activity (table II *ibid.*). Also A-esterase activity (detoxification through hydrolysis) is assumed in all tissues, but effective only (table II *ibid.*) in lung, kidney, liver and blood.

For the PD model, soman is assumed to bind *irreversibly* to B-esterases (*i.e.* quick aging). Irreversible binding of soman to BuChE and CaE is assumed to be non-toxic and is considered as detoxification. Moreover, as BuChE levels are much smaller than CaE levels, BuChE inhibition is neglected. Also not included in the model is the synthesis/degradation process of B-esterases, but presented model calculations indicate a maximum time span of thirty minutes after exposure only for which all processes not considered might be ignored.

Diisopropylfluorophosphate (DFP) in mice and rats

The second PBPK/PD model found in the literature is a model for DFP in mice and rats (Gearhart *et al*., 1990).

The PBPK model, like for soman, consists of ten compartments, but compartments are different from that in Maxwell *et al*. (1988): arterial and venous blood, lung, brain, kidney, diaphragm, liver, lumped richly perfused tissues, lumped slowly perfused tissues and fat. DFP itself is the active agent and needs not to be metabolised. All tissue compartments, exclusive fat, are assumed to have B-esterase activity. A-esterase activity is assumed in blood, brain, liver, kidney and the lumped richly perfused tissues compartment.

The PD model is as in Figure 1, including B-esterases synthesis and degradation. All three B-esterases are considered.

The model is extrapolated in Gearhart *et al*. (1994) to a PBPK/PD model for DPF in humans. Moreover, the model is extended to a PBPK model for parathion. Parathion necessitates the metabolism to its active metabolite paraoxon. Pharmacokinetics of parathion and parathion-oxon was successfully compared to experimental data, but the dynamics of paraoxon was *not considered*.

Paraoxon in rainbow trout

Dynamics of paraoxon is considered in the third PBPK/PD model found in the literature for paraoxon in the rainbow trout (Abbas and Hayton, 1997).

The PBPK model consists of eight compartments: arterial and venous blood, gills, brain, kidney, liver, heart and muscle. Paraoxon itself is the active agent. B-esterase activity is assumed in each tissue, A-esterase activity in liver only.

In the PD model, like for soman, BuChE is not considered and CaE inhibition serves detoxification. Reactivation and aging of AChE is neglected: recovery of AChE activity is through esterase synthesis only.

Chlorpyrifos (CPF) in rats and humans

Based on the work of Gearhart *et al*. (1990), Timchalk *et al*. (2002) developed a fourth inhibition model concerning CPF in rats and humans.

As CPF has to be metabolised to its active CPF-oxon analogue, the PBPK modelling consists of two coupled models for CPF and CPF-oxon. The CPF model consists of the eight compartments: blood, brain, diaphragm, liver, richly lumped perfused tissues, lumped slowly perfused tissues, skin and fat. In addition, for CPF oral bolus administration stomach and intestine CPF content is modelled. The CPF-oxon model does not contain a skin compartment, but the blood compartment is replaced by two compartments: mixed venous blood for free CPF-oxon and arterial blood for total CPF-oxon. Notice

that both represent the *total* blood pool. Tissue-blood transfer of CPF and CPF oxon is modelled as transfer of unbound CPF, CPF-oxon only. See **Figure 3**. B-esterase activity is assumed in arterial blood, diaphragm, brain and liver and A-esterase activity in mixed venous blood and liver only. Additional to these models a third one-compartment for the hydrolysed metabolite TCP is introduced that may serve interpretation of TCP as a biomarker in urine.

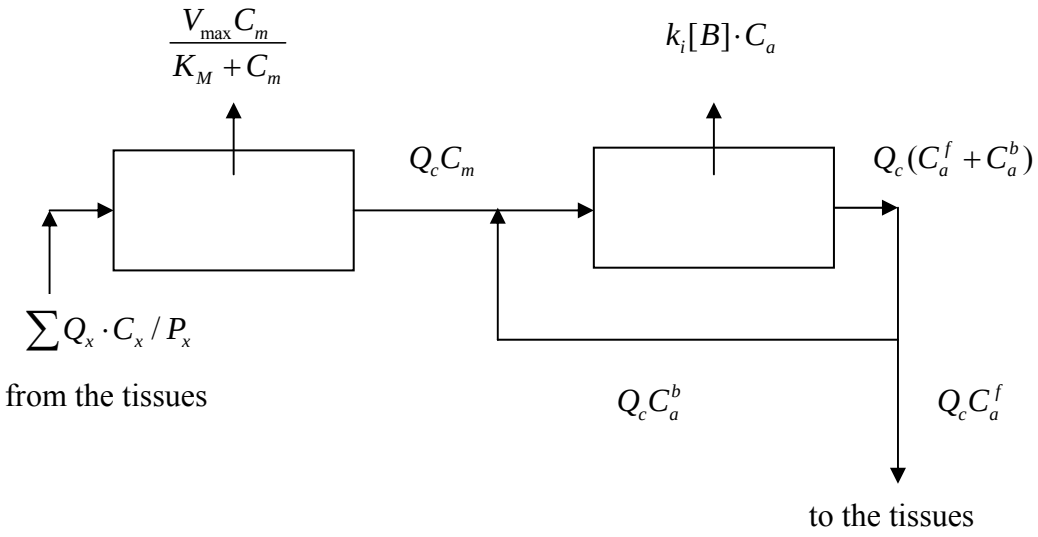

Figure 3. Blood pool model in Timchalk *et al*. (2002). The mixed venous pool (left) receives unbound (free) CPF-oxon from the tissues. The partition coefficients P_x denote the tissue:free-in-blood partition of CPF-oxon. Elimination of CPF-oxon from this pool only is due to A-esterase activity. Free CPF-oxon, leaving the mixed venous pool, enters the blood pool for total, *i.e.*, free and bound, CPF-oxon (right). Elimination due to AChE inhibition is in this total CPF-oxon blood pool. The bound fraction recycles directly for re-mixing with the free fraction from the mixed venous pool and the free fraction is transported to the tissues for CPF-oxon exchange. The same model, but without elimination due to A- and B- esterase activity holds for CPF.

The PD model is as in Figure 1, including B-esterases synthesis and degradation. All three B-esterases are considered. In this model the combined AChE and BuChE inhibition determines the dynamics of CPF. CaE inhibition serves detoxification of CPF.

This model has been extended/modified/applied in several studies. In Timchalk *et al*. (2007) an age-dependent CPF model in the preweanling rat is studied. In Timchalk and Poet (2008) the CPF B-esterase inhibition model for the rat with a is combined with a model for B-esterase inhibition of diazinon in rats (see below). Smith *et al*. (2009) considered comparative PBPK/PD of CPF via different routes of exposure as well as different application vehicles in rats. Foxenberg *et al*. (2011) considered human age- and gender-dependent CYP enzymes profiles and CYP polymorphism and compared AChE and BuChE cholinesterase inhibition by CPF of 1 year old and 19 years old humans. Ellison *et al*. (2011) studied PBPK/PD in rats following repeated subcutaneous exposure. Of special importance for the Acropolis project is the application of the CPF model for dietary exposures (Hinderliter *et al*., 2011). In that study, dietary exposure together with human individual physiology (compartment weights and organ-specific perfusion rates) is combined with the CPF-PBPK/PD model.

Diazinon (DZN) in rats

The fifth inhibition model was introduced by Poet *et al*. (2004) for DZN in rats.

DZN is metabolised to its active metabolite DZN-oxon and hydrolysed to IMHP. Furthermore, this model is a complete analogue of the CPF model in Timchalk *et al*. (2002), with "translation": CPF = DZN, CPF-oxon = DZN-oxon, TCP = IMHP.

The DZN model was combined with the CPF model in Timchalk and Poet (2008) for the inhibition of binary CPF/DZN mixtures in rats.

Parathion in rats

The sixth modelling effort concerns the combined exposure of rats to CPF and parathion (El Masri *et al.*, 2004). As such, it contains a model for parathion in rats, which is based on the PBPK-model for parathion and paraoxon in rats of Gearhart *et al.* (1994), but with inclusion of a PD-model.

The PBPK modelling concept for parathion and its active metabolite paraoxon is almost the same as that in Gearhart *et al.* (1994), however the lung is not considered. Tissue and lumped tissues compartment volumes, regional blood flows and partition coefficients are the same, but the metabolic constants for biotransformation of parathion to paraoxon and p-nitrophenol are quite different from Gearhart *et al.* (1994).

The PD model is as in Figure 1, including B-esterases synthesis and degradation. Only AChE esterase activity in blood is considered.

In this model only the AChE inhibition rate and oral or subcutaneous absorption rate are left as parameters for fitting to data. This results in half-lives of absorption kinetics of 10 and 20 hours for oral and subcutaneous dosing, respectively. These values are quite large. In fact, for CPF (the PBPK/PD model of which is partially based on Timchalk *et al.* (2002) and Gearhart *et al.* (1994) and partially on parameter values obtained from other literature data) these values are 140 and 350 hours, respectively.

The model is applied to find oral dose limits below with combined exposure effects may be assumed to be additive.

Carbofuran (CBF) and 3-hydroxycarbofuran (3HOCBF) in rats

The seventh inhibition model is that for AChE inhibition of CBF, a carbamate, and its metabolite 3HOCBF (Zhang *et al.* 2007).

The PBPK model is obtained from EPA (ERDEM system; Blancato, 2006). This modelling approach consists of 11 compartments: arterial, venous and portal blood, lung, brain, kidney, liver, lumped richly perfused tissues, lumped slowly perfused tissues, skin and fat. Additionally, oral uptake is modelled by carbofuran content of stomach, duodenum, small intestine and colon. Of these uptake compartments, duodenum and small intestine provide for enterohepatic circulation. B-esterase activity is assumed in blood and liver. Detoxification is through several pathways in the liver. As a number of metabolites, of which 3HOCBP is an AChE inhibitor as well, are modelled, the model consists of 17 sub-models.

PD is modelled as AChE inhibition only in blood and brain, BuChE and CaE were not considered due to implied model uncertainties. They follow the PD model in Figure 1 inclusive AChE synthesis, but exclusive AChE degradation. Confusingly, they consider degradation of the *inhibited* enzyme: "k_d: degradation rate constant of the inhibited enzyme", where in the other literature "degradation" refers to the B-esterase itself.

Carbaryl in rats

Modelling of carbaryl, a carbamate, is the eighth published cholinesterase inhibition model (Nong *et al*., 2008).

The PBPK model consists of three sub-models, one for carbaryl, one for its main metabolite 1-naphtol and one for "other" metabolites. Each sub-model consists of five compartments: blood, brain, liver, fat and lumped rest of body tissues. In contrast to the models reviewed thus far, transfer of carbaryl between tissues and blood is modelled as diffusion, rather than perfusion, limited. Additionally, an intestine compartment models the parent and metabolites gut lumen content, together with parent compound uptake, enterohepatic circulation of the parent compound and faecal excretion of the metabolites. Only AChE and BuChE activity is considered in blood and brain. Detoxification of carbaryl is through metabolism in the liver.

The PD model is as in Figure 1. including synthesis and degradation. Carbamate-B-esterase complexes however do not age, so only reactivation is modelled. CaE is not considered, thus detoxification by inhibition of this B-esterase is neglected.

Soman in rats, marmosets, guinea pigs and pigs

The ninth PBPK/PD cholinesterase inhibition model (Chen and Seng, 2011) is again for soman, but differs considerably from the model introduced by Maxwell *et al*. (1988).

In this model, the four stereo isomers of soman are modelled by four different PBPK models. There are eleven model compartments: arterial and venous blood, lung, brain, kidney, diaphragm, liver, heart, lumped richly perfused tissues, lumped slowly perfused tissues and fat. Moreover, the lumped slowly perfused tissues compartment contains a sub-compartment providing for intramuscular and subcutaneous exposure. Like in Maxwell *et al*. (1988) all tissue compartments, exclusive fat and the lumped tissues sub-compartment, are assumed to have B-esterase activity. A-esterase activity is assumed in blood, liver and kidney (but not, as in Maxwell *et al*. (1988), in lung). Like in Maxwell *et al*. (1988), BuChE inhibition contributing to detoxification is neglected with respect to the contribution of CaE inhibition.

The PD model is as in Figure 1, now including B-esterases synthesis and degradation, but, as in Maxwell (1988), still neglecting reactivation.

Model properties

Information on the different models with respect to PBPK and PD is summarized at the next page in **Table 1**. From this table, one can see that there are as many similarities as dissimilarities in the different model approaches.

PBPK model aspects

Blood/plasma

All models contain (a) blood/plasma compartment(s) for transport from the site of exposure to the tissues and from tissues to eliminating compartments. The only model that contains a plasma instead of a blood compartment is that for soman (Maxwell *et al*. 1988). The OPs CPF, DZN, DFP and soman are detoxified through A-esterase activity in blood/plasma itself. For the OP paraoxon no such detoxification is modelled in the rainbow trout. All models assume B-esterase activity in blood.

Only for CPF, DZN and carbaryl venous and arterial blood compartments separated by the lung is not modelled, most probably as these compounds have low volatility and the main routes of exposure and elimination do not include lung. The modelling of a mixed venous and an arterial blood compartment for the models of CPF and DZN, shown in Figure 2, is quite different from the usual approach of modelling separate venous and arterial blood compartments.

Lung (gills)

The models for DFP, CBF and soman contain a lung compartment and the model for paraoxon (in rainbow trout) contains a gill compartment that separates the venous and arterial blood compartments. The models for DFP, paraoxon and soman consider B-esterase activity in this compartment, but the model for carbofuran does not so. There is no B-esterase activity modelled in gills. A-esterase activity in the lung is only modelled in Maxwell *et al*. (1988).

Though explicitly included as a compartment the lung does neither serve inhalatory uptake nor exhalation elimination for DFP, CBF and soman. The gill compartment of the model for paraoxon in rainbow trout does serve these processes.

Liver

The liver is modelled as a compartment in all models and serves A-esterase activity/detoxification. B-esterase activity is assumed in the liver for all OP-models but not for the carbamate models.

Diaphragm

All models but for paraoxon in rainbow trout, which is obvious, and for carbaryl contain a diaphragm compartment. The models with a diaphragm compartment all, but for CBF, model B-esterase activity in that compartment. It is not clear why this activity is omitted in the model for CBF.

Brain

As AChE inhibition in brain seems the most important adverse effect, the brain is a compartment and contains B-esterase activity in all models. Only the model for DFP contains A-esterase activity for detoxification in the brain. The brain has the same function in all other models.

Table 1. PBPK/PD model characteristics

Compound / species	**PBPK** model			**PD** model		
	compartments	B-esterase compartments	A-esterase / detoxification compartments	processes	B-esterases	inhibition effect in plasma
Chlorpyrifos (CPF) / rats & humans	BL, BR, DI, LI, SP, RP, FA [(a)]	BL, BR, DI, LI	BL, LI	SY, DE, IN, RE, AG	AChE, BuChE, CaE	AChE + BuChE
Diazinon (DZN) / rats	BL, BR, DI, LI, SP, RP, FA [(a)]	BL, BR, DI, LI	BL, LI	SY, DE, IN, RE, AG	AChE, BuChE, CaE	AChE + BuChE
Diisopropylfluorophosphate (DFP) / mice & rats	BLV, LU, BLA, BR, DI, LI, KI, SP, RP, FA	all tissues but FA	BL, BR, LI, KI, RP	SY, DE, IN, RE, AG	AChE, BuChE, CaE	AChE
Paraoxon / rainbow trout	BLV, GI, BLA, BR, LI, KI, HE, MU	all tissues (fat is not considered)	LI	SY, DE, IN	AChE, CaE	AChE
Parathion / rats	BLV, BLA, BR, DI, LI, KI, SP, RP, FA	BL	BL, BR, LI, KI, RP	SY, DE, IN, RE, AG	AChE	AChE
Carbofuran and 3-hydroxycarbofuran (CBF, 3HOCBF) / rats	BLV, LU, BLA, BLP, BR, DI, LI, SK, SP, RP, FA[(b)]	BL, BR	LI	SY, IN, RE	AChE	AChE
Carbaryl / rats	BL, BR, LI, FA, RE©	BL, BR	LI	SY, DE, IN, RE	AChE, BuChE	AChE + BuChE
Soman / rats	PL, BR, DI, LI, KI, MU, HE, CA	all tissues (no AChE in carcass)	BL , LU, KI, LI	IN, AG	AChE, CaE	AChE
	BLV, LU, BLA, BR, DI, LI, KI, HE, SP, RP, FA	all tissues but FA	BL, KI, LI	SY, DE, IN, AG	AChE, CaE	AChE

Compartments: BL: blood, BLA: arterial blood, BLP: portal blood, BLV: venous blood, BR: brain, CA: carcass, DI: diaphragm, FA: fat (adipose tissue), GI: gastrointestinal tract, HE: heart, KI: kidney, LI: liver, LU: lung, MU: muscle, PL: plasma, RE: remaining tissues, RP: richly (rapidly) perfused, SK: skin, SP: slowly (poorly) perfused

Processes: AG: aging, DE: degradation, IN: inhibition, RE: reactivation (regeneration), SY: synthesis

a: models for CPF and CPF-oxon or for DZN and DZN-oxon, the biomarker metabolites TCP and IMHP models have 1-compartment only

b: models for the active parent CBF, its active metabolite 3HOCBF and 15 other metabolites

c: models for carbaryl, its main metabolite and “other” metabolite

Slowly perfused tissues

The models for CPF, DZN, DFP, and soman (Chen and Seng, 2011) contain a lumped slowly perfused tissues (SP-) compartment, representing muscle, bone and skin. The model for CBF has an explicitly defined skin compartment and its SP-compartment consists of muscle and bone only. However, none of the authors explicitly declare the composition of the SP-compartment. The models for CPF and DZN consider the SP-compartment as non-active, but the other two assign B-esterase activity to it. The models for paraoxon in rainbow trout, carbaryl and soman (Maxwell, 1988) do not contain such a compartment. The latter two define a "rest tissues" and a "carcass" compartment, respectively, which may contain richly perfused tissues as well: this is not declared.

Richly perfused tissues

The models for CPF, DZN and CBF contain a lumped richly perfused tissues (RP-) compartment including kidney. Those for DFP and soman (Chen and Seng, 2011) contain an explicitly defined kidney compartment besides a RP-compartment. The models for paraoxon in rainbow trout, carbaryl and soman (Maxwell, 1988) do not contain such a compartment. The latter two define a "rest tissues" and a "carcass" compartment, respectively, which may contain slowly perfused tissues as well: this is not declared. The models for CPF, DZN and CBF consider the RP-compartment as non-active, but the other two assign B-esterase activity to it. A-esterase activity is assumed in the RP-compartment for the DFP-model and for none of the other ones.

Kidney

A kidney compartment is modelled for DFP, paraoxon and soman (both models). B-esterase activity is assumed in kidney for all four models. But for the model of paraoxon in rainbow trout, A-esterase activity is also assumed for kidney.

Fat

Fat is a compartment in all models but for paraoxon and soman (Maxwell *et al*., 1988). The latter may contain fat in the defined "carcass" compartment. In all models fat is a non-active compartment, obviously modelled as a storage for the lipophilic compounds.

Heart

Heart is explicitly considered in the model for paraoxon and soman. It is assumed to contain B-esterase activity.

Muscle

Muscle is explicitly considered in the model for paraoxon and soman (Maxwell *et al*., 1988). It is assumed to contain B-esterase activity.

GI-tract

GI-tract is explicitly considered in the model for paraoxon only. It is assumed to contain B-esterase activity.

Rest and carcass

The models for carbaryl and soman (Maxwell *et al*., 1988) contain remaining tissues. In the model for carbaryl, this compartment is inactive, in the model for soman (Maxwell *et al*., 1988) it contains CaE activity, but no AChE activity (table II *ibid.*).

PD-model aspects

Inhibition

Obviously, all model describe B-esterase inhibition

Reactivation

Reactivation of the B-esterase-OP complex is not considered in the models for paraoxon and soman (both models). It is assumed for paraoxon to be insignificant. For soman Maxwell (1988) states that soman is bound irreversibly and Chen & Seng (2011) state that the complex just ages, with is effectively equivalent to the viewpoint of being irreversibly bound.

Aging

The two carbamates do not age. The B-esterase-CBF complex is assumed to "degrade" which in the usual terminology would be called to "age", while the B-esterase-carbaryl complex is assumed to be

reactivated only. Aging was not modelled for the OP paraoxon, but for this compound reactivation was considered insignificant, which may considered to be effectively equivalent to state that the B-esterase-paraoxon just ages, as for soman.

Synthesis

Only the model for soman Maxwell (1988) does not consider *de novo* synthesis of B-esterases. This might be due to ignoring synthesis as this process provides a negligible contribution to B-esterases activity on the time scale of their experiments of 30 minutes only.

Degradation

By degradation we mean "degradation" in the usual sense of AChE degradation and not in the sense of Zhang *et al.* (2007). Obviously, the model for soman Maxwell (1988) does not consider B-esterase degradation.

B-esterases considered

Obviously, AChE is considered in all models.

Inhibition of BuChE and CaE are considered as detoxification processes. **Figure 4** at page 12 shows the sensitivity of AChE inhibition on detoxification by BuChE and CaE. The model for plasma inhibition (Timchalk *et al*., 2002) was applied for an oral bolus dose of 500 μg CPF/kg body weight and the inhibition rates for BuChE and CaE were alternatively set to zero. The figure shows that detoxification of BuChE is negligible. BuChE activity was omitted in the models for paraoxon, carbofuran and soman (both models).

The sensitivity on CaE detoxification is 1% for this dose, this raises to 8% for a dose of 5000 μg CPF/kg bw and 18% for a dose of 50000 μg CPF/kg bw. However absolute values are 1%, 5% and 5% inhibition loss. See **Figure 5** at page 13.

CaE activity was not considered in the models for both carbamates.

Inhibition effects in plasma

The models for CPF, DZN and carbaryl consider plasma inhibition of total cholinesterase inhibition: the sum of AChE and BuChE activities with respect to the sum of their base-line activity, although only AChE inhibition is toxicologically relevant. Other models consider AChE activity inhibition only. **Figure 6** at page 14 shows that differences can be substantial. Nevertheless, plasma ChE inhibition, as well as RBC AChE inhibition serves as inhibition biomarkers.

In our study RBC AChE inhibition will be considered as biomarker. Note that RBC AChE inhibition itself is toxicologically irrelevant.

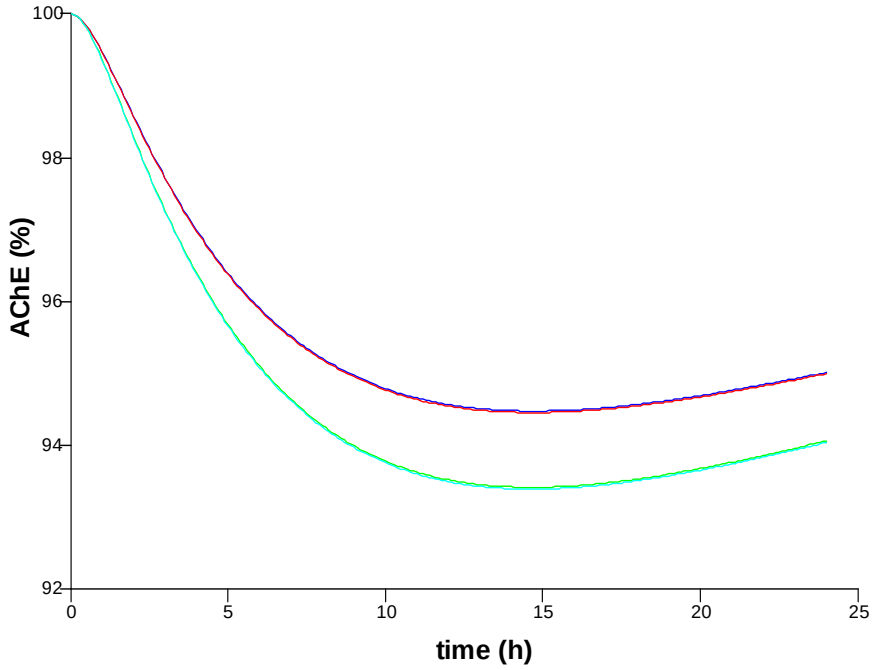

Figure 4. The two upper lines (hardly discernable), show AChE inhibition when the detoxification of CaE is active with and without BuChE activity. The two lower lines (hardly discernable), show AChE inhibition when the detoxification of CaE is inactive with and without BuChE activity.

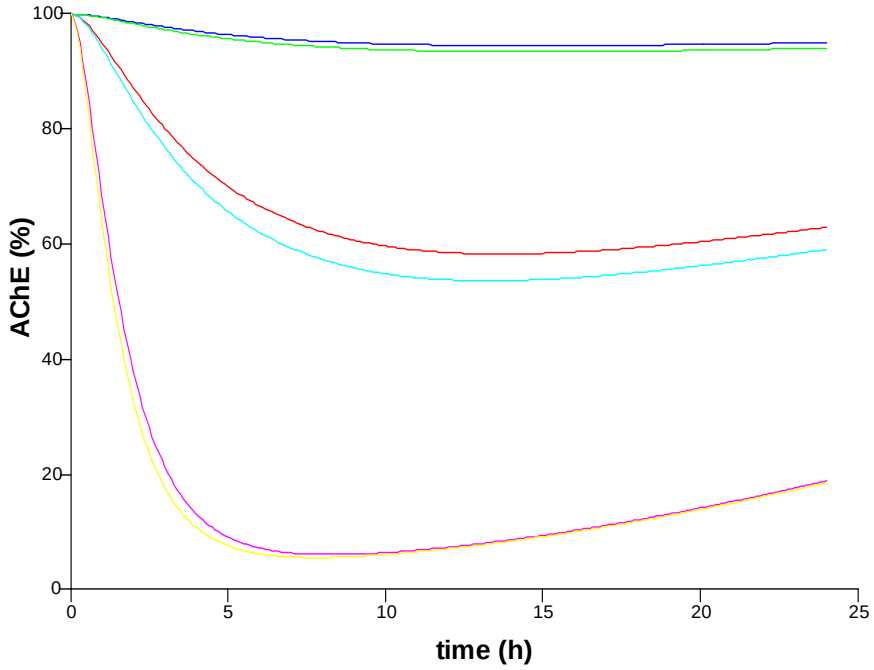

Figure 5. AChE inhibition for oral bolus doses of 0.5, 5 and 50 mg CPF/kg bw with (upper of line pairs) and without (lower of line pairs) CaE activity.

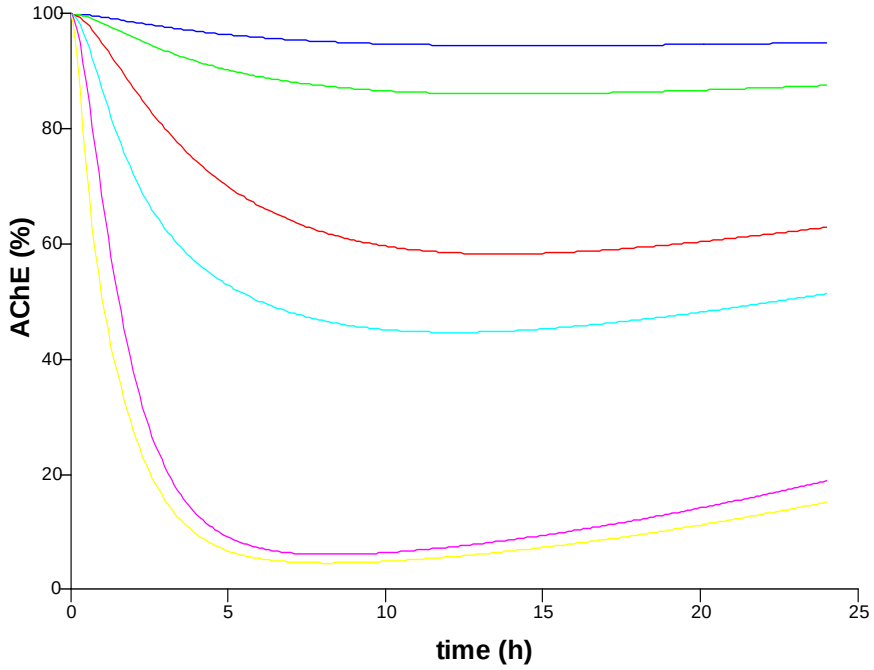

Figure 6. Total ChE (lower line of line pairs) and AChE (upper line of line pairs) inhibition for oral bolus doses of 0.5, 5 and 50 mg CPF/kg bw.

Modelling relevance for WP4

The Acropolis project states that pesticide residues on foods are one of the principal worries of EU consumers when it comes to the risks associated with their food. WP4 aims at the development of a methodology for the risk assessment of dietary exposure including variability due to food intake and consumers physiology.

From the start of the project, it was clear that such a methodology should be based on mathematical models that not only take into account the internal fate of pesticides after oral exposure but the internal dose-effect as well. In this framework PBPK/PD modelling seems a promising approach. Such an approach should be supported by an example. Therefore PBPK/PD models for neurotoxic pesticides that have been developed in the literature could be used as a starting point. In the following a choice will be made which of the models in the overview would be promising candidates for this objective.

As both soman and diisopropylfluorophosphate are not used as pesticides, these compounds will not be further considered for exemplary dietary exposure risk assessment, *i.e.* possible effective internal dose.

Of the three other OPs, PBPK modelling of parathion in the rat has been developed (Gearhart *et al.*1994) and further extended to a PBPK/PD model for AChE inhibition in the rat by El Masri *et al.* (2011). However, model parameterization of these authors leads to an oral absorption half live of parathion in the rat of 10 hours, *i.e.* after a period of about two days still about 5% of the dose is not absorbed yet. Nevertheless, they introduce a promising methodology for checking dose additivity in the combined oral exposure to parathion and CPF in rats. However, seen the extreme oral absorption half life of CPF of 140 hours, their results are in doubt. In relation to the dose additivity limit, it would

be interesting also whether these limit doses still lead to observable (measurable) AChE inhibition levels, which the authors do not consider. A PBPK/PD model for paraoxon, the active metabolite of parathion in rainbow trout has been developed (Abbas & Hayton, 1997). However, it is unclear how this model should be scaled to a PBPK/PD model for parathion itself in rats or humans. So, parathion also will not be further considered for exemplary dietary exposure risk assessment.

The two carbamates will not be considered too. First of all these compounds are less persistent than OPs, secondly their PBPK/PD models were developed for rats only and third, they are banned by EU legislation (though, of course, it could be found on EU-imported food (components).

DZN, banned as a pesticide by EU legislation, is used outside the EU and may be found on imported food (components). A PBPK/PD model of DZN and its active metabolite DZN-oxon in rats has been modelled by Poet *et al*. (2004). This model has not only been developed as such, but has been applied to a PBPK/PD model for cumulative exposure in rats to DZN and CPF (Timchalk & Poet, 2008). So, it could serve at least as exemplary for risk assessment due to cumulative exposure, be it in rats. However, in Poet *et al*. (2004), the model also has been linked to human biomarker kinetics. It seems appropriate to further consider this model for WP4.

CPF is in use world wide as a pesticide and is allowed in the EU. Timchalk *et al*. (2002) developed a PBPK/PD model for CPF and its active metabolite CPF-oxon in rats and **humans**. As such, it is the ideal model for use in WP4. Moreover, the model was not only developed as such, but it was applied to a PBPK/PD model for the combined exposure to CPF and DZN in rats (Timchalk & Poet, 2008) and to the stochastic biomarker (AChE inhibition in RBC) effect of dietary exposure of 3 years old children and a 30 years old adults including stochastics of intake as well as of the subjects physiology (Hinderliter *et al.*, 2011). **This seems exemplary to the objective of WP4**.

However that be, their modelling results indicate that for the average daily dose of 9 ng CPF/kg bw/day, estimated for adults in the U.S., biomarker red blood cells AChE activity would be still 99.985% of control. This raises the questions whether such a low inhibition effect is relevant and is measurable. Moreover, it indicates that effects of concomitant exposure would, in a conservative risk assessment approach and not regarding kinetics, be additive and still very low.

Literature

Abbas, R. and W.L. Hayton; A physiologically based pharmacokinetic and pharmacodynamic model for paraoxon in rainbow trout; *Toxicol. Appl. Pharmacol.*, **145** (1997) 192-201

Blancato, J. N., Power, F. W., Brown, R. N., and C. C. Dary; *Exposure Related Dose Estimating Model (ERDEM) a physiologically-based pharmacokinetic and pharmacodynamic (PBPK/PD) model for assessing human exposure and risk*; U.S. Environmental Protection Agency, Washington, DC EPA/600/R-06/061 (NTIS PB2006-114712).

Bosgra, S. van Eijkeren, J.C.H., van der Schans, M.J., Langenberg, J.P. and W. Slob; Toxocodynamics of the combined cholineterase inhibition by paraoxon and methamidophos in human wholw blood; *Toxicol. Appl. Pharmacol.*, **236** (2009) 9-15

Chen, K. and K-Y. Seng; Calibration and validation of a physiologically based model for soman intoxication in the rat, marmoset, guinea pig and pig; *J. Appl. Toxicol.*, (2011) (wileyonlinelibrary.com) DOI 10.1002/jat.1671

Crowell, S.R., Henderson, W.M., Kenneke, J.F. and J.W. Fisher; Development and application of a physiologically based pharmacokinetic model for triadimefon and its metabolite triadimenol in rats and humans; *Toxicol. Lett.*, **205** (2011) 154-162

Ellison, A.E., Smith, J.N., Lein, P.J. and J.R. Olson; Pharmacokinetics and pharmacodynamics of chlorpyrifos in adult male Long-Evans rats following repeated subcutaneous exposure to chlorpyrifos; *Toxicology*, **287** (2011) 137-144

El-Masri, H.A., Mumtaz, M.M. and M.L. Yushak; Application of physiologically-based modeling to investigate the toxicological interaction between chlorpyrifos and parathion in the rat; *Environ. Toxicol. Pharmacol.*, **16** (2004) 57-71

Foxenberg, R.J., Ellison, C.A., Knaak, J.B., Ma, C. and J.R. Olson; Cytochrome P450-specific human PBPK/PD models for the organophosphorus pesticides: Chlorpyrifos and parathion; *Toxicology*, **285** (2011) 57-66

Gearhart, J.M., Jepson, G.W., Clewell III, H.J., Andersen, M.E. and Conolly, R.B.; Physiologically based pharmacokinetic and pharmacodynamic model for the inhibition of acetylcholinesterase by diisopropylfluorophosphate; *Toxicol. Appl. Pharmacol.*, **106** (1990) 293-310

Gearhart, J.M., Jepson, G.W., Clewell, H.J., Andersen, M.E. and Conolly, R.B.; Physiologically based pharmacokinetic model for the inhibition of acetylcholinesterase by organophophate esters; *Environ. Health Perspect.*, **102(Suppl 11)** (1994) 51-60

Hinderliter, P.M., Price, P.S., Bartels, M.J., Timchalk, C. and T.S. Poet; Development of a source-to-outcom model for dietary exposures to insecticide residues: An example using chlorpyrifos; *Regul. Toxicol. Pharmacol.*, **61** (2011) 82-92

Maxwell, D.M., Vlahacos, C.P. and D.E. Lenz; A pharmacodynamic model for soman in the rat; *Toxicol. Lett.*, **43** (1988) 175-188

Nong, A., Tan, Y-M., Krolski, M.E., Wang, J., Lunchick, C., Conolly, R.B. and H.J. Clewell III; Bayesian calibration of a physiologically based pharmacokinetic/pharmacodynamic model of carbaryl cholinesterase inhibition; *J. Toxicol. Environ. Health, A*; **71** (2008) 1363-1381

Poet, T.S., Kousba, A.A., Dennison, S.L. and C. Timchalk; Physiologically based pharmacokinetic/pharmacodynamic model for the organophosphorus pesticide diazinon; *NeuroToxicology*, **25** (2004) 1013-1030

Smith, J.N., Campball, J.A., Busby-Hjerpe, A.L., Lee, S., Poet, T.S., Barr, D.B. and C. Timchalk; Comparative chlorpyrifos pharmacokinetics via multiple route of exposure and vehicles of administration in the adult rat; *Toxicology*, **261** (2009) 47-58

Timchalk, C., Nolan, R.J., Mendrala, A.L., Dittenber, D.A., Brzak, K.A. and J.L. Mattsson; A a physiologically based pharmacokinetic and pharmacodynamic (PBPK/PD) model for the organophosphorus insecticide chlorpyrifos in rats and humans; *Toxicol. Sci.*, **66** (2002) 34-53

Timchalk, C., Kousba, A.A. and T.S. Poet; An age-dependent physiologically based pharmacokinetic/pharmacodynamic model for the organophosphorus insecticide chlopyrifos in the preweanling rat; *Toxicol. Sci.*, **98** (2007) 348-365

Timchalk, C. and T.S. Poet; Development of a physiologically based pharmacokinetic and pharmacodynamic model to determine dosimetry and cholineterase inhibitioenfor a binary mixture of chlopyrifos and diazinon in the rat; *NeuroToxicoloy*, **29** (2008) 428-443

J.C.H. van Eijkeren; Tebuconazole kinetics in male Japanese white rabbit; *internal WP4-memo*; RIVM, Bilthoven, the Netherlands, 2011

Zhang, X., Tsang, A.M., Okino, M.S., Power, F.W., Knaak, J.B., Harrison, L.S. and C.C. Dary; A physiologically based pharmacokinetic/pharmacodynamic model for carbofuran in Sprague-Dawley rats using the exposure-related dose estimating model; *Toxicol. Sci.*, **100** (2007) 345-359